INFORMATION TO USERS

This manuscript has been reproduced from the microfilm master. UMI films the text directly from the original or copy submitted. Thus, some thesis and dissertation copies are in typewriter face, while others may be from any type of computer printer.

The quality of this reproduction is dependent upon the quality of the copy submitted. Broken or indistinct print, colored or poor quality illustrations and photographs, print bleedthrough, substandard margins, and improper alignment can adversely affect reproduction.

In the unlikely event that the author did not send UMI a complete manuscript and there are missing pages, these will be noted. Also, if unauthorized copyright material had to be removed, a note will indicate the deletion.

Oversize materials (e.g., maps, drawings, charts) are reproduced by sectioning the original, beginning at the upper left-hand corner and continuing from left to right in equal sections with small overlaps.

Photographs included in the original manuscript have been reproduced xerographically in this copy. Higher quality 6" x 9" black and white photographic prints are available for any photographs or illustrations appearing in this copy for an additional charge. Contact UMI directly to order.

ProQuest Information and Learning
300 North Zeeb Road, Ann Arbor, MI 48106-1346 USA
800-521-0600

What's Happening Around Herbig Ae Stars?

Investigating Circumstellar Activity in
Young Intermediate Mass Stars
with Optical and Near-Infrared Spectroscopy

Bernadette Rodgers

A dissertation submitted in partial fulfillment
of the requirements for the degree of

Doctor of Philosophy

University of Washington

2001

Program Authorized to Offer Degree: Astronomy

Bell & Howell Information and Learning Company
300 North Zeeb Road
P.O. Box 1346
Ann Arbor, MI 48106-1346

In presenting this dissertation in partial fulfillment of the requirements for the Doctoral degree at the University of Washington, I agree that the Library shall make its copies freely available for inspection. I further agree that extensive copying of this dissertation is allowable only for scholarly purposes, consistent with "fair use" as prescribed in the U.S. Copyright Law. Requests for copying or reproduction of this dissertation may be referred to Bell and Howell Information Learning, 300 North Zeeb Road, Ann Arbor, MI 48106-1346, to whom the author has granted "the right to reproduce and sell (a) copies of the manuscript in microform and/or (b) printed copies of the manuscript made from microform."

Signature 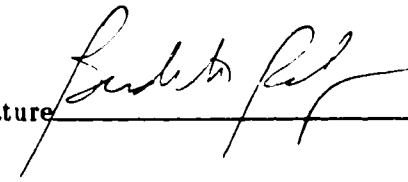

Date 7 June 2001

University of Washington

Graduate School

This is to certify that I have examined this copy of a doctoral dissertation by

Bernadette Rodgers

and have found that it is complete and satisfactory in all respects,
and that any and all revisions required by the final
examining committee have been made.

Chair of Supervisory Committee:

Bruce Balick

Reading Committee:

Bruce Balick

Suzanne Hawley

Paula Szkody

George Wallerstein

Diane H. Wooden

Date: 6/5/01

University of Washington

Abstract

What's Happening Around Herbig Ae Stars?

Investigating Circumstellar Activity in
Young Intermediate Mass Stars
with Optical and Near-Infrared Spectroscopy

by Bernadette Rodgers

Chair of Supervisory Committee

Professor Bruce Balick
Astronomy

We have investigated the optical and near-infrared spectral behavior of the intermediate mass, pre-main sequence Herbig Ae stars, with particular emphasis on variability and evolution. The evolutionary state of Herbig Ae (HAe) stars is intermediate between very young, pre-main sequence objects and the young main sequence Vega, or β Pic-like, stars. The majority of HAe stars are estimated to span a small range in ages, between 2 and 6 million years. Near-infrared spectra reveal an evolutionary sequence from strong Brackett emission in the youngest sources to photospheric absorption in main sequence Vega-like stars. HAe stars exhibit nearly featureless spectra in the near-infrared, a combination of photospheric absorption veiled by strong excess continuum, and weak Brackett line emission. In the evolutionary sequence, the hot gas creating the Brackett emission disappears before the hot dust responsible for the thermal emission. The data suggest that the strength of the Brackett emission decreases with age between 1 and 10 Myrs, while the thermal emission drops for stars >10 Myrs. Our high resolution spectra of Brγ in 2 HAe stars indicate that the Brackett emission is associated with accreting gas. Therefore, near-infrared Brackett emission offers an important diagnostic of inner disk evolution in late pre-main sequence

intermediate mass stars.

A large fraction ($\sim 25 - 50\%$) of HAe stars, called UXORs after the prototype UX Ori, exhibit large optical variability ($\Delta V > 1.5$ mag), commonly attributed to obscuration of the central star by circumstellar dust. Optical spectra of the UXOR star RR Tau over factor of 10 in brightness ($V = 11$ to $V \sim 13.5$ mag), reveal a system in which the photosphere of the star (Balmer wings and weak metal lines) and the wind flux ([OI], [FeII], and Hα lines) are unaffected by the brightness minima while permitted metal lines (FeII, CaII, OI, NaI) change from absorption to emission when the star fades. We suggest a model that attributes the metal absorption to a higher density region obscured with the star, while the metal emission lines come from a more extended unobscured region. More importantly, this result exemplifies the value of spectral monitoring in constraining the location of obscuring material and its effects on the circumstellar environment.

TABLE OF CONTENTS

LIST OF FIGURES

LIST OF TABLES

ACKNOWLEDGMENTS

Someone once said "It takes a village to get a PhD[1]". There are a great number of people that have contributed to this endeavour, in ways large and small, and to whom I am indebted. First and foremost of course, are my primary advisors, Diane Wooden and Bruce Balick. My thanks to Diane for friendship, wisdom and encouragement, but most of all for being willing to jump in and get her fingernails dirty when I needed it most! To Bruce I am indebted for his enthusiasm and support, and for allowing me the freedom to pursue my own topic. I am grateful to my supervisory committee: Suzanne Hawley, Paula Szkody, and George Wallerstein for their time and guidance. To my collaborators, who often acted more as advisors: Chick Woodward, Vladimir Grinin, Antonella Natta and Dmitry Shakhovsky, a special thanks. I couldn't have done it without you. For data taking and/or data sharing, I would like to acknowledge George Wallerstein, Christopher Laws, Steve Strom, Bo Reipurth and Chris Johns-Krull. Chris also falls in the category of people who have generously shared their knowledge through many enlightening conversations, of whom I also mention Robbins Bell, Joan Najita, David Hollenbach, Suzan Edwards, Frank Shu and many other members of the Center for Star Formation, my scientific home away from home.

For my start in astronomy, I credit two people. My dear friend Al Glassgold, who took me under his wing at NYU in 1987 and whose excellent mentoring has gone far beyond the masters degree I obtained there. And Dr. Harry Shipman, my Astronomy 101 professor at the University of Delaware, whose infectious enthusiasm gave me the astronomy bug my senior year in college (and of course, Mom and Dad for getting me there in the first place!). Back to the present, a special thanks to Vandana, who went above and beyond the duties of an officemate so many times– even changing diapers! For good times and bad food, I can thank the astro-grads, w(h)ine time, the GV, Big Time boxes, and the pizza mafia.

[1]Borrowed from the book with a similar title by Hilary Rodham Clinton

Through the course of this endeavour I received financial support from a number of sources. The majority of my research was funded by a NASA Graduate Student Research Program (GSRP) grant from NASA Ames Research Center, for which Diane Wooden was my NASA mentor. When that money ran out, I received a one year Dissertation fellowship from the American Association of University Women (AAUW) to focus on the writing of my dissertation. As this took longer than anticipated (primarily due to the arrival of a new family member!), I also received one quarter of funding from the Space Grant Consortium during my final year. This research has made extensive use of the SIMBAD database, operated at CDS, Strasbourg, France. Most data reduction was performed with the Image Reductiuon and Analysis Facility (IRAF), distributed by the National Optical Astronomy Observatories, which are operated by the Association of Universities for Research in Astronomy, Inc., under cooperative agreement with the National Science Foundation. I have also used, and acknowledge with thanks, data from the American Association of Variable Star Observers (AAVSO) International Database, based on observations submitted to the AAVSO by variable star observers worldwide.

Finally, and above all, I couldn't have done this without the love of my family. Peter, for the emotional and financial support to abandon a lucrative job and follow my heart, your payback's coming! Joshua and Amy, you light up my life and always keep my priorities where they should be ("no 'puter Mommy").

Chapter 1

INTRODUCTION

Stars of spectral type A are interesting creatures in the galactic zoo. On the main sequence, there are the magnetic Ap stars, the metal-rich Am stars, A shell stars with narrow absorption lines, and δ Scuti variable stars. On the H-R diagram, these A stars fall in the "instability strip", where opacity effects in the atmospheres of the stars cause them to pulsate, with luminosity fluctuations up to a few tenths of a magnitude. And then there are the β Pic-like or Vega systems, the majority of which are of spectral type A. These systems, first discovered in large numbers as a result of the Infrared Astronomical Satellite mission, are main sequence stars with infrared continuum emission well above that which is emitted by their photospheres. The excess emission is thermal energy emitted from warm dust organized in circumstellar disks (cf., Backman & Paresce 1993). These secondary, or "debris" disks, harbor particles which are too small to have survived for the ages of the stars, and therefore must be replenished, presumably as a result of collisions from larger solid bodies in orbit around the stars. Since their discovery, the β Pic-like stars have generated a lot of excitement as astronomers believe they offer the best opportunity to witness young planetary systems in the making.

The evolutionary pre-cursors to main sequence A stars are the Herbig Ae stars. Herbig Ae (HAe) stars, along with Herbig Be (HBe) stars, were discovered in 1960 (Herbig 1960), and are now known to be pre-main sequence stars of intermediate mass ($2 - 8\mathcal{M}_{\odot}$). They have many characteristics in common with their lower mass counterparts, the T Tauri stars, but significant empirical and theoretical differences as well. While intense observational and theoretical focus on the T Tauri (TT) stars has successfully produced a fairly complete and comprehensive picture of disk formation, accretion, outflow, and evolution to the main

sequence, it is unclear how well this picture fits the intermediate-mass stars. As a group, Herbig Ae and Be systems have historically been lumped together, and this has hampered the understanding of their physical nature. They are much smaller in number and more heterogenous than the T Tauris, making concensus even more difficult. However, the Herbig Ae/Be stars (HAEBEs, pronounced "hay-bees") have enjoyed considerable observational attention over the past decade, and very recently some theoretical progress as well. As a result, we now know that HAe and HBe stars have significant differences between them and must be considered seperately if we are to forward our understanding of either. The emerging picture of HAe stars is one of young stars surrounded by fairly massive, primary disks, possibly in the late stages of stellar accretion and early stages of disk dispersal and/or solid body growth. Fundamental unanswered questions include: how does material accrete onto these stars? do the stars harbor significant magnetic fields? how do the disks evolve? are there radial gaps or large scale inhomogenities in the disks? if so, what causes them? is there evidence for grain growth/planet formation?

The circumstellar environments of Herbig Ae stars are the focus of this thesis. Much of the work in this field (in both HAEBEs and TTs) has concentrated on optical light curves to quantify variability, spectral energy distributions (ultra-violet to infrared photometry) to measure solid material in the disks, and Hα profiles to study gas kinematics. Building on these, we have obtained optical and near-infrared spectra of moderate resolution for more than two dozen targets, spanning spectral types from B to F and ages from 0.1 Myr to >10 Myr. Quasi-simultaneous spectra covering most of the visible spectrum ($\sim 3900 - 8800$Å) offer a unique perspective on the physics of the gas in the immediate circumstellar environment. A spectral monitoring campaign conducted for a subset of five stars, including four large amplitude photometric variables, has produced the most detailed picture yet available of spectral behavior associated with optical brightness variations. Our near-infrared spectra suggest that hydrogen Brackett emission offers a previously unrecognized evolutionary diagnostic, with possibly better age resolution than the evolution of infrared continuum emission suggested by others.

1.1 *A Brief History of Herbig Ae/Be Stars*

1.1.1 Identification

George Herbig (1960), in a deliberate search for higher mass counterparts to the T Tauri stars, originally identified 26 candidates according to three criteria: 1) Hα emission; 2) early spectral type; and 3) surrounding nebulosity. This work pre-dated infrared (IR) observations of stars, and in particular the Infrared Astronomical Satellite (IRAS) mission, and so the strong continuum emission in the infrared associated with young stars, which is in excess of that expected from a blackbody at the stellar temperature, was not yet known. Nonetheless, the pre-main sequence nature of these objects was confirmed by Strom *et al.* (1972) who placed 14 of them above the main sequence on the H-R diagram. The next complete list of HAEBEs came from Finkenzeller & Mundt (1984) who compiled a list of 54 objects, adding 28 to Herbig's original list. This was the first work to consider the "IR excess" emission, in addition to the original criteria used by Herbig. As a result, a few objects, such as BF Ori, were added to the list based on excess infrared emission and similarity to other HAEBEs, even though they did not light up nearby nebulosity. These are the so-called "isolated" HAEBEs, a group that includes most of the "UXOR" subgroup of HAe stars (see Ch. 2). Although these stars are pre-main sequence and similar in all other respects to classical HAEBEs, it remains an open question how they come to be unencumbered by a nearby star formation region. Did these objects form in isolation? Or did they travel far from their birthplace in a very short time ($\lesssim$1 Myr)?

The most recent attempt to inventory Herbig Ae/Be stars comes from Thé *et al.* (1994), who identify a much more extensive list of 287 candidate objects, including several stars of spectral type F. They use IR excess and spectral type (B – F) as the primary criteria, with Hα emission, nebulosity and variability being optional but noted characteristics. This list is particularly useful for statistical analysis and to extend current studies beyond the small number of "classic" HAEBEs. However, they point out that many of the objects are "candidate" HAEBEs, and in fact the pre-main sequence nature of many in this list is not secure. This list also identifies a number of previously suggested candidates that are confirmed NOT to be Herbig Ae/Be stars.

Despite the success in identifying HAEBEs, the nature of these objects and their circumstellar environments is still controversial. In general, we know they are optically visible (ie, not significantly embedded, although some do have substantial reddening), emit considerable IR excess, presumably from heated circumstellar dust, and lie for the most part close to, but above, the zero-age main sequence (Finkenzeller & Mundt 1984). These are characteristics in common with T Tauri stars. Beyond that, the Herbig Ae/Be stars present a heterogenous group empirically, due at least partly to the wide range in spectral type, which has complicated attempts to pin down their physical nature.

1.1.2 Spectral Energy Distributions and the Evidence for Disks

Since the detection of excess continuum emission in the infrared, much work has been done on the total spectral energy distributions (SED) of young stars, including HAEBEs. Hillenbrand *et al.* (1992) constructed SEDs for 47 HAEBE stars and found that 30 of them ("Group I") exhibited a characteristic shape in the IR, and notably less near-IR excess. This is known as the "2 μm gap" or "3 μm bump" and is not commonly seen in T Tauris. HAEBEs also do not have the classic disk/accretion signatures of T Tauris: they exhibit no detectable excess continuum emission ("veiling") in the optical and UV, and only a few have blue-shifted forbidden emission. They occupy a separate space from T Tauris on a J–H/H–K color-color diagram (Finkenzeller & Mundt 1984). The IR excess has been modeled using a disk with the near-IR dip caused by a physical gap in the disk close to star presumably due to dust sublimation (Hillenbrand *et al.* 1992). However, Harvey (1984) and others have found strong Brackett emission in several HAEBE stars which points to dense, ionized gas very close to the star.

While the presence of disks is well-documented and accepted for T Tauri stars, for HAEBEs it has been more controversial. Modeling of IR excess alone is not sufficient evidence, as other authors have successfully reproduced the continuum emission with more spherical circumstellar dust configurations (Hartmann & Kenyon 1996) or very small grains (Natta *et al.* 1993). Perhaps the most convincing evidence for disks comes from Mannings and Sargent (1997, 2000). By mapping the distribution of CO with submillimeter observa-

tions, they have resolved flattened structures in several HAEBEs, and observed the telltale sign of Keplerian disk motion in a few systems. Natta *et al.* (2000b) provide a summary of the status of disks around these stars. Using the CO flux and a standard gas to dust ratio of 100, they calculate disk masses for 25 systems, and find values between 0.01 and 1 $\mathcal{M}_{\odot}$, comparable to T Tauri disks.

1.1.3 Spectral Characteristics

Spectral investigations of HAEBEs have generally focused either on Hα (Strom *et al.* 1972; Finkenzeller & Mundt 1984), or on one or two specific objects. Notable exceptions include Herbig's original report (1960), Hamann & Persson (1992) in the optical, Grady *et al.* (1996) in the UV, and Harvey (1984) in the near-infrared. These papers have confirmed that HAEBEs are clearly not "normal" main sequence objects. Emission and absorption features due to circumstellar gas are seen to a widely varying degree in all objects. Some features again are similar to T Tauri stars, others are not. Both groups, by definition, show Hα in emission. However, T Tauri stars generally exhibit emission in upper level Balmer lines and metal lines, while HAEBEs often show circumstellar absorption as well as emission in these lines. High resolution spectra help to distinguish between lines from wind material, exhibiting P Cygni profiles, and accreting gas, which form inverse P-Cygni profiles. Both outflow and inflow signatures are seen, although not in all objects (Grady *et al.* 1996). In addition, gas in circumstellar disks and envelopes contribute spectral features. Sorting out the origins of the numerous circumstellar contributions to the spectra is an on-going, and often controversial, exercise.

1.1.4 Optical Variability

Photometric variability is ubiquitious in pre-main sequence stars, and HAEBEs are no exception. Herbst *et al.* (1984) provide a good overview of the different types of variability observed in all young stars. In T Tauris, most of the observed variability is prescribed to either hot or cold spots on the surface of the star associated with accretion. Both HBe and HAe stars commonly exhibit variability of relatively low amplitude, $\Delta V \leq 1.5$ mag, of

unknown origin but possibly similar to the variations exhibited by TTs.

As many as 50% of HAe stars (spectral type A – F) exhibit large amplitude, aperiodic photometric variability not commonly seen in T Tauri stars. This group of objects is discussed in more detail in Chapter 2. The fact that this phenomenon appears to be limited to stars of spectral types A and F must be accounted for in any model to explain their variability. The most common explanation for the brightness variations attributes them to obscuration of the central star by circumstellar dust. However, the nature of the obscuring material is not well-constrained. We shall return to this topic in Chapter 8.

1.2 A Brief History of this Dissertation

This dissertation research has focused on the spectral behavior of Herbig Ae stars, with particular emphasis on multi-epoch observations to examine the variable nature of these stars. Work began in the near-infrared, where we had hoped to learn something about the hot, dense gas close to the star through monitoring hydrogen Brackett lines in the H and K passbands. These data provide original information on the strength of Brackett emission across a wide range of objects, which is discussed in Chapter 6. However, limitations of the instrument, both in resolution and stability, hampered efforts to investigate variability at these wavelengths and precluded kinematic analysis of the gas. For the latter, we began a program to obtain high spectral resolution observations of Brγ line profiles of HAe stars. The initial results of this work are presented in Chapter 7.

At the same time, the monitoring program was redirected into the optical regime. Taking advantage of the short time block scheduling at Apache Point Observatory (APO), we obtained multi-epoch observations covering most of the optical spectrum at moderate resolution, of a handful of HAe stars, specifically 3 strongly varying objects (CQ Tau, RR Tau, UX Ori) and 1 non-varying Ae star (AB Aur). In addition, a larger number of Herbig Ae/Be stars were observed on two epochs. These data are the subject of Chapters 3 – 5. We were particularly successful in the case of RR Tau, where the spectra span nearly 3 magnitudes in V. Through the stability of certain features and the correlated variability of others, these spectra provide strong evidence in support of an obscuration mechanism

for the optical variability, and a unique window into how the circumstellar environment is affected by the occulting material. The analysis of RR Tau is presented in Chapter 4. In Chapter 8, we discuss the evidence for evolution in these data and revisit variations on the obscuration hypothesis for photometric variability in light of these data. Finally, Chapter 9 recaps the main conclusions.

Chapter 2

PHOTOMETRY AND "UXOR" STARS

Herbig Ae/Be stars have been the subject of photometric observations for many years. Many of the stars are bright ($V < 11$ mag) and a number have been known variables since before the class was identified in 1960. The largest collection of HAEBE photometry has been compiled by Herbst and collaborators with UBVRI data on over 80 HAEBEs from various sources (Herbst *et al.* 1984; Herbst & Shevchenko 1999, hereafter, the Wesleyan Database). These data allow detailed analysis of the photometric behavior of a statistically significant sample of these objects. The data confirm characteristics previously identified by others based on much smaller samples and provide the potential for learning more. Another photometric source is the visual observations of the American Association of Variable Star Observers (AAVSO)[1]. These data are contributed by many observers. They generally provide excellent coverage of the target stars, but in a single color ($\sim V$) and with limited accuracy.

In this chapter, the photometric behavior of HAe and HBe stars is reviewed, with particular emphasis on an empirical subgroup of Herbig Ae stars known as "UXORs". In addition, *UBVRI* data for four HAe stars targeted in this dissertation are presented and discussed.

2.1 Herbig Ae and Herbig Be Stars

Herbig Ae/Be stars are a heterogeneous group, which has often complicated attempts to understand their nature. Taken together, their spectral types alone span a range from G0 to B0, or $8000 \leq T_{eff} \leq 30000K$. Several authors have pointed out the differences between Herbig Be stars and Herbig Ae stars (e.g., Natta *et al.* 2000a). HBe stars are significantly hotter than HAe stars and so have much stronger UV flux. They generally have very little

[1]www.aavso.org

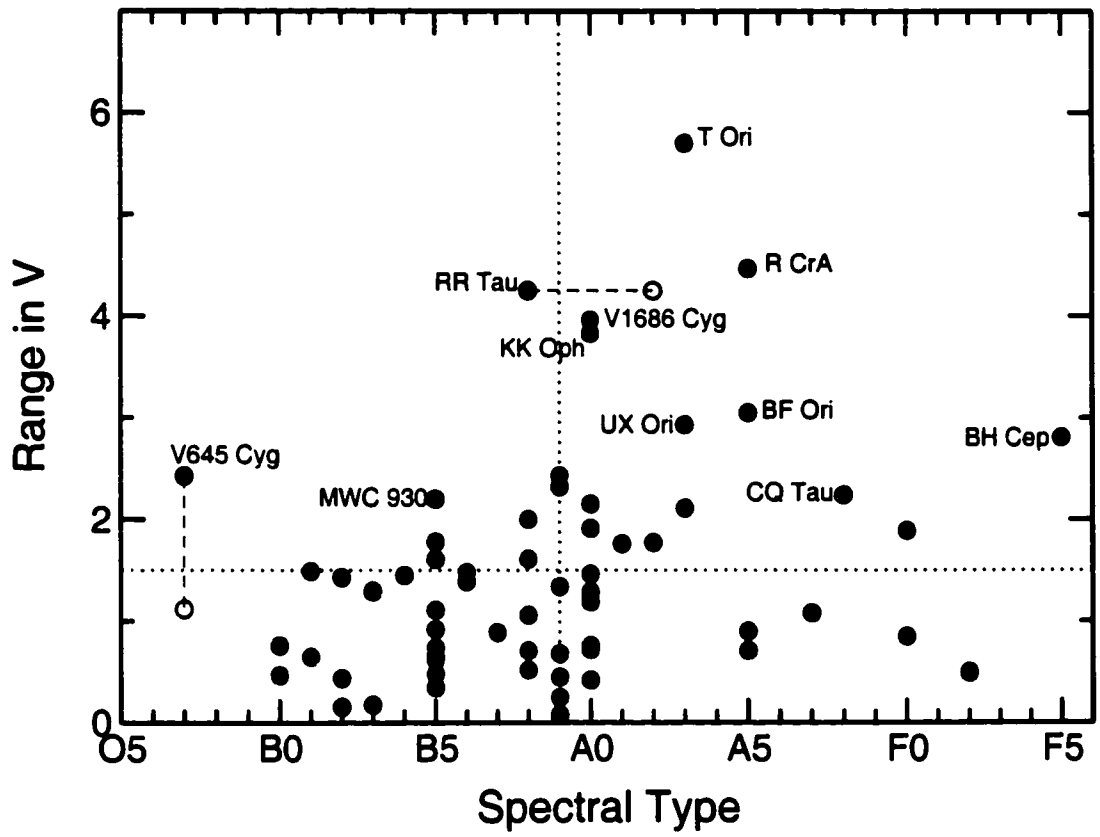

Figure 2.1 Range in V magnitudes versus spectral type for HAEBE stars in Wesleyan database. Sixty-five stars are plotted. Spectral types are from Herbst & Shevchenko (1999). Stars identified as "Be" only have been plotted as B5. Dashed lines and open circles indicate positions of a) V645 Cyg with one datapoint deleted, and b) RR Tau with spectral type A2 as reported here and by others.

excess near-IR emission, and very few HBes show silicate emission in the mid-infrared which is nearly ubiquitous among HAe stars. In addition, the photometric variability of HBe stars is markedly different than that of HAe stars. HBe stars exhibit lower amplitude variability, $\Delta V \leq 1.5$ mag, while all of the large amplitude variables are HAe stars. Low amplitude variables are also seen among the HAes. This was first noted by Finkenzeller & Mundt (1984) based on a fairly small number of data points, but has been borne out subsequently in larger datasets (Bibo & The 1991; Herbst & Shevchenko 1999, Fig. 2.1).

The dependence of V band photometric variability on effective temperature is shown in Figure 2.1. All the Herbig Ae/Be stars from the Wesleyan database for which reliable

spectral types are known are plotted, 65 objects in all. The correlation with spectral type is marked, with a clear distinction between B8 and B9. In Figure 2.2 we plot a histogram of the data from Figure 2.1. In the Wesleyan database, we find 47% (16/34) of HAe stars have $\Delta V \geq 1.5$ magnitudes. Of the HBe stars, 22% (7/31) meet the same criteria. However, we caution that spectral types are often uncertain in HAEBEs, and can vary by a full spectral class or more. The one object with $\Delta V > 4$ mag in the left panel of Fig. 2.2 is RR Tau, which we identify as an early A star in Chapter 4.

The reason for this ΔV dependence on spectral type is not well understood, and must be explained by any quantitative model for the photometric variability. Several qualitative explanations have been put forth elsewhere to account for this phenomenon, which we summarize briefly. HBe stars in general exhibit much less excess IR emission than HAe stars, suggesting they may have significantly less circumstellar dust. The stronger UV radiation fields of HBe stars can photodissociate, or prevent the formation of, dust in the densest circumstellar regions close to the star. The higher luminosities of HBe stars may mask the effects of a variable accretion luminosity in these systems. From a theoretical standpoint, HBe stars have much shorter-lived pre-main sequence lifetimes and therefore are more likely to be on the main sequence by the time they become optically visible. There is also some question whether these higher mass stars have a different formation mechanism than HAe stars, which are probably more similar to the T Tauri class of stars. Thus the correlation between photometric variability and spectral type may not be a strong discriminant between different variability models, although rigorous testing of these suggestions is still needed.

Nevertheless, it is clear that HBe and HAe stars are very different, both empirically and theoretically. In order to effectively compare objects within each group, or consider statistical behavior of many stars together, it is necessary to separate the two. In this work I am primarily interested in the variable nature of intermediate mass young stars and so I will consider only Herbig Ae stars, except where specifically noted.

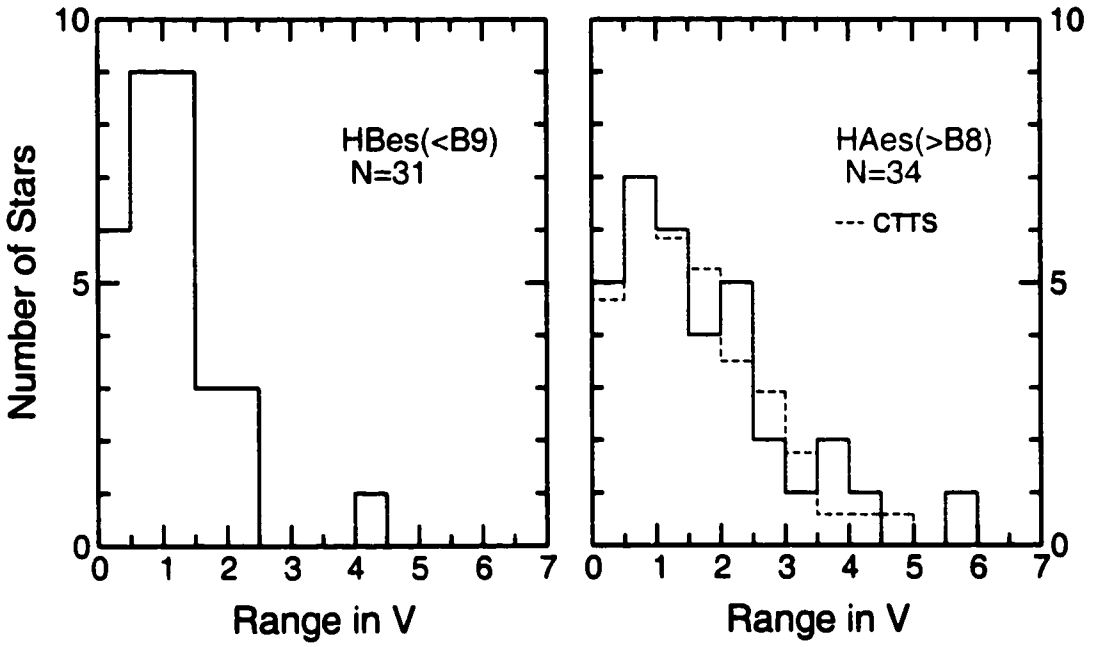

Figure 2.2 Histogram of range in V magnitudes for HBe stars (left) and HAe stars (right). Data and spectral types are as in Figure 2.1. Right panel also shows data for 56 classical T Tauri stars (also from Wesleyan database) for comparison.

2.2 What are UXORs?

A subset of Herbig Ae stars are singled out empirically by their unique photometric and polarimetric behavior. These objects have been named "UXORs", after the prototype of the class, UX Orionis. Given the ubiquitous optical variability of HAEBE stars, and the uncertainty in the nature of the variability, exactly what constitutes a UXOR star is not completely clear. We shall use the following defining characteristics: 1) Large photometric amplitude ($\Delta V > 1.5$); 2) "Blueing effect", in which the stars initially redden as they get fainter but turn bluer at the deepest part of the minima; and 3) Increased polarization during optical minima. We have chosen the cutoff in ΔV somewhat arbitrarily, based on the data in Figure 2.1. Although the polarization behavior is a key piece of evidence in interpreting the variability, it is known for only a small number of objects, ~9 stars (Natta *et al.* 1997). Generally, the first and second characteristics are considered sufficient to identify objects in this group.

Inspection of Figure 2.1 reveals that while no large amplitude variables exist with SpT earlier than B9, the converse is not true. For stars with SpT later than B8, both low and high amplitude variables are common, such that UXORs represent a subset of the Herbig Ae class. Various estimates puts the number of UXORs at ~25 - 30% of Herbig Aes (Natta *et al.* 1993; van den Ancker *et al.* 1998). Given our definition and the data in Figures 2.1 and 2.2, we find the number to be closer to 50%.

The leading theory to explain these variations is variable extinction from dense circumstellar material that obscures the star along our line of sight during minimum light (cf., Grinin 1994). The source of the circumstellar dust varies in different models, from large orbiting clouds, to "clumpy accretion" by infalling comet-like objects, to instabilities in the disk itself that cause it to temporarily "puff up", obscuring the star. These models and their implications are discussed further in Chapter 8. Alternative accretion theories include boundary layer accretion and magnetospheric accretion (popular for low-mass T Tauri stars), both of which assume a more steady state accretion. An excellent review of Herbig Ae/Be and UXORs is given by Natta et al (2000b) in Protostars and Planets IV.

2.3 Photometry of Dissertation Targets

In this dissertation, we shall look specifically at the spectral behavior of 4 stars: AB Aur, CQ Tau, RR Tau, and UX Ori. Three of these are documented UXORs, exhibiting all three characteristics (large ΔV, color reversal and anti-correlated polarization). The fourth, AB Aur, is the prototype Herbig Ae star, a non-UXOR. Its visual magnitude is stable to within ≈0.2 magnitudes.

The long term behavior of these four stars is shown in Figure 2.3, which plots three databases of V magnitude data over time. The photometric stability of AB Aur is apparent, as is the large scatter in the multi-user AAVSO database. CQ Tau is the least well-sampled of our four targets, with only ~ 200 points. UX Ori appears to show a long term periodicity, with deep minima more common during the times of shallow periodic minima. This has been interpreted in terms of large-scale perturbations due to a stellar (or giant planet) companion (Grinin *et al.* 1998).

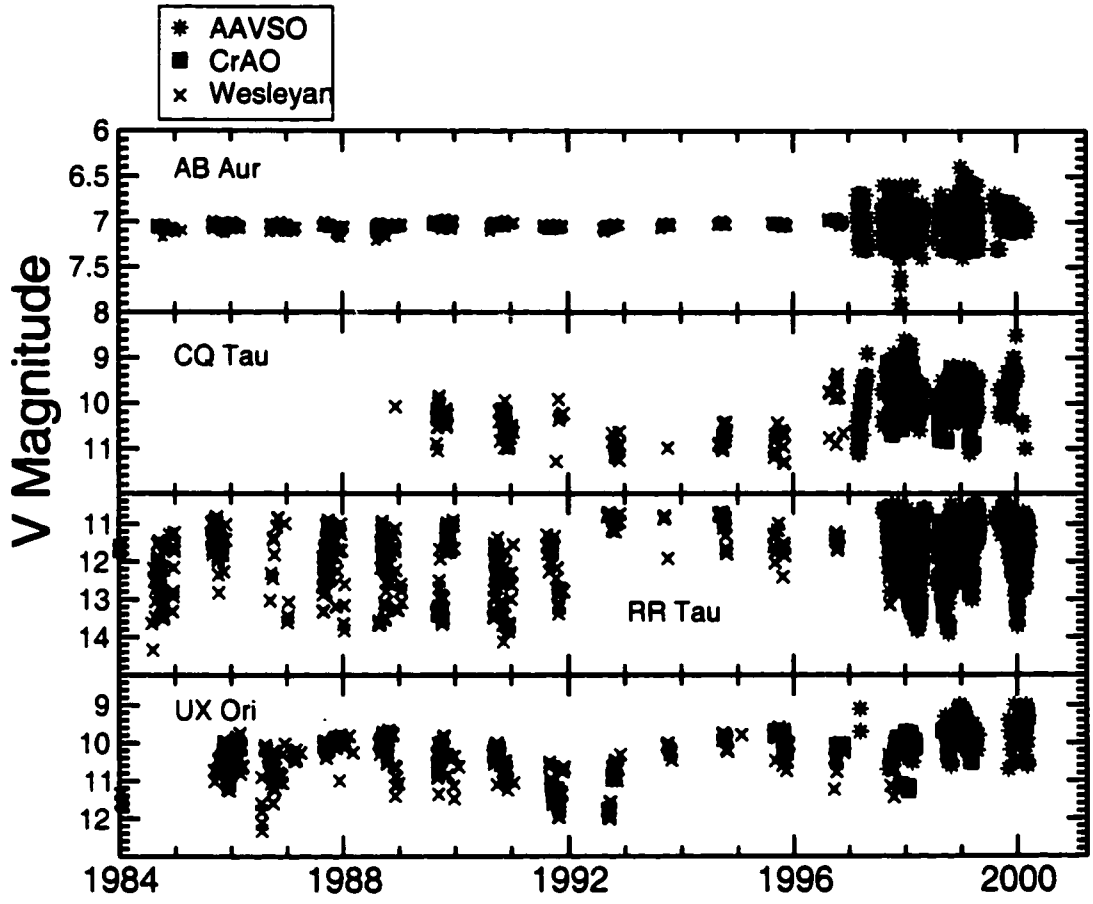

Figure 2.3 V band light curves of four HAe stars, spanning nearly two decades in time. Historical data are from the collected Wesleyan database (crosses), recent data are from Crimean Astrophysical Observatory (squares) and AAVSO (stars).

The color behavior with brightness for the four stars is shown in Figure 2.4. AB Aur has only very small scatter around a single value in each color, while the other stars show strong magnitude-dependent color behavior. The color reversal or blueing phenomenon at deep minimum is clearly seen in all three of the UXORs. This effect is strongest in CQ Tau, although this star does not show as large a range in V as the other two stars.

Although CQ Tau, RR Tau and UX Ori are all UXORs, they are not a homogeneous group. To illustrate the differences in their photometric behavior, histograms of their V magnitudes are plotted in Figure 2.5. UX Ori has a strongly preferred bright state at V = 10.0 with occasional sightings at slightly brighter magnitude and more frequent occurences of

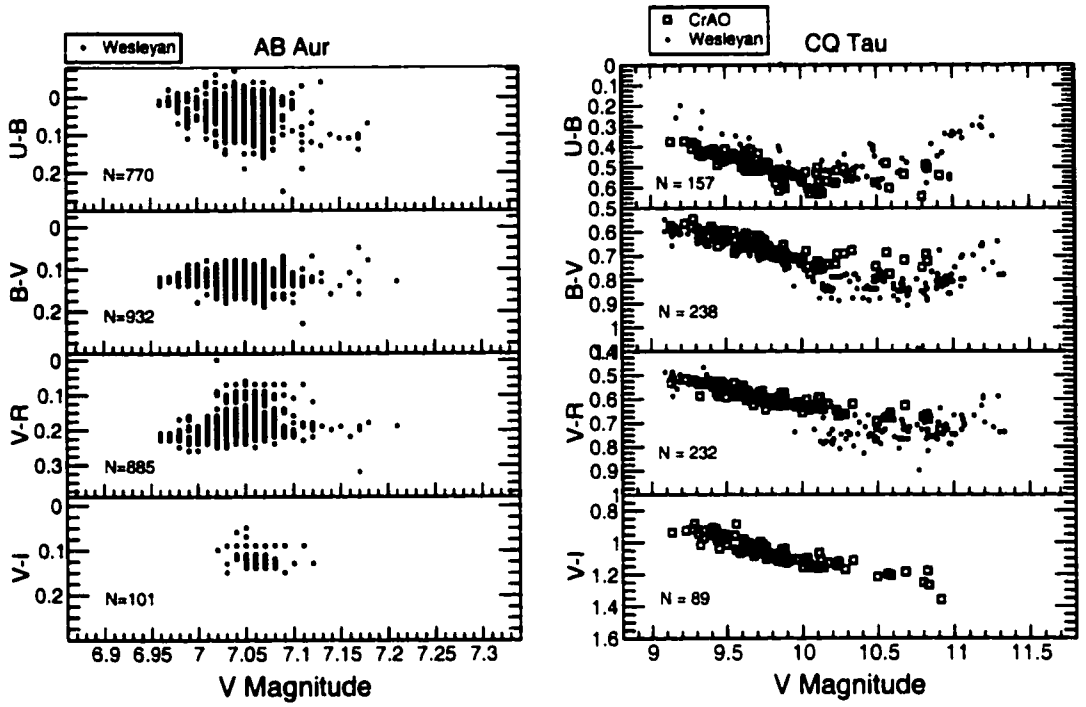

Figure 2.4 Color behavior with V magnitude of AB Aur and CQ Tau.

fainter states. RR Tau exhibits a relatively flat histogram, populating a range of magnitudes nearly equally. CQ Tau may be similar, although the histogram contains significantly fewer points than those of the other 3 stars. The stability of AB Aur is apparent.

2.4 Future Work

A wealth of information remains to be mined from the extensive photometric database of Herbig Ae/Be stars that now exists. Recently, Grinin *et al.* (1998) have reported reliable detections of cyclic behavior in a few UXOR stars, including RR Tau, suggesting binary or multiple systems could explain some of the variability. A recent report by Yudin (2000) explores the connection between polarization and near-infrared excess, finding the two to be strongly correlated for a statistically significant (~400) number of young stars. The Weseleyan database includes $UBVRI$ data for about 80 Herbig Ae/Be stars, offering the potential for statistical analysis. The difference in the variable nature of Herbig Ae and Herbig Be stars is already well documented (see Fig. 2.1). However, further study of the

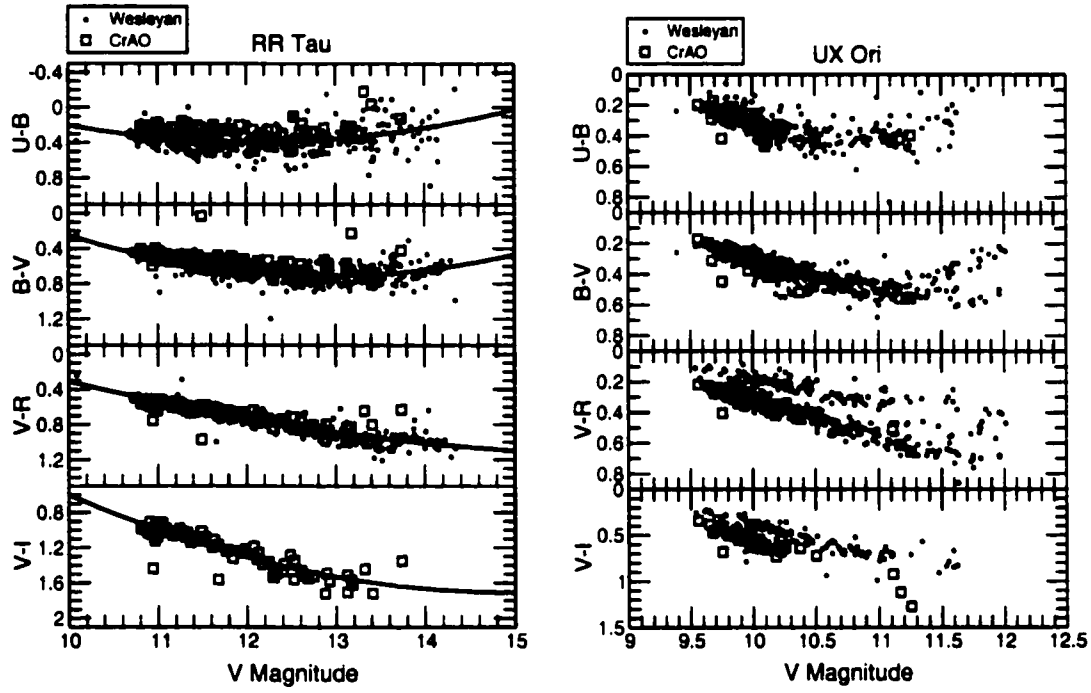

Figure 2.4 (continued) RR Tau and UX Ori.

variable and color behavior among the Herbig Ae stars is warranted. Both low and high amplitude variables are observed. Natta *et al.* (1997) do not find any correlation between ΔV and system age or mass in their Herbig Ae star sample. Among the variables, Bibo *et al.* (1992) distinguish between stars showing reddening only during minima and those that show the "blueing effect" associated with UXORs and find that the second group generally exhibit larger ΔV. Their work is based on a small sample of ~20 stars, and deserves revisiting with the larger Wesleyan dataset.

The nature of individual minima is also an interesting avenue to explore. Most minima are not well-sampled (i.e., >1 day between measurements), but those that are usually show asymmetry into and out of minima, and structure within the minima. Most commonly the objects exhibit a sudden drop in brightness, often recovering to intermediate brightness during minima, and a more gradual recovery to maximum light. These data can place constraints on orbital geometry or physical timescales for variability.

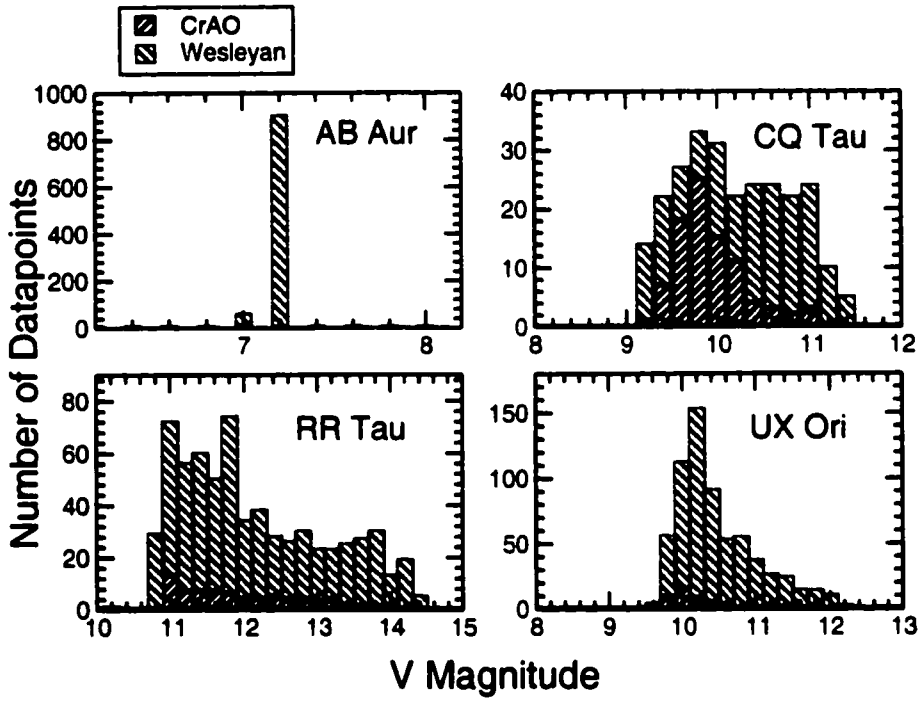

Figure 2.5 Histogram of V magnitudes for AB Aur, CQ Tau, RR Tau, and UX Ori. Datapoints from Wesleyan and CrAO have been combined. AAVSO data is not included due to low accuracy. Note different abcissa values in each plot.

Chapter 3

OPTICAL SPECTRA: SURVEY TARGETS

(Rodgers and Balick, to be submitted)

This chapter describes moderate resolution optical spectra of about two dozen Herbig Ae (and a few Be) stars. Herbig Ae/Be stars are a notoriously heterogeneous class of objects and this dataset reinforces this characterization. Spectra of 26 stars are presented exhibiting a wide range of spectral characteristics. We have divided them into three empirical categories: strong emission line stars, strong Balmer emission and/or peculiar metal line stars, and Hα emission only stars. Even within each category we find notable differences between objects, but there are a number of similar characteristics that justify our categorization. Five of the stars were observed several times to investigate spectral variability. These stars are discussed in detail separately in Chapters 4 and 5.

3.1 Description of Data

3.1.1 Target Selection

The most complete list of Herbig Ae/Be and candidate Herbig Ae/Be stars comes from the tables of Thé *et al.* (1994). To investigate the nature of photometric variability in HAe stars, we selected all objects from Tables 1 – 4 with Right Ascension of 3, 4 or 5 hours and $\Delta V > 1$ mag. There were 18 targets selected by these criteria, and we obtained spectra of 14 of them. Five more large amplitude variables ($\Delta V > 1$) were added, one from Table 5 (MR Ori), and four outside the initial RA limits. Spectra of six other HAe (and one HBe) stars with $\Delta V < 1$ mag were obtained for comparison. The only low mass star in the sample, DG Tau, was observed as part of another project (Wooden *et al.* 2001).

Table 3.1 presents a complete list of the targets and the dates of observations. Other information provided is spectral type, amplitude of photometric variability (ΔV), age and

comments about the target. Values for ΔV are taken from either Thé *et al.* (1994) or Herbst & Shevchenko (1999). Ages are from Natta *et al.* (1998) or Rostopchina (1999) in the case of UXOR stars. Under the comments we have listed identifying remarks from the literature, not from our own data. The majority of the targets are early A stars, with two stars earlier than B9 (MWC1080 and HD45677), three F/G stars (CQ Tau, RY Ori, and CO Ori) and one T Tauri star (DG Tau). Of the 20 HAe stars, six have small amplitude variability ($\Delta V < 1$), five are known UXORS (large ΔV and corresponding polarimetric and color variations, see Ch. 2), seven have $\Delta V > 1$, according to Thé *et al.* (1994), and the remaining two have unknown ΔV. Two of the Fe stars (CQ Tau and RY Ori) are also known UXORs.

3.1.2 Observations

The optical spectra presented in this dissertation (here and in the next two chapters) were obtained at the Apache Point Observatory (APO) 3.5m telescope located in Sunspot, New Mexico, using the Dual Imaging Spectrograph (DIS), between October 1997 and March 1999. This instrument employs a dichroic to split the beam simultaneously onto blue and red CCD chips. In this way we observed Hα and Hβ, as well as nearby features, in one integration. On most nights we also used a second pair of grating positions to observe both bluer and redder bandpasses encompassing higher Balmer lines and the CaII H&K lines in the blue, and Paschen and CaII infrared triplet (CaII-IRT) lines in the red. Each target was observed at two positions along the slit to improve signal-to-noise. In high resolution mode using the 1.2″ slit, the dispersion is 1.6Å/pixel for the blue chip and 1.3Å/pixel for the red. This corresponds to a two-pixel resolution of $\lambda/\Delta\lambda \approx 1500$ (200 km s^{-1}) at Hβ and $\lambda/\Delta\lambda \approx 2500$ (120 km s^{-1}) at Hα respectively.

There were two aspects to this observing program: a monitoring program to observe variability in a small number of objects and a survey program to obtain similar spectra of a range of HAEBEs. The monitoring program consisted of five objects which are discussed individually in Chapters 4 and 5. The 22 survey targets were observed mostly during two runs on 19OCT97UT and 20NOV97UT, with additional observations at various dates

Table 3.1. APO Dual Imaging Spectrograph Observations of Survey Targets

Object	Spec.Type	Epochs [UT]	ΔV	Age[Myr]	Comments
AB Aur	A0	see Chapter 5	.25 H	3	outflow
BF Ori	A5	19OCT97,20NOV97 24Feb98	3.0 H	2.3	UXOR, isolated
CO Ori	G5	see Ch. 5	3.5 T	0.5	vis.binary
CQ Tau	F2	see Ch. 5	2.2 H,T	10	UXOR
DG Tau	K/M	04JAN99,25MAR99			T Tauri star w/jet
HD 34282	A0V	19OCT97,20NOV97	1.5 T	1	
HD 35187	A2/3	19OCT97,20NOV97			
HD 45677	B3	25MAR98	1.3 T		
HD250550	B9/A0eq	19OCT97,20NOV97	.4 T		outflow
HK Ori	A5	19OCT97,20NOV97 07FEB98	.71 H	6	
IP Per	A3e	19OCT97,20NOV97	1.1 T		
LkHa 208	B5/F0V	19OCT97,20NOV97	.85 H	7	
MR Ori	A2V	19OCT97,20NOV97	1.7 T		non-emission star
MWC 480	A2/3ep	29MAR99,31MAR99		6	
MWC 1080	B0	22JUN97	.76 H		outflow
RR Tau	A0/2	see Ch. 4	4.25 H	3	UXOR
RY Ori	F6/8ep	19OCT97,20NOV97	3.1 T		UXOR[a]
T Ori	A3/5e	19OCT97,20NOV97	3.9 T	0.1	
UX Ori	A2/3	see Ch. 5	2.93 H	4	UXOR
V346 Ori	A5III	19OCT97	2.0 T		
V350 Ori	A0e	19OCT97	1.7 T		
V351 Ori	A7	19OCT97	<1		
V380 Ori	B8/A1e	19OCT97,20NOV97	.85 T	1	outflow
V586 Ori	A2Ve	04JAN99,06MAR99	1.5 T		
VV Ser	B1/9e	22JUN97	1.9 H	5	UXOR
WW Vul	A0/3Ve	22JUN97	2.15 H	4	UXOR
XY Per	B6+A5	19OCT97,20NOV97 17JAN98	1.8 T		vis.binary

Note. — ΔV from Herbst & Shevchenko (1999; "H") or Thé *et al.* (1994; "T"). Ages are from Natta *et al.* (1992), except stars noted as "UXOR" for which ages come from Rostopchina (1999).

[a]Bibo & Thé (1991), Yudin (2000)

between June 1997 and Mar 1999. The observing epochs are listed with the targets in Table 3.1.

3.1.3 Data Reduction

Standard data reduction (bias subtraction, flat-fielding, cleaning and spectral extraction) was performed with IRAF[1]. Spectra of arc lamps obtained during each night of observing were used to determine the dispersion solution. Once wavelength-calibrated, multiple spectra of each target (from a given night) were combined. If a flux standard was available, the data were flux-calibrated and then normalized, otherwise they were simply normalized. Normalization was achieved by fitting a low (4th or 5th) order Legendre polynomial to the continuum, excluding emission and absorption features. This procedure over-compensates for broad, weak absorption features, which can introduce a small, wavelength-dependent error in the normalized continuum level. We estimate this error to be $< 5\%$ for the lines of interest in this discussion.

No flats were obtained on 22 June 97 UT and so both spurious and broad features should be considered suspect in the three objects observed that night (MWC 1080, VV Ser, and WW Vul). They are included only for comparison of the prominent features that they have in common with other objects.

3.2 Spectral Characterization

The 27 objects in this sample exhibit a wide range of spectral characteristics, only some of which are attributable to their spectral types. For convenience in this discussion, we have divided the objects into three empirical categories:

1. Strong emission line objects: AB Aur, DG Tau, HD 45677, HD 250550, HK Ori, MWC 1080, MWC 480 and V380 Ori;

---

[1]IRAF is distributed by the National Optical Astronomy Observatories, which are operated by the Association of Universities for Research in Astronomy, Inc., under contract with the National Science Foundation.

2. Peculiar metal lines: BF Ori, LkHα 208, RR Tau, T Ori, UX Ori, V586 Ori, VV Ser, WW Vul, and XY Per;

3. Emission apparent at Hα only: CQ Tau, HD 34282, HD 35187, IP Per, RY Ori, V346 Ori, V350 Ori, and V351 Ori.

One object, MR Ori, exhibits no emission lines at all. It does show a few peculiar narrow absorption lines, attributable to the large nebulosity in which it is embedded. However, the rest of the spectrum looks like a normal main sequence A2 star, and will not be discussed further here. The G star CO Ori is a known binary with a variable primary star and has often been categorized as a UXOR. Our spectra show that the emission lines in this system are associated with the secondary star. This star is discussed further in Chapter 5.

The assignment of objects to each category has been done subjectively, and a few objects are borderline between the categories. However, there are a number of similarities between the targets in each group. The targets which have been identified as outflow sources, including both HBe stars and the T Tauri star, all fall in the first category. Four of the seven known UXOR stars are in the second category, primarily because of the peculiar metal lines exhibited in their spectra. The last category includes the two late type UXOR stars, CQ Tau and RY Ori. Each category is discussed in detail below.

In most cases we have observed each survey target at least twice, however, with the exception of Hα, we found very little evidence of variability between epochs. We present one spectrum of each star here which is either the highest S/N observation, or an average of multiple dates to improve S/N. We have included the four monitoring targets (AB Aur, CQ Tau, RR Tau, UX Ori) in the categories and present a single epoch of each star in the figures. Only RR Tau exhibited dramatic variations in these spectra, and the spectrum presented represents the more common "bright state" of the star (see Ch. 4). For the other three, the spectrum shown is representative of all of the spectra obtained by us.

3.2.1 Strong Emission Line Objects

This group includes the only HBe stars in our sample, HD 45677 and MWC 1080 (Fig. 3.1a), the T Tauri star DG Tau and the only strong emission HAe star V380 Ori (Fig. 3.1b). The

other HAe stars included in this group are the four weaker emission stars shown in Figure 3.1c.

HD 45677 exhibits very strong Paschen emission, and permitted and forbidden OI (at 8446Å and 6300Å, respectively). The latter is indicative of a low density outflow region. CaII is absent from its spectrum. Balmer emission is apparent through Hγ but is very weak or absent in higher Balmer lines. This is in sharp contrast with the hydrogen emission in the far-red, where both Paschen and Brackett (see Ch. 6) emission is seen to at least Pa21 and Br17 respectively, indicating a large HII region around the star. The discrepancy between these lines and the Balmer lines may be a result of the much stronger blue continuum relative to the red in this hot star, such that the circumstellar component of the upper level Balmer lines does not stand out above the stellar continuum.

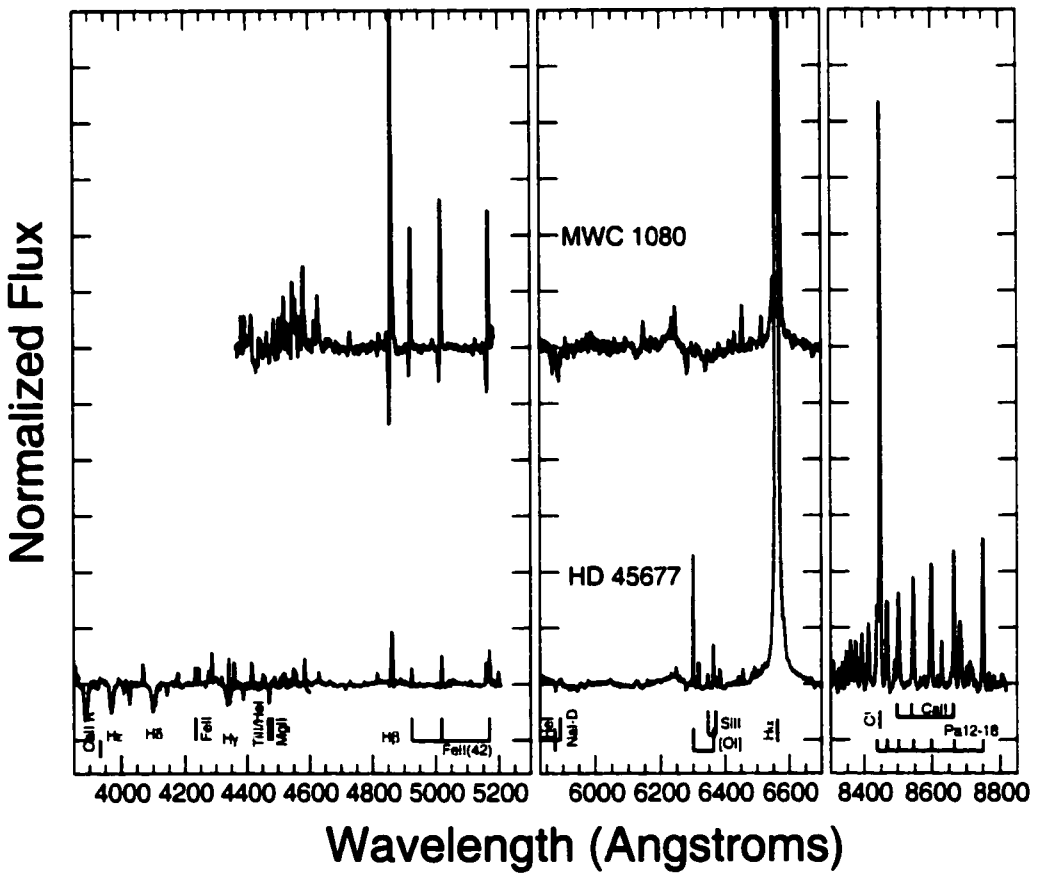

Figure 3.1a DIS spectra of two early B strong emission line stars: MWC 1080 and HD 45677.

Forbidden [OI] is not seen in MWC1080, however P-Cygni profiles are clearly seen in Hβ and in the FeII(42) triplet lines, and an absorption dip that does not reach below the continuum is seen in the blue shoulder of Hα. The velocities of these blue dips are ~400 km s^{-1} in each case, indicating a fast outflow and a common origin for the Balmer and FeII(42) triplet lines. HeI 5876Å is seen in absorption in both Be stars.

The T Tauri star DG Tau is a well-known outflow source. Its spectrum also exhibits [OI] as well as pronounced Balmer, FeII and CaII emission. All the lines appear singly-peaked with no evidence of P-Cygni profiles. The stronger Balmer emission relative to Paschen emission in this cool star is the opposite effect seen in HD 45677, and may also be due to the relative continuum levels. The HeI line and the OI 8446Å lines are seen weakly in emission, but notably absent in emission are the NaI D lines.

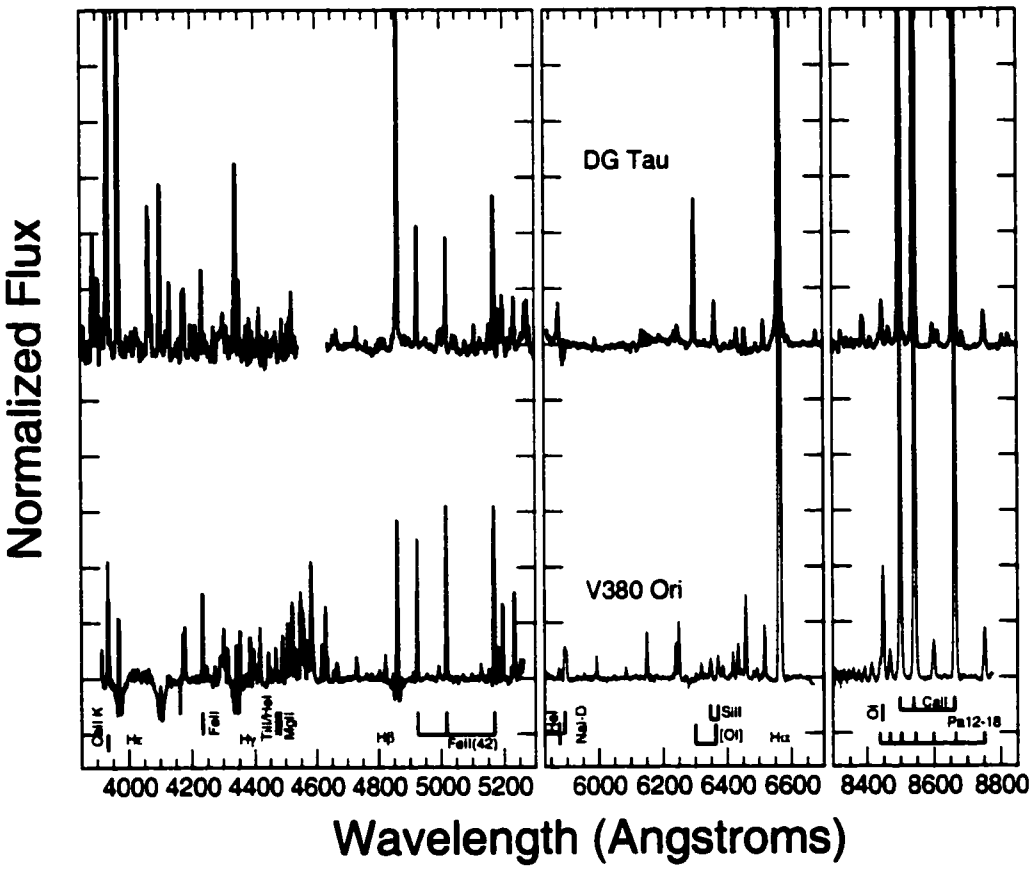

Figure 3.1b Strong emission line objects DG Tau, a T Tauri star, and V380 Ori, an HAe star.

V380 Ori is an interesting emission line star. It is the only HAe star among the strong emission line objects. The only absorption features seen in this spectrum are the wings of Hβ - Hϵ, which identify it as an early A star. However its emission spectrum is similar to DG Tau in the strong CaII, FeII and Balmer emission. In addition HeI and NaI are in emission. Although this star has been identified as an outflow source (Hamann & Persson 1992), it does not exhibit [OI] or P-Cygni profiles.

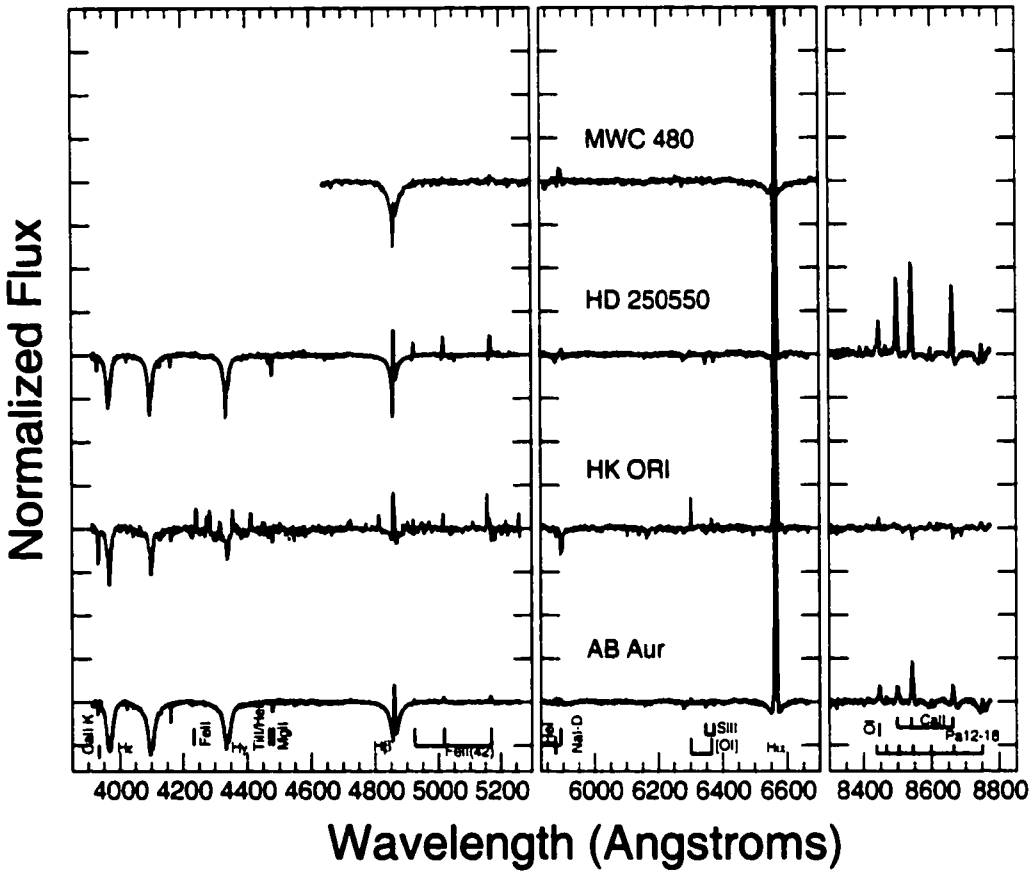

Figure 3.1c HAe stars with metal emission: AB Aur, HK Ori, HD 250550 and MWC 480.

The four Ae stars shown in Figure 3.1c are borderline members of the emission group. They are included because each shows emission to varying degree in the core of Hβ and in the FeII(42) triplet. [OI] is apparent in HK Ori and marginally detected in AB Aur and HD 250550. These three show filled in Paschen lines, and AB Aur and HD 250550 have CaII IR triplet lines in emission. All but HK Ori also exhibit Na I emission, while HK Ori is the

only one with [FeII] lines. Finally, the Hα and Hβ lines of MWC480 and HD 250550 are P Cygni, as is the FeII(42) triplet lines in the latter.

Seven of the eight stars in this group show evidence for outflow, either through [OI] emission from a low density wind, or P Cygni profiles in the Balmer and FeII(42) triplet lines. V380 Ori is unique among the A stars in the complexity of its emission spectrum, and similarities between it and DG Tau suggest that a search for a low mass YSO companion to V380 Ori may be warranted.

3.2.2 Peculiar Metal Line Objects

The combination of broad, pronounced Balmer absorption, appropriate to early A stars, and significant metal absorption lines, distinguishes this group of Ae stars, shown in Figure 3.2. The spectral types of these stars range from late B to mid-A, and so the presence of strong metal absorption lines is inconsistent with their spectral types. All of the stars show strong absorption in the FeII(42) triplet lines, and the five for which we have blue spectra also show enhanced absorption (for their spectral types) in CaII K and in a number of primarily FeII lines between 4200 and 4600Å. BF Ori is the extreme example of this: the metal absorption lines in this star are deeper than observed in CQ Tau and RY Ori (see Fig. 3.3b), both of which are approximately one spectral class cooler.

These stars exhibit moderate Hα line strengths, with the exception of VV Ser which has EW(Hα) $\sim$ -50Å. In seven of the eight stars the Hα line is double-peaked and evidence of emission and added absorption are apparent in the Hβ line. LkHα 208 is the exception. The CaII IR triplet lines in RR Tau, UX Ori, and BF Ori show weak emission in an inverse P Cygni profile with enhanced absorption, indicating infalling gas. All five stars with available data show approximately photospheric hydrogen absorption in the upper level Paschen and Balmer lines. Unlike the first group of emission stars, none of these objects exhibit HeI or NaI in emission and only RR Tau emits a weak [OI] line indicating an outflow.

This group includes all five HAe UXOR stars. V586 Ori is listed as an "algol-minima" star (aka UXOR) by Yudin (2000), but shows smaller percent increase in polarization ($\sim$ 2% versus 5–6% for the other stars and 10% for VV Ser) and also does not exhibit color reversal

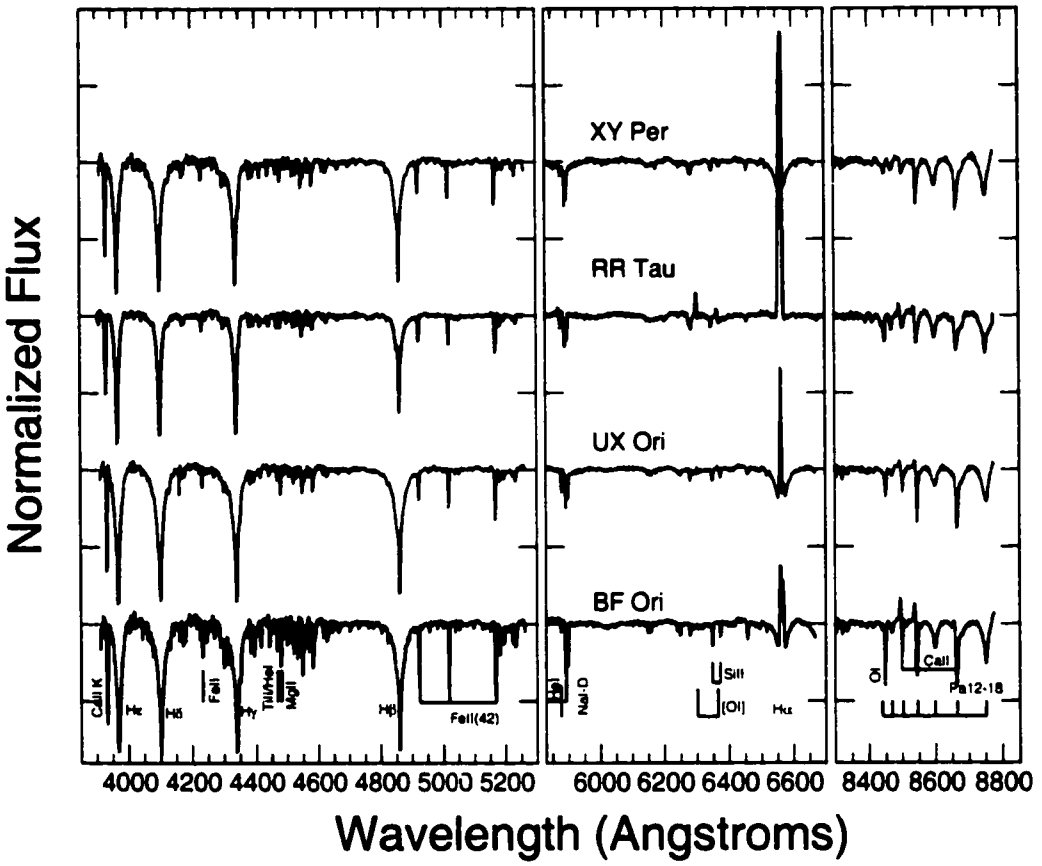

Figure 3.2a DIS spectra of peculiar metal line stars: BF Ori, UX Ori, RR Tau and XY Per. These stars show absorption features abnormal for their spectral type: notably in the FeII(42) triplet, NaI D and CaII IR triplet lines, and enhanced Balmer shell absorption. BF Ori is an extreme example with strong absorption in the blue.

in $B-V$. The other two stars in this group are relatively low amplitude variables: LkHα 208 and XY Per. LkHα 208 appears to be unique among this group, exhibiting weaker and singly-peaked Hα, and virtually no circumstellar component to the Hβ line. XY Per is a visual binary. The spectrum shown is the combined light from the A6 and B5 stellar components. However, the strengths of the metal lines are unusual, even for an A6 star.

It should be noted that UXOR stars are highly variable, both photometrically and spectroscopically. We have information on system brightness only for RR Tau, the subject of the next chapter. For this star we know that the FeII(42) triplet and CaII IR triplet lines can switch from absorption to emission, in conjunction with photometric minima. We have

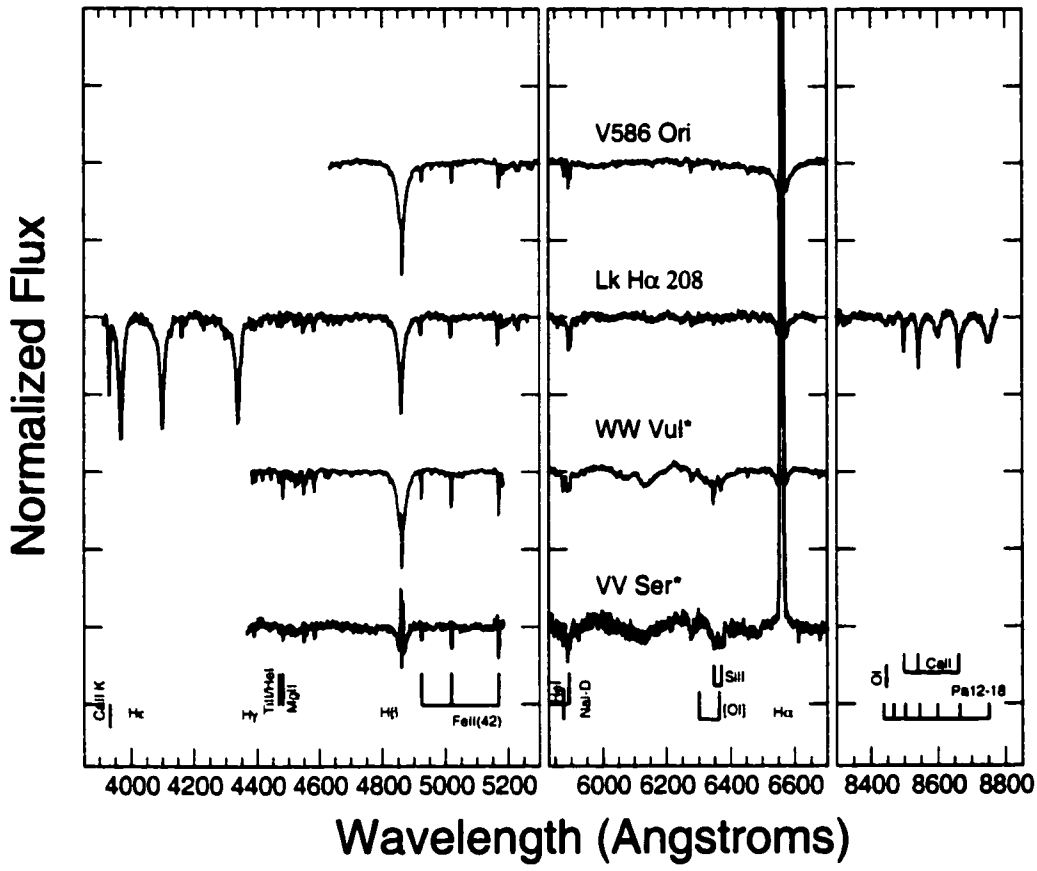

Figure 3.2b Peculiar metal line stars: VV Ser, WW Vul, Lk Hα 208 and V586 Ori. The uneven continua of the stars marked with "*" are due to poor data reduction.

shown here a typical spectrum of this star in its bright state; in its faintest state, we would have placed RR Tau in the first category of emission line stars.

3.2.3 Hα Emission Only Objects

The remaining 9 stars in our sample exhibit emission at Hα only, and show metal line absorption roughly consistent with their spectral types. The early A stars are shown in Figure 3.3a. They exhibit strong upper level Balmer absorption and weak metal absorption lines. Hα emission strength is greatest in IP Per and T Ori, relatively weak in HD 35187 and HD 34282. The latter two stars have been identified as "young Vega-like" stars (Sylvester *et al.* 1996), suggesting a later evolutionary state. T Ori is a large ΔV star, but

does not exhibit strong increases in polarization or color reversal in $B-V$.

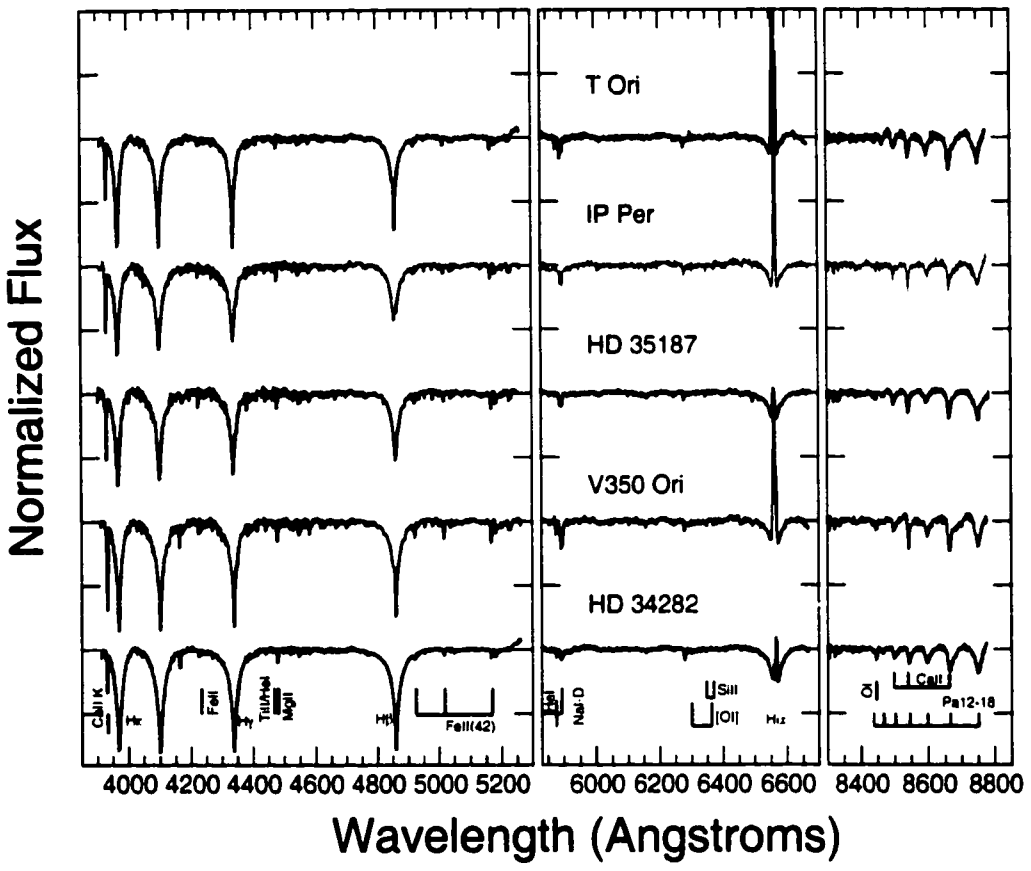

Figure 3.3a DIS spectra of Hα emission only stars. These stars show essentially photospheric spectra with the exception of Hα emission, and in some cases, slight Hβ emission in the core.

The four stars plotted in Figure 3.3b are late A and early F stars, and correspondingly show significantly more metal absorption features. RY Ori is an ~F6 star that is reported to be a UXOR by Yudin (2000), with variable polarization of 4.8 % (comparable to other UXOR stars). CQ Tau, an F2 star, is also a known UXOR. Both stars exhibit circumstellar Hα emission with inverse P Cygni profiles, indicating accretion. Little, if any, excess emission or absorption is apparent in CaII, FeII, or the higher Balmer or Paschen lines. RY Ori shows He I 5876 Å line in absorption which must be circumstellar, and the same line is barely detected in CQ Tau. The other two stars in Figure 3.3b are late A stars with double-peaked circumstellar Hα emission barely detectable in the photospheric absorption lines.

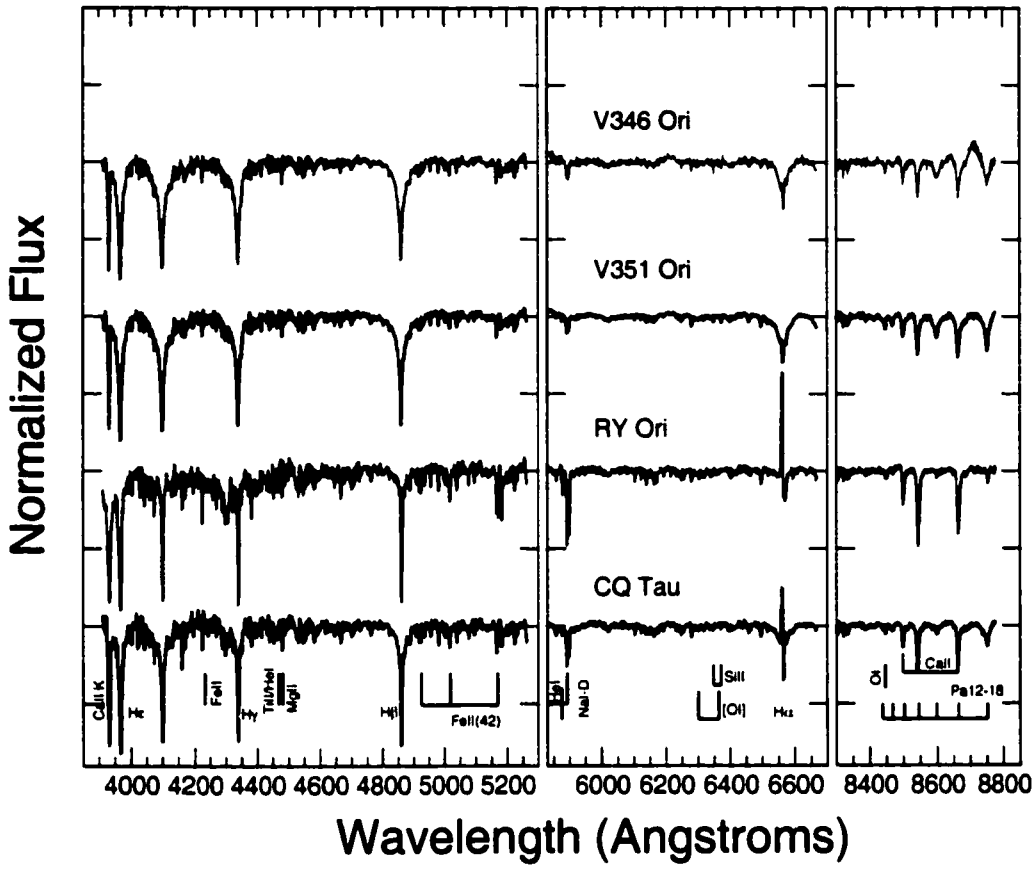

Figure 3.3b Hα emission only stars. The bottom two: RY Ori and CQ Tau are spectral type F stars and so have much stronger metal absorption lines.

3.3 Discussion

3.3.1 Comparison to previous observations

Spectra of most of these stars have been reported in the literature, in some cases as far back as Herbig (1960) or even before. Usually, the reports focus on a few specific lines such as Hα, [OI] or NaI D. In comparing our spectra with Herbig (1960), Finkenzeller & Mundt (1984) and Hamann & Perrson (1992), we find the overall spectral behavior of most of the stars to be consistent over these decades-long timescales. Although the strength of Hα is variable in most, if not all, of the objects, the overall line profile remains the same. This is true of the emission stars and, although less information is available, probably also the "Hα

only" stars. The exception is the UXOR stars in the second group. Many spectral features have been observed in common in these widely seperated observations, including Hα profile and metal emission/absorption behavior, suggesting a preferred state of the star. However, detailed monitoring has shown that individual lines can change dramatically on daily, and possibly even shorter, timescales. This has been shown for UX Ori (Grinin *et al.*1994), BF Ori (De Winter *et al.* 1999), RY Tau (Holtzman *et al.* 1986), and RR Tau (Chapter 4).

3.3.2 Correlations

Having divided the stars into three categories based on their optical spectra, we now consider other system characteristics listed in Table 3.1. Figure 3.4 plots histograms of the three categories against spectral type, range in V, and age estimates, taken from the literature. We see some tendency for the stars to separate into categories by spectral type, with category I (strong emission) stars of earlier type and category III (Hα only) stars later type. But there is a mix among the Ae stars, where all but one of the category II (peculiar metal lines) stars lies. The low ΔV of cat. I stars is clearly seen in the middle panel, which can only partially be accounted for by the early spectral types of two stars in this group. The other two categories are mixed against δV. We had anticipated an evolutionary sequence from Category I to II to III, but no clear trend is seen with age (right panel). While age estimates are not available for all objects, even in this small sample the Category I and III objects are scattered across the range. However Cat. II stars, which are all HAe stars and most of the UXOR stars, span a small range of ages, roughly 2–7 Myrs. We shall return to this point in Chapters 6 and 8.

Natta *et al.* (1997) find no correlation between ΔV and age, suggesting that the UXOR phenomenon is not an evolutionary effect but rather a geometric one where the UXOR stars are viewed nearly edge-on through their disks. Our data suggest that the UXOR stars do separate themselves in the strength of their circumstellar metal absorption, however, some low amplitude variables exhibit similar behavior. Unfortunately, the small number of low ΔV stars in this sample is not statistically significant. Two fall in each of the three categories defined here. For those stars with $\Delta V > 1$ mag, seven are known UXORs and

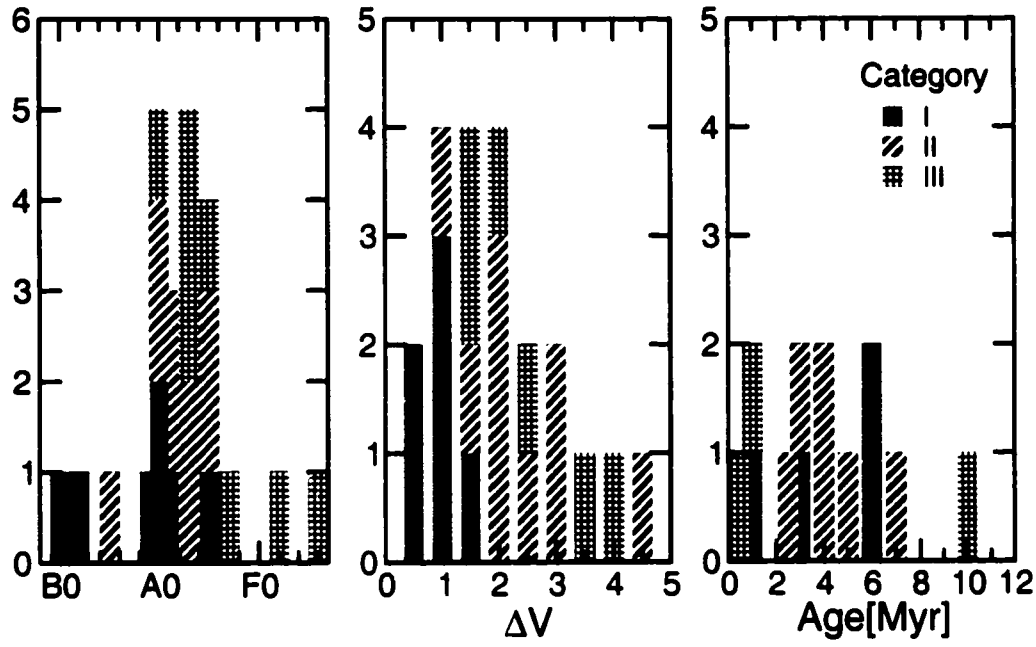

Figure 3.4 Histograms of Spectral Groups vs. Spectral Type, ΔV, Age. Age estimates are not available for all objects.

seven are not. Of these, five UXORs fall in Category II, and five non-UXOR variables fall in Category III.

Chapter 4

SPECTRAL VARIABILITY I.: RR TAU

Rodgers, Wooden, Grinin, Shakhovsky and Natta, **ApJ**, *submitted*

4.1 Summary

We present moderate resolution optical spectra of the highly variable Herbig Ae star RR Tau over 12 epochs spanning $\sim$ 2.5 magnitudes in V. Combining normalized spectra with contemporaneous photometry from two databases, we analyze both equivalent width and flux behavior as a function of system brightness for lines from the CaII K line in the blue to the Paschen lines in the far-red. The wings (Δv > 400 km s^{-1}) of the Balmer lines and the equivalent widths of several weak metal lines are essentially constant, indicating very little change in the underlying photosphere over a factor of ten change in brightness. We detect no measurable change in spectral type. Variability is apparent in the cores of Hα and Hβ, but the total flux in these lines is not correlated with photometric variability. Forbidden oxygen ([OI]6300Å) has essentially constant flux, indicating a stable low density wind component. The low-ionization permitted lines of FeII, CaII, OI, and NaI are seen strongly in absorption for $V \leq$ 12.2 in these normalized spectra, but change dramatically from absorption to emission during deep minima ($V \gtrsim$ 12.6). Analysis of the FeII(42) triplet indicates that these lines originate in circumstellar gas which is partially affected by the photometric minima, in that the opacity of the absorbing gas remains constant with the changing stellar continuum (conserving equivalent width) while a weak emitting region is unaffected (roughly constant flux). Our results are consistent with a model in which the stellar minima are caused by an occulting screen of size such that it obscures the stellar surface and the innermost region of circumstellar gas producing permitted metal absorption

lines, but not the outer parts, or the wind. The circumstellar hydrogen, while variable, is not strongly affected by the occultations.

4.2 *Introduction*

RR Tauri is an intermediate mass young star, a member of the original Herbig Ae/Be (or HAEBE) class of stars (Herbig 1960). Its pre-main sequence status was confirmed by Strom *et al.* (1972) who placed it above the main sequence on the H-R diagram based on analysis of the wings of the Balmer lines. Like other pre-main sequence stars, it has significant excess infrared emission indicative of a substantial circumstellar environment (e.g., Hillenbrand *et al.* 1992). As noted by Herbig (1960) and others, RR Tau is highly optically variable on timescales as short as a day, with photometric variability of up to 3 magnitudes ($11 \lesssim V \lesssim 14$) observed every year since 1980 (Herbst & Shevchenko 1999). As the star fades, it becomes redder in its $B-V$ and $V-R$ colors, but at deepest minima the $B-V$ color reverses, becoming bluer for $V \gtrsim 13$. Photopolarimetric measurements show sharp increases in the percentage of linearly polarized light during photometric minima, with a wavelength dependence such that stronger polarization is seen at shorter wavelengths (Rostopchina *et al.* 1997). These characteristics: large, aperiodic optical minima, reddening followed by a blueing at deepest minima, and anti-correlated polarization, place RR Tau firmly in the so-called "UXOR" sub-class of Herbig Ae/Be stars, after the prototype UX Ori (Herbst *et al.* 1984).

While extensive photometric monitoring of UXORs has been done, relatively few reports of spectroscopic monitoring exist. Those that do show dramatic spectral variability, either linked to photometric variations (Eaton & Herbst 1995; Grinin *et al.* 1994; Holtzman *et al.* 1986) or not (Natta *et al.* 2000a; de Winter *et al.* 1999; Graham 1992). The HAEBE star AB Aur exhibits variable spectral features on timescales of hours (Catala *et al.* 1999, 1997; Böhm *et al.* 1996). This star does not currently show large amplitude photometric variability, and so is not included in the UXOR class. Except for the initial work by Herbig (1960), spectra of RR Tau reported in the literature generally consist of single epoch observations, primarily focusing on Hα (e.g., Finkenzeller 1985; Finkenzeller & Mundt 1984).

We have conducted a spectroscopic monitoring program of several UXOR and non-UXOR Herbig Ae/Be stars. Here we present the results for the UXOR star RR Tau, for which we have obtained spectra at 12 epochs spanning more than an order of magnitude in optical brightness. Section 4.3 describes the relevant observations and data reduction, and section 4.4 presents the spectra. In section 4.5 we highlight the behavior of several features, including the hydrogen Balmer and Paschen lines, forbidden [OI], and permitted lines of FeII, CaII, HeI, and NaI. Section 4.6 discusses the implications of these data in the context of the photometric variability models and section 4.7 summarizes our conclusions.

4.3 Data

4.3.1 Spectroscopy

The details of the spectral observations and data reduction procedure are provided in Chapter 3. For the monitoring program, many of the observations were obtained under a short time block scheduling program at APO, often utilizing just an hour of telescope time per night. Because of this, flux standard stars were not obtained every night and no attempt has been made to flux calibrate the data. A log of the observations and the estimated V magnitude at each spectral epoch (discussed below) are provided in Table 4.1. Throughout the text we designate each epoch by its UT date, e.g., 25MAR98 is 25 MARCH 1998 UT. In addition to the data reduction steps described in the previous chapter, the IRAF tasks *fxcor* and *specshift* were used to correlate telluric features on multiple nights in order to adjust all spectra to a common heliocentric velocity.

4.3.2 Photometry

Photo-polarimetric UBVRI observations over the same period were obtained at the Crimean Astrophysical Observatory (CrAO), as part of the on-going monitoring program being conducted there. This program is described in Grinin *et al.* (1991). Because of the rapid variability of RR Tau, we require photometric observations within $\sim$1 day of the spectral observations to reliably estimate the visual magnitude. Despite efforts to coordinate our programs, simultaneous spectral and photometric observations were made on only a few oc-

Table 4.1. Apache Point DIS Observations of RR Tau

Date (UT)	Jul.Date (JD−2.4 × 10^6)	V[a] Magnitude	N[b]	Δt[c] (days)	Designation
19OCT1997	50740.85	10.9±0.3	1	0.71	11a
20NOV1997	50772.84	11.1±0.2	4	0.29	11e
15JAN1998	50828.61	11.0±0.1	4[d]	0.11	11b
14FEB1998	50858.60	12.6±0.3	6	0.26	12c
24FEB1998	50868.61	12.2±0.3	6[d]	0.11	12b
05MAR1998	50877.60	13.4±0.3	1	0.30	13b
10MAR1998	50882.63	12.0±0.3	1	0.33	12a
12MAR1998	50884.64	13.2±0.1	2	0.30	13a
25MAR1998	50897.64	13.7±0.2	2	0.08	13c
01FEB1999	51210.60	11.0±0.1	2	0.28	11c
25MAR1999	51262.61	11.0±0.5	2	0.11	11d
29MAR1999	51266.64	11.1±0.2	3	0.31	11f

[a]See text for discussion of error bars.

[b]Number of photometry points considered in average.

[c]Minimum time difference between photometry and spectra. (Max. time difference $\leq$ 0.75 day.)

[d]1 point from CrAO, others AAVSO.

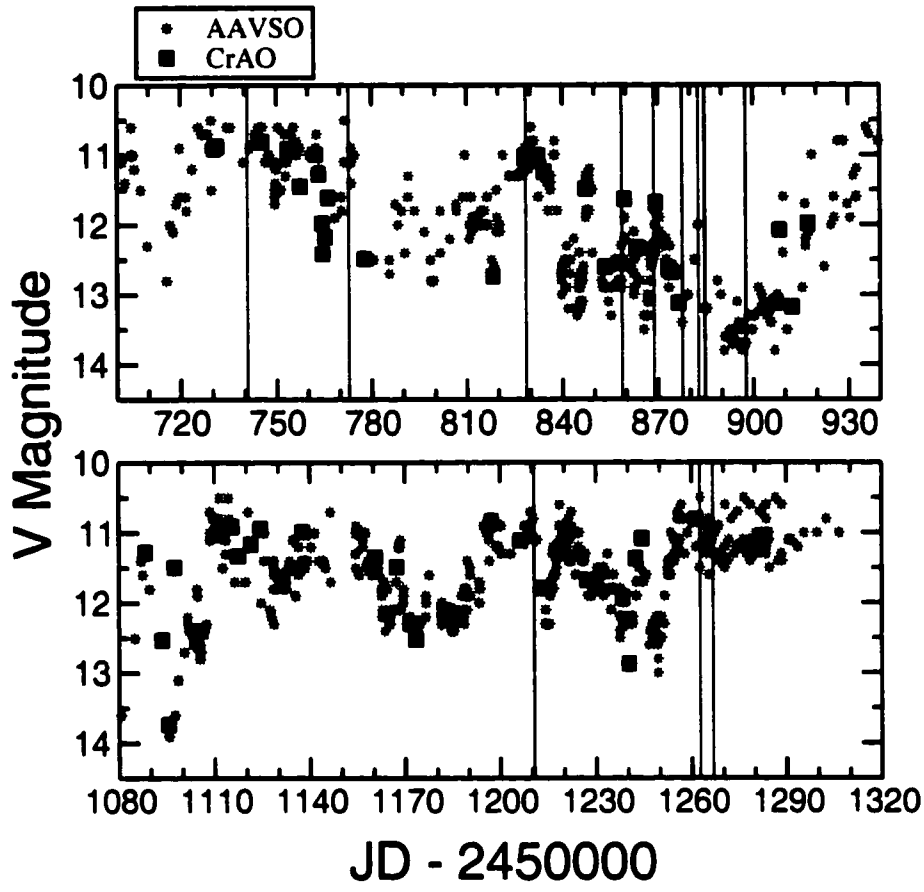

Figure 4.1 Light Curve for RR Tau: V band photometry as a function of Julian date. Stars are AAVSO data, squares are data from CrAO. Two observing seasons are plotted: approximately September thru April 1997 - 1998 on top, 1998 - 1999 on the bottom. The dates of spectral observations are indicated with vertical lines.

casions (see Fig. 4.1). Fortunately, we are able to supplement these data with the extensive V band database of the American Association of Variable Star Observers (AAVSO), which has over 900 measurements of RR Tau during the same two seasons. Figure 4.1 shows the light curve of RR Tau between 1997–1999, with the dates of spectral observations indicated by vertical lines. Although there is considerable scatter among the AAVSO data, the figure shows generally good agreement with the points obtained at CrAO.

Using these data we have obtained reliable estimates of the star's V magnitude at each spectral epoch. To account for the scatter in the AAVSO data, we considered all photom-

etry points within ~0.75 day of the spectral observation, but placed the highest weighting on the point (or points) closest in time. In most cases, two or more measurements contributed to the determination of the estimated V. We estimate the errors to be between 0.1 and 0.3 magnitudes in V, with the range being a function of both the scatter among the considered points and the number of points available at each epoch. On three dates (19OCT97, 05MAR98 & 10MAR98) there is only one AAVSO photometry point within one day of the spectral observation, and we have allowed for a slightly higher uncertainty in these cases. Table 4.1 lists the estimated V magnitudes along with the number of points that contributed to the average, and the Δt of the closest point. The resulting V magnitude corresponding to each spectral epoch are shown in Figure 4.2. Half of the twelve spectra were obtained when the star was bright, $V \approx 11$, while the other half were obtained at fainter magnitudes, $12 < V < 13.7$. The "faint spectra" were all obtained over a six week period during February and March of 1998, during which time the star's brightness appears to have bounced around within this range. The "bright spectra" bracket the faint spectra chronologically and span 1.5 years of elapsed time (October 1997 to March 1999).

The AAVSO data provide V band magnitudes only. To determine the magnitudes in other bands, we use long-term data to examine the typical color behavior of RR Tau over time. A quadratic solution is fit to each color of the combined data from the CrAO $UBVRI$ photometry and the Wesleyan $UBVR$ database (Herbst & Shevchenko 1999), as shown in Figure 2.4b (see 2). The color reversal ("blueing effect") is apparent in the $U-B$ and $B-V$ colors, and barely seen at faintest epochs in the sparser $V-R$ and $V-I$ data.

4.4 *Results*

4.4.1 The Spectra

The spectra in their entirety are shown in Figure 4.4.1, ordered by Vmagnitude, with the faintest spectra shown at the top. Prominent features are identified. As expected for an early A type star, the Balmer lines dominate the spectra. Hα is seen strongly in emission at all epochs, while the upper level Balmer lines show broad absorption wings with either narrow shell absorption or emission in the cores. At all epochs, numerous weak absorption lines,

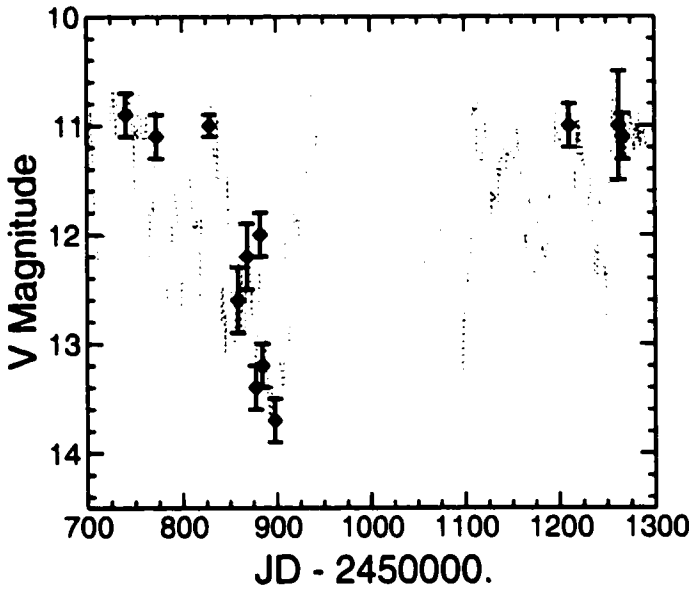

Figure 4.2 Estimated V magnitudes of spectral epochs versus Julian date. Dotted line indicates visual behavior of RR Tau over the whole period (running average of data in figure 4.1). Note that the point at V = 12.0 lies between the points at V = 13.4 and V = 13.2. See text for discussion of the error bars.

primarily FeI, FeII, and TiII, are seen in the blue (4000 - 4600 Å, hereafter "blue forest"). The forbidden lines [OI]6300&6363 Å are seen in emission. A broad diffuse interstellar band (DIB) feature at ~6150Å is present in most spectra, and affects the normalization between 5900 and 6200 Å, particularly in the lower signal-to-noise data. A narrow feature seen at 6283Å in all spectra is likely due to telluric absorption.

At bright epochs, prominent features seen in absorption include the higher order Balmer and Paschen lines, CaII K and the CaII IR triplet, the FeII(42) triplet redward of Hβ, HeI 5876, and the NaI D lines as well as numerous weaker absorption lines. The HeI 5876Å and CaII IR triplet lines also exhibit some emission in inverse P-Cygni profiles. The brightest spectrum obtained on 19OCT97 is an anomaly: the [OI] and many of the absorption features are similar, but the cores of Hα, Hβ and the CaII IR triplet are much stronger, while the FeII(42) triplet line absorption is much weaker. As discussed in section §4.5.5, we believe this spectrum has captured a unique epoch in these data.

There are strong similarities among all of the normalized spectra for $V \leq 12.2$, but the

four spectra taken when the system was faint, $12.6 \leq V \leq 13.7$ (top of Fig. 4.4.1), appear very different. The increased equivalent widths of the [OI] lines and the core of Hβ are readily apparent. Emission is clearly seen in the cores of the upper level hydrogen lines, and the upper level Paschen absorption lines are filled in. In addition, the three faintest epoch spectra reveal a number of additional emission lines. The strongest of these are the CaII K, FeII(42) triplet, NaI D, OI 8446, and CaII IR triplet, all of which are seen in absorption when the system is brighter. These are primarily low excitation lines, normally only seen weakly in absorption in late B/early A type stars. The spectrum from 25MAR98, the faintest state in these data, also reveals a number of weak emission lines in the blue forest identified with forbidden [FeII] transitions. The combination of weak emission mixed with weak absorption and decreased signal-to-noise in this spectrum, makes the line and continuum identification more uncertain at this epoch.

In this chapter we focus on the relative strengths of the lines as a function of system brightness. We discuss briefly the kinematic behavior of the Hα and Hβ lines, but defer a quantitative report on the gas kinematics to analysis of higher resolution Echelle data now under analysis (B. Rodgers *et al.*, in preparation).

4.4.2 Equivalent Widths

The equivalent widths (EW) of a number of prominent lines at all epochs are presented in Tables 4.2 and 4.3. We have selected a few of the most prominent and least blended lines from the "blue forest" (4000 - 4600 Å). Note also that the region below 4500 Å is not available on two of the three faintest epochs. Of the hydrogen lines, only Hα and Pa14 that present the simplest profiles, are included in the table. The hydrogen and CaII IR triplet lines (which are blended with Paschen lines), are discussed further in §4.5.1 and §4.5.3.

The EW behavior of the lines naturally separate themselves into three categories, shown in Figure 4.4. The first group is the "emission only" lines: Hα, [OI], and [FeII] (Fig. 4.4a). These lines show the greatest change in the normalized spectra, but in fact the emitting gas is changing very little. The dramatic increase in EWs are a result of the dropping continuum; the emission flux is not changing. The solid lines shown in the figure indicate

Figure 4.3 DIS Spectra of RR Tau versus wavelength, in order of decreasing V magnitude (faintest spectra at the top). All data are normalized and plotted offset from each other by 0.5 (vertical tickmarks). Dates and corresponding V magnitudes are indicated and prominent spectral features labeled. Along the right side, spectral designations from Table 4.1 are shown.

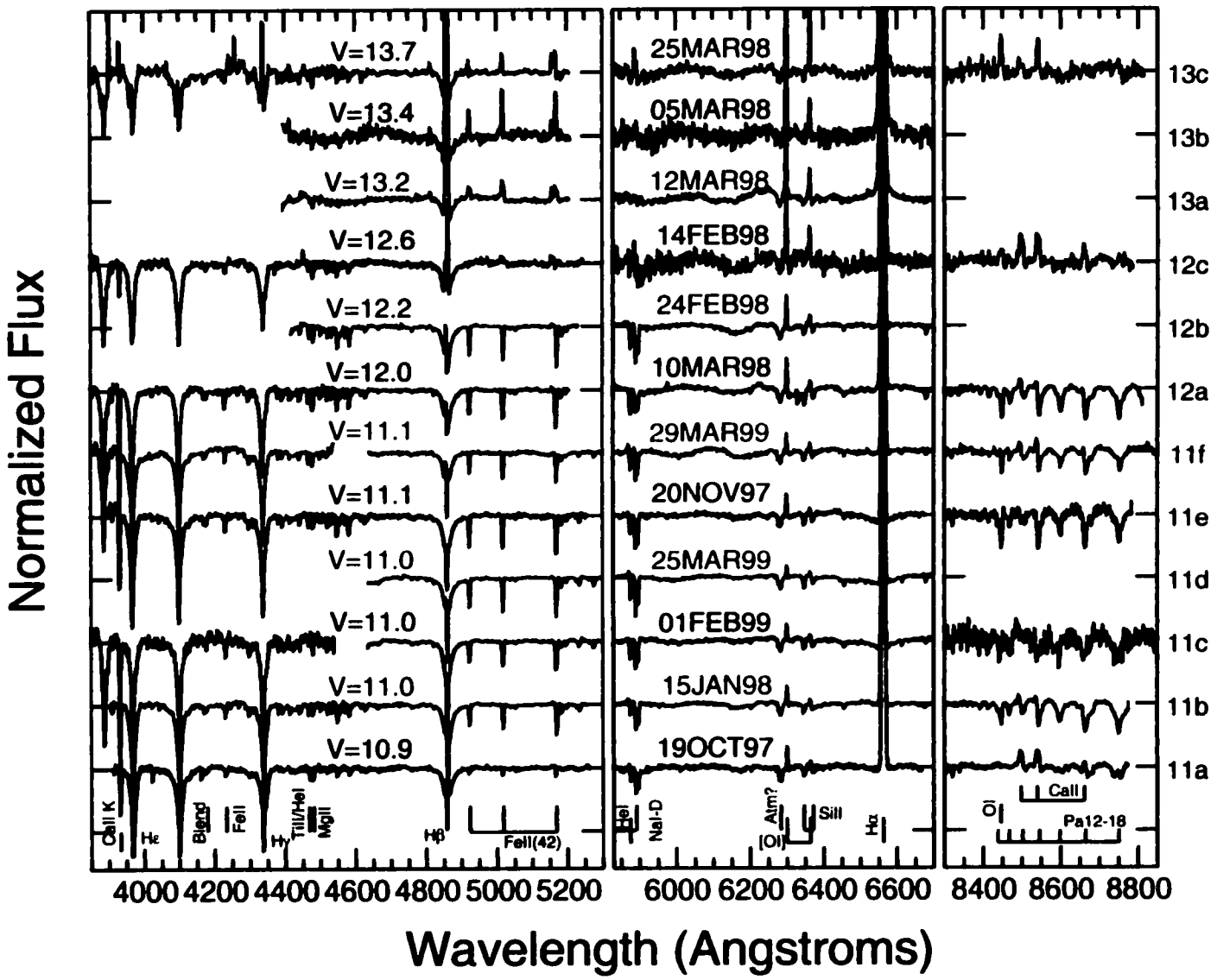
Normalized Flux
V=13.7
V=13.4
V=13.2
V=12.6
V=12.2
V=12.0
V=11.1
V=11.1
V=11.0
V=11.0
V=11.0
V=10.9
25MAR98
05MAR98
12MAR98
14FEB98
24FEB98
10MAR98
29MAR99
20NOV97
25MAR99
01FEB99
15JAN98
19OCT97
13c
13b
13a
12c
12b
12a
11f
11e
11d
11c
11b
11a
CaII K
Hε
Blend
FeII
HγTiII/HeI
MgII
Hβ
FeII(42)
HeI
NaI-D
Atm?
[OI]
SiII
Hα
CaII
OI
Pa12-18
4000 4200 4400 4600 4800 5000 5200
6000 6200 6400 6600
8400 8600 8800
Wavelength (Angstroms)

Table 4.2. RR Tau Equivalent Widths During Bright State

Line ID	11a V = 10.9	11b 11.0	11c 11.0	11d 11.0	11e 11.1	11f 11.1
CaII K	1.39	2.10	... [a]	...	2.39	-1.15
Fe I 4045	0.13	0.17	0.30	...	0.15	0.05
Fe II 4233	0.23	0.42	0.44	...	0.56	0.36
He I 4471	0.15	0.37	0.16	...	0.39	0.44
Mg II 4481	0.45	0.37	0.54	...	0.49	0.54
Fe II 5018[c]	0.18	0.79	0.86	1.12		
[FeII] 5158	-0.05	-0.06	-0.05	-0.07	0:	-0.06
HeI 5876	0.47	0.51	0.73	0.85	0.80	0.72
NaI D[d]	0.5	1.07	0.82	1.06	0.95	0.72
DIB 6283	1.16	0.91	0.96	0.95	0.94	1.10
[OI] 6300	-0.60	-0.59	-0.46	-0.42	-0.53	-0.49
Si II 6348	0.55	0.45	0.56	0.51	0.52	0.60
Hα[e]	-36.01	-21.25	-13.62	-21.03	-27.34	-28.65
OI 8446	-0.02	0.83	...	...	1.58	0.89
Pa14	0.92	2.20	...	...	2.10	1.89

Note. — EWs are measured in Å. Negative EW indicates emission. Spectral designations at the top of each column are defined in Table 4.1.

[a]Data not available.

[b]: Denotes uncertain value.

[c]Middle line of triplet.

[d]First line of doublet.

[e]Observed EW (without photospheric subtraction).

Table 4.3. RR Tau Equivalent Widths During Faint States

Line ID	12a V = 12.0	12b 12.2	12c 12.6	13a 13.2	13b 13.4	13c 13.7
CaII K	2.73	... [a]	2.72	...	2.37	0.77
Fe I 4045	0.09	...	0.17	...	...	0.19
Fe II 4233	0.56	...	0.25	...	...	0.30
He I 4471	0.59	0.59	0.19	0.06	0.18:[b]	0.32
Mg II 4481	0.63	0.58	0.49	0.46	0.52	0.57
Fe II 5018[c]	1.05	1.04	-0.14	-1.12	-1.36	-0.63
[FeII] 5158	-0.14	-0.10	-0.24	-0.34	-0.46	-0.70
HeI 5876	1.24	1.03	0.33:	0.28:	-0.27:	0.22:
NaI D[d]	0.73	1.18	-0.4:	0.11:	-0.37:	-1.03
DIB 6283	1.05	1.21	1.80	1.25	1.11	1.35
[OI] 6300	-0.96	-1.05	-2.34	-3.28	-3.61	-7.42
Si II 6348	0.79	0.56	0.70	0.82	0.19:	0.57
Hα[e]	-44.57	-40.61	-73.05	-132.20	-174.97	-211.80
OI 8446	1.39	...	-0.75	...	...	-2.35
Pa14	2.63	...	0.50:	...	...	0.78:

Note. — EWs are measured in Å. Negative EW indicates emission. Spectral designations at the top of each column are defined in Table 4.1.

[a]Data not available.

[b]: Denotes uncertain value.

[c]Middle line of triplet.

[d]First line of doublet.

[e]Observed EW (without photospheric subtraction).

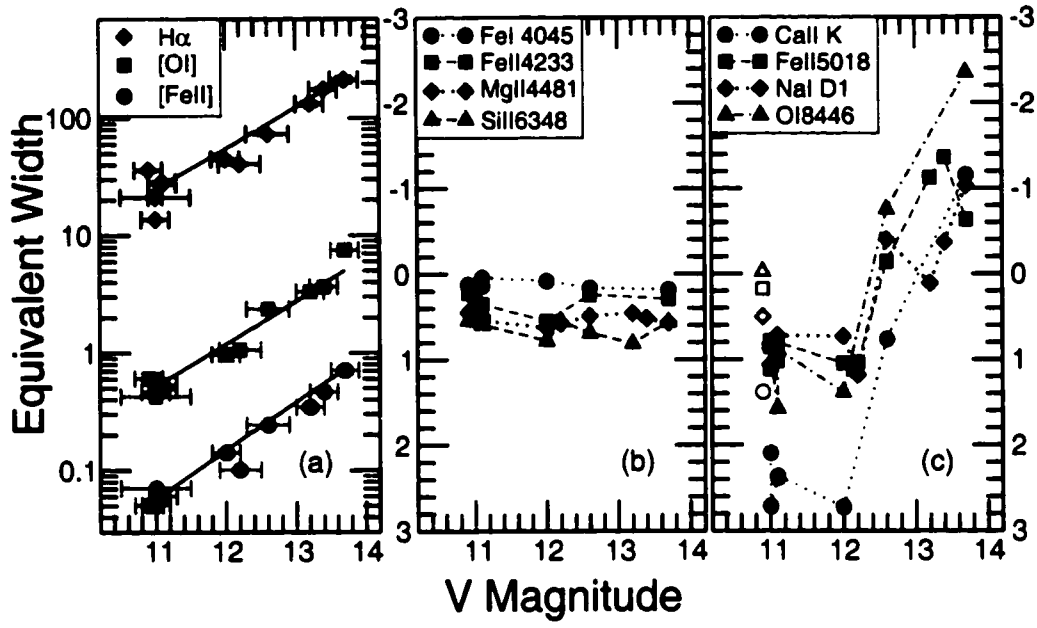

Figure 4.4 Measured equivalent widths versus V magnitude of selected lines from Tables 4.2, 4.3. (a) Emission lines. EW is plotted as absolute value on logarithmic scale. Solid lines are not fits to data but indicate paths of constant flux. (b) Lines seen in absorption at all epochs. (c) Lines seen in absorption for $V \leq 12$ and absent or in emission for $V > 12$. Open symbols are 19OCT97 points. Vertical axes are the same in the center and right panels. Errors in V are shown in (a) only. Errors in EW are generally smaller than the size of the symbols.

expected EW for lines of constant flux (where the flux is set by the average of the EWs at $V = 11$). For the [OI] and [FeII] lines, the measured points lie within the error bars of the constant flux line. The Hα line flux is more variable, but to first order it also shows that the EW behavior is due to the contrast between a stable line flux and a decreasing continuum.

The lines in the second group (Fig. 4.4b) exhibit essentially constant EW, i.e., the absorption in the line scales with the continuum over >2 magnitudes in V. This group consists of weak absorption lines such as FeI 4045, FeII 4233, MgII 4481, and SiII 6348 Å in all spectra. Note that many of these lines are in the blue forest, which is not available at all epochs.

Thirdly, and most intriguing, are a number of strong permitted lines, FeII, OI, NaD, CaII, plotted in Figure 4.4c. Note that the vertical scale is the same in the second and third

panels of the figure. At bright epochs the lines are in absorption, at intermediate epochs the lines disappear, and at faint epochs the lines go into emission. The open symbols in Fig. 4.4 are taken from the 19OCT97 spectrum, which is unique among the bright spectra (§4.5.5). These lines when seen in absorption are significantly deeper than expected from the photosphere alone.

4.4.3 Line Fluxes

For the lines whose EW changes with system brightness (Figs. 4.4a and 4.4c), the relevant measurement is the flux in the line. We calculate the observed line flux at each epoch from the EW and the stellar continuum flux. The integrated line flux is

$$F_{line} = F_\lambda * EW_{line}$$

where F_λ is the continuum flux at the wavelength of the line derived from the simultaneous V band magnitude, the interpolated colors (Fig. 2.4), and the zero-magnitude fluxes given by Johnson (1966). The EW in this formula is $F_{line}/F_\lambda - 1$ such that $EW > 0$ for emission lines. Throughout the text, we present the flux normalized by 1.6×10^{-13} erg cm^{-2} s^{-1}Å^{-1} which is the continuum flux at 5500 Å in the bright state ($V = 11$; Johnson 1966). The errors in the line fluxes are dominated by the uncertainty in the continuum flux (see Table 4.1).

4.5 Discussion

4.5.1 Photosphere

The broad absorption wings of Balmer lines are clearly seen in Hβ through Hϵ at all epochs. The wings of Hα are barely seen on a few epochs, but are generally dominated by the strength of the circumstellar Hα emission. While the cores of all the Balmer lines are variable, beyond $\Delta v \sim 400$ km s^{-1} the wings of the lines are quite stable at all epochs. In addition the weak metal absorption lines identified in Figure 4.4b show constant EW at all epochs. Both of these characteristics are associated with the photosphere of the star

and indicate that the photosphere of RR Tau is not varying though the system brightness changes by an order of magnitude.

In early A stars, the Balmer wings are more strongly dependent on gravity than on effective temperature. Therefore, they provide a sensitive test of changes in the underlying photosphere. We compare the wings of Hβ, Hγ and Hδ to synthetic Kurucz (1979) line profiles for T_{eff} = {7000, 8000, 9000, 10000, 12000 K} and log g ranging from 1.5 to 5.0 in increments of 0.5. The synthetic profiles have been broadened to the instrumental profile of DIS, which dominates the line width for $50 \leq v \sin i \leq 150$ km s^{-1}. The observed line profiles are identical at all epochs to within Δ log $g \lesssim 0.5$ for a given T_{eff}. This is shown in Figure 4.5 for T_{eff} of 9000 and 12000K and a range of log g. The average of the bright epochs are shown as the heavy solid line and each intermediate and faint epoch is plotted individually. A total of seven spectra are plotted for Hβ, four for Hγ and Hδ (see Fig. 4.4.1); the observed spectra are identical between the left and right panels of the figure. The weak emission lines which become visible at faintest epoch are seen on either side of Hγ. We find the wings can be well fit for different combinations of effective temperature and gravity with best fits at log g =2.5, 3.0, 3.5 and 4.0 for T_{eff} = 8000, 9000, 10000, and 12000, respectively.

Due to the degeneracy in the effect of temperature and gravity on the Balmer line profiles, we cannot rule out a change in spectral type from the Balmer wings alone. However, any such change would require a change in temperature exactly offset by an opposite change in surface area such that the observed wings remain constant. For example, an increase in T_{eff} from 9000 to 10000K, would require a factor of $\sim$2 decrease in radius (for fixed mass), to produce an increase of 0.5 in log g, resulting in essentially the same Balmer wing profile according to the Kurucz models. We find such fine-tuning unlikely and conclude instead that the surface temperature and gravity of the central star in RR Tau are essentially unchanging.

In addition to the Balmer wings, there are a number of weak metal absorption lines that are invariant in all spectra. The EWs of a few representative lines are plotted in Figure 4.4b. In Figure 4.6, the entire blue forest region is shown. An average of five bright spectra is compared with the two fainter spectra of 14FEB98 (V = 12.6) and 25MAR98 (V = 13.7). Despite the lower S/N of the two fainter spectra and the presence of several weak emission

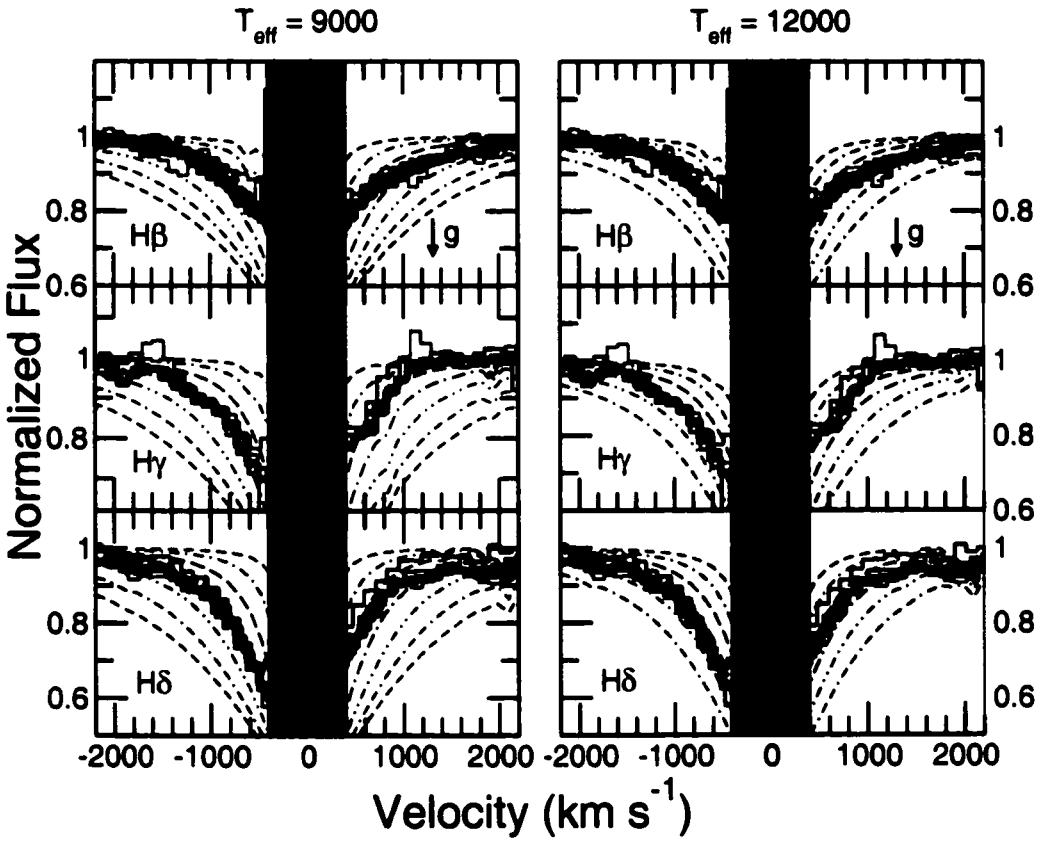

Figure 4.5 Wings of Hβ, Hδ and Hγ versus velocity. Observed data (solid lines) are overlaid on synthetic Kurucz spectra (dashed lines) for $T_{eff} = 9000K$ and $1.5 < \log g < 4.5$ (*left*) and $T_{eff} = 12000K$ and $2.5 < \log g < 5.0$ (*right*). Gravity is increasing top to bottom in all panels. The same observed data are plotted on the left and right side. Variable cores ($\Delta v \leq 400$ km s^{-1}) have been blocked out. Heavy solid line is the average of bright spectra, excluding 19OCT97, and each intermediate and faint spectrum is plotted separately. A total of 7 spectra are plotted for Hβ, 4 each for Hγ and Hδ.

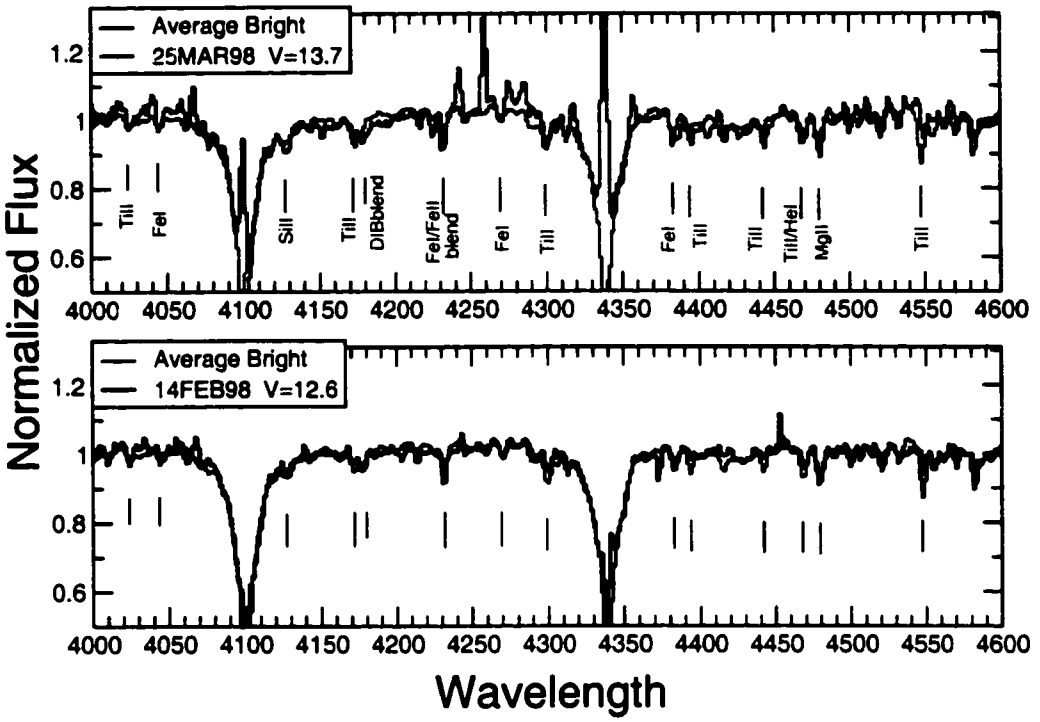

Figure 4.6 Comparison of blue forest spectra on different epochs. Thin line is the average of three bright epoch spectra (same in both panels): top panel overlaid with 25MAR98 spectrum (V=13.7); bottom panel overlaid with 14FEB98 (V=12.6). Labels identify a number of weak metal features present on all epochs. Emission lines visible blueward of Hγ in the top panel are [FeII] lines seen when the system is faint.

features, particularly on 25MAR98, the similarity in a number of weak absorption features is clearly seen. This indicates that these lines, whose strengths are consistent with an early A spectral type, are photospheric in nature and the photosphere (or continuum source) is not changing temperature significantly with system brightness.

The depth of the metal lines can be used to constrain the effective temperature. We did not find a good match at T_{eff} = 7000K, in either the Balmer wings or the metals. At T_{eff} =12000K, the line strengths of metals in the synthetic spectra are too weak to match the observed spectra. The best fit to the majority of the metal lines present in the spectra is 9000 $\leq T_{eff} \leq$ 10000K. Taken together, the Balmer wings and the metal lines match an early A spectral type with slightly lower gravity (3 $\leq \log g \leq$ 3.5) than a main-sequence star. This is in agreement with the A2 spectral type of Strom *et al.* (1972), also based on the Balmer

wings. Our result is consistent with a more accurate spectral type analysis, based on higher resolution data (V.P. Grinin *et al.*, in preparation) that finds $T_{eff} = 9750K$, $\log g = 3.5$ and $v \sin i = 140$ km s^{-1}. These are in contrast to the B9 spectral type originally assigned by Herbig (1960) based primarily on HeI absorption. Our spectra show the HeI 5876 line to be variable, decreasing in strength at faint epochs, and exhibiting blue-shifted emission on some epochs. We conclude that this line is not photospheric. The HeI 4471Å line is a blend with TiII at this resolution, and thus not useful for spectral classification.

The constant EW of weak metal absorption lines and of the wings of Balmer lines suggests no significant change in spectral type between bright epochs and faint epochs. This condition was first noted in RR Tau by Herbig (1960) and has also been reported for other UXOR systems (Eaton & Herbst 1995).

4.5.2 Wind Emission: [OI] and [FeII]

Forbidden [OI] lines at 6300Å and 6363Å are seen in emission at all epochs. A forbidden iron line, [FeII] 5158 Å, is barely detected in emission when the system is bright but easily seen in the faint spectra. Both lines show EW increasing in proportion to the decreasing continuum as the star fades (Fig. 4.4). Figure 4.7 plots the integrated line flux in the [FeII] and [OI] lines with V magnitude (see §4.4.3). Both lines exhibit essentially constant flux, within the error bars, and no dependence on V. The faintest [OI] point has slightly higher flux that is not matched by the other two faint epochs, nor by [FeII], and we caution that the continuum flux in R is somewhat more uncertain for $V \gtrsim 13$ (Fig. 2.4).

Forbidden emission lines arise in a low density region, and specifically the presence of [OI] is commonly associated with a circumstellar wind. These data show that this wind is stable at all epochs and therefore is not affected by the change in observed brightness. The [FeII] lines, of which [FeII]5158 is the brightest of several observed, appear to behave in concert with [OI] indicating a wind origin for these lines as well. No increase in flux is seen in [FeII] or [OI] when the one high point in Hα flux is seen (Fig. 4.7, bottom panel), suggesting that the gas responsible for the forbidden emission is distinct from the hydrogen emission region.

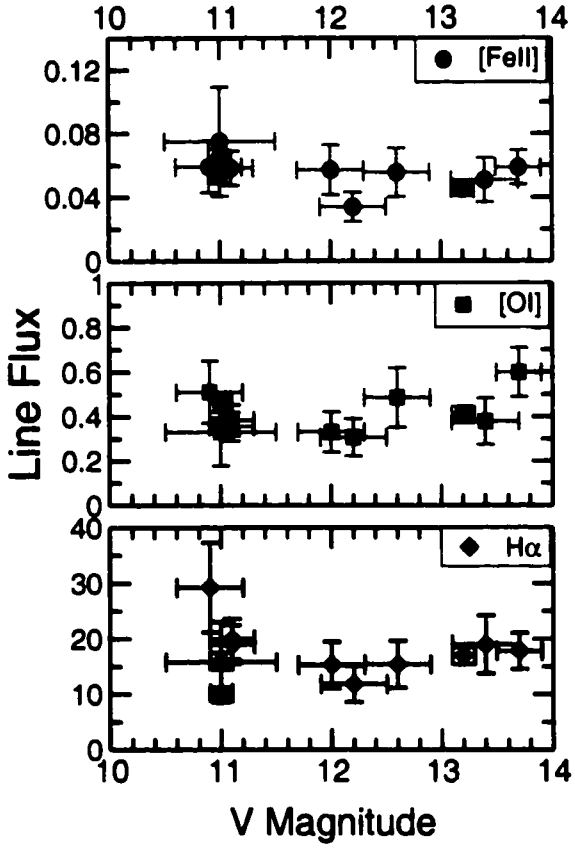

Figure 4.7 Integrated flux of emission lines as a function of V magnitude: [FeII] *(top)*, [OI] *(center)* and Hα*(bottom)*. Flux is in units of 1.6×10^{-13} erg cm^{-2} s^{-1} (§4.4.3). Errors in line flux are propagated from uncertainty in V magnitude.

The constant flux in [OI] emission makes the EW of this line an excellent indicator of system brightness in the absence of concurrent photometry or absolute flux information. Specifically, we offer the following empirical relation,

$$V = 11.8 + 2.75 \log(EW_{[OI]6300})$$

where $EW_{[OI]6300} > 0$ in emission. The error in this relation based on our data is ≤ 0.3 magnitudes for $11 \leq V \leq 13.4$, comparable to the errors in the V estimates (Table 4.1), and 0.5 magnitudes for the one epoch with $V = 13.7$.

4.5.3 Circumstellar Hydrogen

Balmer lines

The Hα line is a complex composite of various circumstellar regions possibly including a wind, a disk atmosphere and an accretion stream. The Hα line flux plotted in Figure 4.7 shows roughly constant flux with no dependence on V, but with larger scatter than the forbidden lines, particularly at bright epochs. A correlation between [OI] and Hα in single epoch observations of a selection of stars is often cited as an indicator of accretion-outflow connection in T Tauri stars (Cabrit *et al.* 1990). It is unclear whether a temporal correlation in a single source is expected. Since the two lines sample very different densities and volumes, one might expect a time lag between the accretion (Hα) and the wind ([OI]). Here we are comparing spectra from the same star at different epochs, and we see a general tendency in RR Tau for Hα to be correlated with [OI], in that both lines exhibit nearly constant flux, independent of V. However, the flux in Hα at bright epochs is more variable than [OI], and in particular the largest Hα flux on 19OCT97 is not matched by an increase in [OI] or [FeII].

To recover the circumstellar flux in the Balmer lines, we subtract a Kurucz (T_{eff} = 9000, $\log g = 3.0$) profile from each spectrum and scale the residual emission by the relative continuum flux. The circumstellar line fluxes in Hα and Hβ are shown in Figure 4.8. The labels in each box correspond to the spectral designations listed in Table 4.1. Although the fluxes in these lines are not strongly correlated with V, the shapes of the lines do show

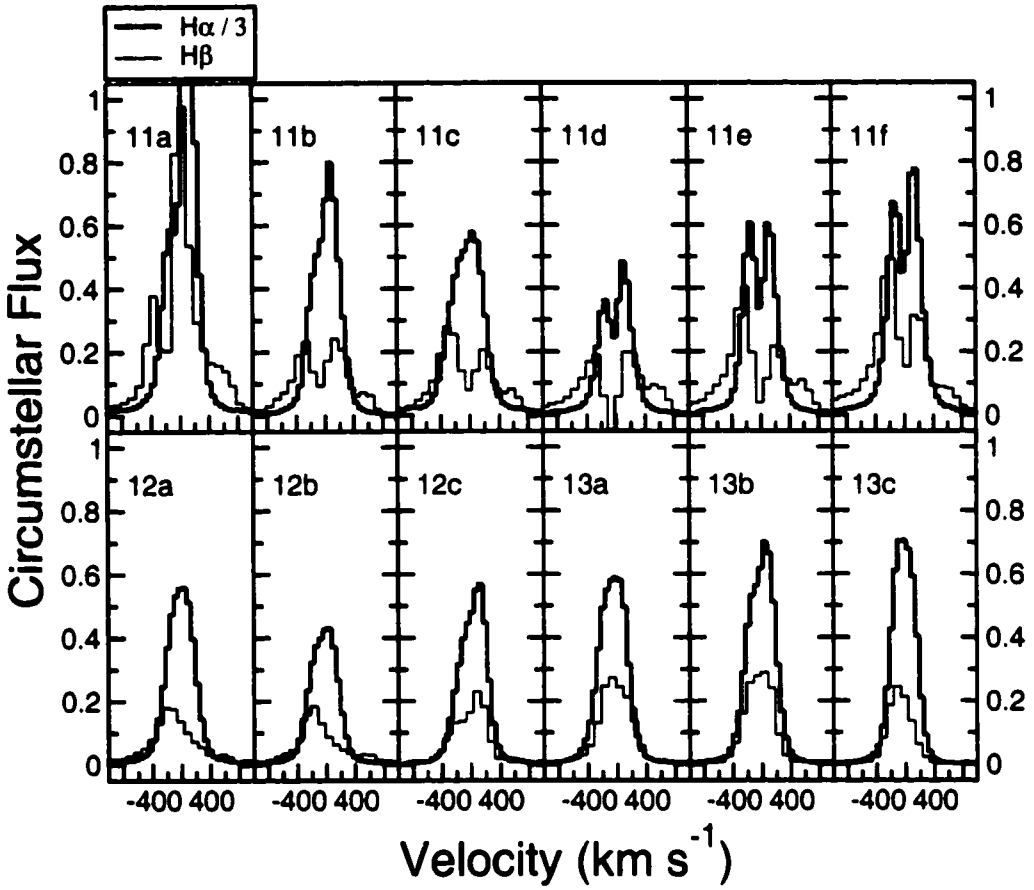

Figure 4.8 Hα (thick line) and Hβ (thin line) circumstellar line fluxes versus velocity. Hβ flux is in units of 1.6×10^{-13} erg cm^{-2} s^{-1} Å^{-1} (§4.4.3); Hα flux is further divided by 3 to plot on similar scale. Kurucz line profiles (T_{eff} = 9500, log g = 3.0) have been subtracted from all spectra. Spectral designations are defined in Table 4.1.

some correlation. Even at this resolution, the Hβ profiles are clearly double-peaked in all of the bright spectra, and appear more singly-peaked at fainter epochs. Hα emission shows well separated peaks on three of the bright epochs (11d, 11e and 11f). The separation of the peaks is $\sim$ 250 km s^{-1} in Hα and $\sim$ 450 km s^{-1} in Hβ. The full width at zero intensity of Hα is unchanged at all epochs, $\sim$800 km s^{-1}. The Hβ line shows similar width at faint epochs, but exhibits broad shoulders at bright epochs that are absent when the star fades.

From these data, we conclude that the circumstellar gas responsible for most of the hydrogen emission is inherently variable but independent of the photometric variability.

However, the source of the central self-absorption in Hα and Hβ, and the highest velocity gas seen in Hβ, are linked to system brightness, disappearing when the star fades.

Paschen lines

Paschen absorption and emission is seen in the far-red portions of the spectra. The Pa13, Pa15 and Pa16 lines are blended with CaII IR triplet lines at 8498, 8542 and 8662Å. At bright epochs these lines show broad photospheric Paschen absorption, narrow Paschen shell absorption and CaII emission and absorption in an inverse P-Cygni profile. At fainter epochs, the Paschen lines are essentially completely filled in. The CaII IR triplet lines appear more strongly in emission at faint epochs, but this is primarily due to the increased Paschen emission. We find the behavior of the Paschen lines is similar to that of the upper level Balmer lines at each epoch.

4.5.4 Variable Metals

The lines in the first two panels of Figure 4.4 are easy to understand in terms of a stable photosphere and stable optically thin emission region, both unaffected by photometric variability. In contrast, the behavior of the metal lines in Fig. 4.4c is clearly linked to photometric brightness. The CaII K, FeII(42) triplet, NaI D, and OI 8446 lines, all low-ionization permitted lines, are seen strongly in absorption, with small variations in EW, for epochs with $11.0 \leq V \leq 12.2$; are essentially absent at the intermediate epoch of $V = 12.6$ on 14FEB98; and are then prominent in emission when $V \geq 13.2$ (three epochs for FeII(42) triplet, one for CaII K and OI 8446). While there appears to be a sudden change in the behavior of these lines for $V > 12.5$, the normalized spectra can be misleading. In Figure 4.9, we show these lines scaled to their relative flux levels. In this figure it is clear that the absorption line depths decrease at intermediate epochs (and disappear in the case of FeII(42) triplet) and reappear in emission at faintest epochs.

These metal lines are predominantly circumstellar. Not only do they show circumstellar emission at some epochs, but their absorption line depths are much larger than typical photospheric lines for an A2 star, as compared with either a Kurucz spectrum or comparable

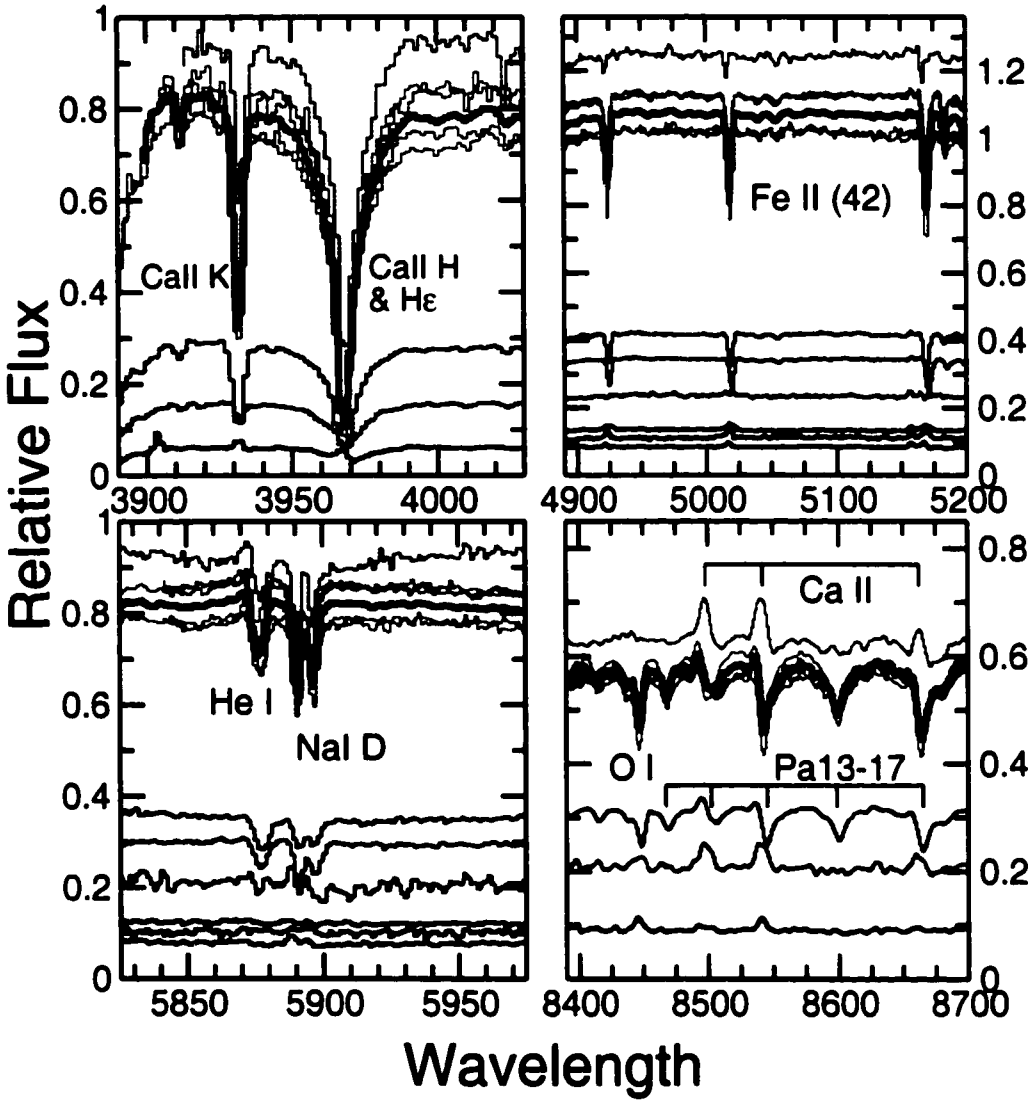

Figure 4.9 Relative flux of variable lines versus wavelength. Flux units are as in figure 4.8. Heavy solid line represents average of bright spectra. Except HeI 5876, the prominent features in each panel switch from absorption at bright epochs to emission at faint epochs. The brightest spectrum is 19OCT97, discussed in §4.5.

standard stars (V.P. Grinin *et al.*, in preparation). To investigate the behavior of these lines at all epochs, we first need to calculate the circumstellar line flux.

Following Bertout (1994), for the simplified case of a spherically symmetric envelope the observed flux is given by

$$F_\nu = \int_0^{R_{max}} I_\nu(\infty, p) 2\pi p dp \tag{4.1}$$

where R_{max} is the full extent of the system and p is the impact parameter with respect to the star. The emergent intensity is

$$\begin{aligned} I_\nu(\infty, p) &= S_\nu(1 - e^{-\tau_\nu(p)}) + \\ &\quad \epsilon(p) I_\nu(0) e^{-\tau_\nu(p)} \end{aligned} \tag{4.2}$$

and S_ν is the source function, $\tau_\nu(p)$ is the optical depth, and $I_\nu(0)$ is the continuum intensity. $\epsilon(p) = 1$ for $p \leq R_*$ and 0 otherwise. We have neglected the contribution of scattered light to the continuum. In RR Tau the scattered light is estimated to be very small compared to the stellar continuum, ~3% of $I_\nu(0)$ (Rostopchina *et al.* 1997). This is an important continuum source at minimum light, however, it is not a significant component in these line flux calculations. In terms of the stellar and circumstellar parts,

$$\begin{aligned} F_\nu = 2\pi \{ &\int_0^{R_*} I_\nu(0) e^{-\tau_\nu(p)} p dp + \\ &\int_0^{R_{env}} S_\nu(1 - e^{-\tau_\nu(p)}) p dp \} \end{aligned} \tag{4.3}$$

where R_* and R_{env} are the radii of the star and the circumstellar region, respectively. For our purposes, $I_\nu(0)$ includes the photospheric contribution to the line.

In order to make progress in understanding the behavior of these lines, we consider two contributing regions: one that is affected by the brightness variations, and one that is not. We further assume the variability is caused by an obscuring screen with a time-dependent continuum opacity, $\tau_S(t)$, and radius, R_S, such that $R_* < R_S < R_{env}$. We rewrite equation 4.3 as

$$\begin{aligned} \frac{1}{2\pi} F_\nu(t) = e^{-\tau_S(t)} \times \\ [\int_0^{R_*} I_\nu(0) e^{-\tau_\nu(p)} p dp + \int_0^{R_S} S_\nu(1 - e^{-\tau_\nu(p)}) p dp] \end{aligned}$$

$$+\int_{R_S}^{R_{env}} S_\nu(1-e^{-\tau_\nu(p)})pdp \tag{4.4}$$

Note that in the bright state, $\tau_S(t) = 0$, we recover equation 4.3. The continuum flux is $F_{\nu,*}(t) = I_\nu(0)e^{-\tau_S(t)}\pi R_*^2$.

The form of $\tau_\nu(p)$ is a function of the (unknown) geometry and inclination of the circumstellar region. For simplicity only, let us assume that τ_ν is independent of p (i.e., a uniform column depth slab). Integrating equation 4.4 and dividing by the continuum, the normalized flux is

$$\begin{aligned} F_\nu/F_{\nu,*} = & \\ & e^{-\tau_\nu} + \frac{S_\nu(1-e^{-\tau_\nu})}{I_\nu(0)}\frac{R_S^2}{R_*^2} \\ & + \frac{S_\nu(1-e^{-\tau_\nu})}{I_\nu(0)e^{-\tau_S(t)}}\frac{(R_{env}^2 - R_S^2)}{R_*^2} \end{aligned} \tag{4.5}$$

The observed spectra clearly show that the absorption (the first term) is the dominant component at bright epochs (Fig. 4.4.1). Therefore, we derive the emission component (the second and third terms) at every epoch in the following way. We use the bright epoch with the strongest absorption (largest EW), as an approximation to the first term, neglecting any contribution from S_ν. This normalized spectrum is subtracted from each of the other epochs, and the difference is multiplied by the continuum flux on that epoch. That is,

$$F_\nu^{\rm Em} = (F_\nu/F_{\nu,*} - F_\nu^{\rm Abs}/F_{\nu,*}^{\rm Abs})F_{\nu,*} \tag{4.6}$$

$$\cong \; S_\nu(1-e^{-\tau_\nu})[R_{env}^2 - R_S^2(1-e^{-\tau_S(t)})] \tag{4.7}$$

where equation 4.6 is the empirical procedure and equation 4.7 is what the resulting flux represents. The procedure is shown in the top panel of Figure 4.10 for the FeII(42) triplet lines at 4924, 5018 and 5159 Å (for which we have the most epochs and the highest S/N). We use the 25MAR99 spectrum as the "absorption only" template, shown in the top of the figure and overlaid on the normalized spectrum of 05MAR98. The bottom curve in the panel is the derived emission flux for 05MAR98. The emission fluxes for the other 10 epochs (19OCT97 excluded) are shown in the lower panels.

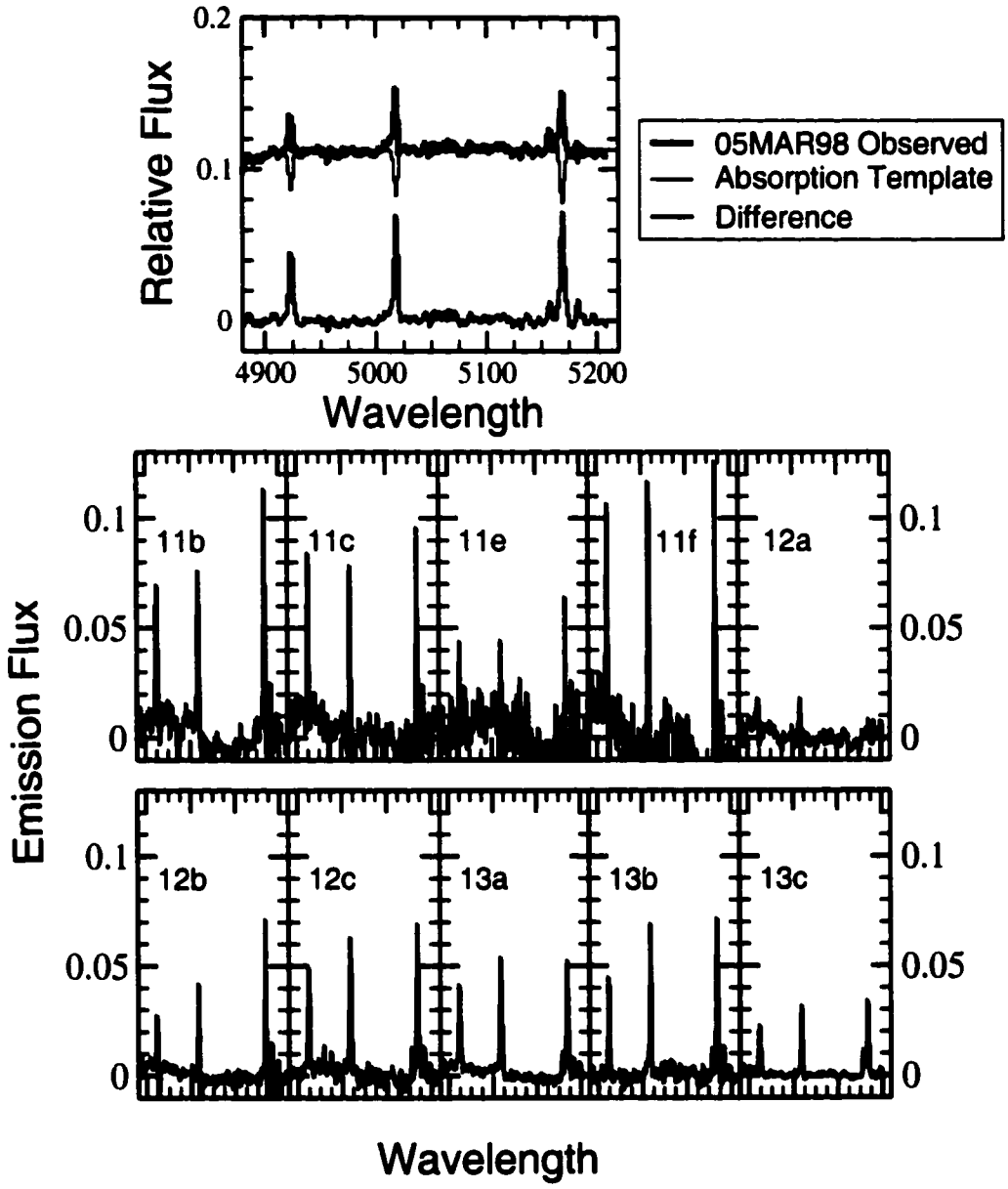

Figure 4.10 Derived emission flux of FeII(42) triplet at each epoch. The top panel shows the procedure: a maximum absorption template (25MAR99) is subtracted and the difference scaled to the relative flux level for each epoch. The bottom panels show the resulting flux for 10 epochs (excluding 19OCT97 and 25MAR99). Units of flux are as in Fig. 4.8.

The recovered emission flux at all epochs is roughly time-independent, with slight variations uncorrelated with V. The total flux is small relative to the stellar continuum at maximum light. Therefore the slight variations in equivalent width at bright epochs *and* the emission seen at faint epochs can be explained by a single emitting region that is always present and unobscured, i.e., the region between R_S and R_{env}. In addition, the lack of any correlation with brightness leads us to conclude from equation 4.7 that $R_S << R_{env}$.

The identical procedure was performed for the other lines in Figure 4.9, with the 20NOV97 epoch used as the absorption template for the CaII K and OI 8446 line regions. The calculated emission fluxes, integrated over each line, are plotted with V in Figure 4.11. In each case, a small emission flux, relative to the continuum at bright epochs, is recovered at all epochs. The emission fluxes are slightly variable but independent of system brightness. Because we have neglected any contribution from the emission in our template absorption spectrum, the absolute fluxes in the figure represent a lower limit. However, any additional contribution to the faint emission must be very small to go undetected at faint epochs. Also note that the CaII K line includes a photospheric component and the NaI D lines include an interstellar component, both of which result in underestimated fluxes in these lines.

This derivation has employed an obscuring screen as the cause of the continuum variability. It is conceivable that a similar result might be achieved with another mechanism. What is required is that the cause of the variability affect the absorbing gas in proportion with the continuum, and not affect the emitting gas significantly. We have utilized the simplifying assumptions of spherical symmetry and constant optical depth to illustrate this result. A more realistic geometric model is desirable to explore the behavior of these lines in more detail.

We conclude that the low-ionization permitted metal lines in RR Tau have an absorption component that varies with the continuum and an emission component that is unaffected by the photometric variability.

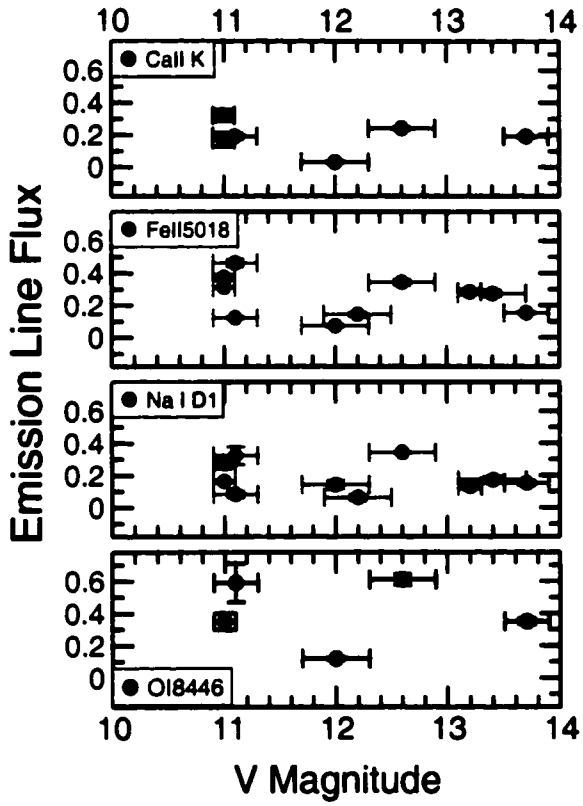

Figure 4.11 Integrated emission line flux of metal lines shown in figure 4.10 and integrated over the line. Units of flux are as in Fig. 4.7. The 19OCT97 epoch is not shown.

4.5.5 Unique Epoch: 19OCT97

The 19OCT97 spectrum is unique among the epochs presented here. The EW of [OI] and the signal-to-noise of the spectrum both indicate that the system is in the bright state, in agreement with the one AAVSO photometry measurment of $V = 10.9$ obtained 0.7 days after the spectral epoch and $V = 11.1$ obtained 1.35 days before. Six additional photometry points, including one taken at CrAO four days later, indicate that RR Tau brightened slightly and remained bright, between $10.6 \leq V \leq 10.8$, for ~ 5 days after the spectrum was taken.

This epoch displays a mix of faint and bright spectral features in the normalized spectum shown in Figure 4.4.1. The emission seen in [OI], the absorption in the HeI 5876 and NaI D lines and the upper level Balmer lines (Hγ to Hϵ) are similar to other bright spectra. However, the Hα and Hβ lines show strong increase in equivalent width and the FeII(42) triplet, OI 8446, and upper level Paschen lines are filled in, similar to the intermediate spectrum on 14FEB98. The CaII K line is seen in absorption, but with smaller EW than other bright spectra (see Fig. 4.4). The CaII IR triplet lines stand out in emission, although this may be primarily a result of the filled in Paschen lines.

Given that the continuum is bright at this epoch, these changes in equivalent width indicate significant changes in line flux at this epoch. We recover the circumstellar flux in the Balmer lines and metal lines as described in §4.5.3 and §4.5.4, respectively. That is, a Kurucz profile is subtracted from the hydrogen lines, which removes the strong photospheric component, and a template epoch is subtracted from the metal lines, which removes the strong absorption component (non-photospheric) seen at other bright epochs. The circumstellar emission recovered is shown in Figure 4.12, compared to another bright epoch (15JAN98) and the intermediate epoch of 14FEB98. In all of the hydrogen lines and most of the metal lines, the flux is $\sim$3 times brighter on 19OCT97. Interestingly, no increased emission is seen in HeI 5876 or NaI D. The Balmer emission is double-peaked with a much stronger red-shifted component. The red peak in the Hβ, Hγ and Hδ lines has a recession velocity of ~ 50 km s^{-1} while the peak in Hα is ~ 120 km s^{-1}. The FeII(42) triplet emission is also red-shifted with approximately the same value as the upper level Balmer lines.

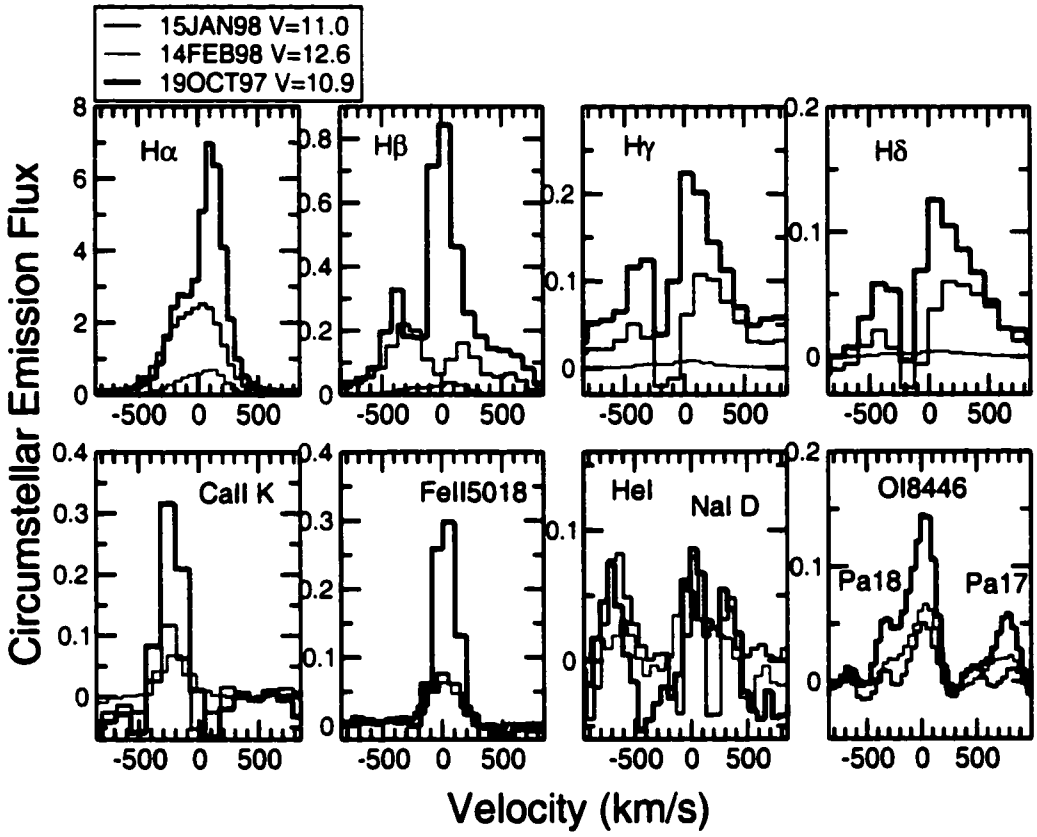

Figure 4.12 Emission flux on 19OCT97 (heavy line) compared to two other epochs, 15JAN98 and 14FEB98. Balmer lines (top panels) have had synthetic Kurucz profiles subtracted from them (§4.5.3); metal lines (bottom panels) have had a bright epoch template subtracted (§4.4). Units of flux are as in Figure 4.8.

In the blue forest of weak metal lines between 4000 and 4600 Å, we see a subtle change in the stable absorption features identified and discussed in §4.5.1. On 19OCT97, when the star is $\sim$ 10% brighter than its "normal" state (V= 11), several of these lines have somewhat smaller EW (see Table 4.2). The decrease is not seen in all lines, as would be expected for a veiling event. Instead, the effect appears preferentially in the cooler lines of TiII and FeII, while the MgII 4481Å line is unchanged. The 4470 Å line, a blend of HeI and TiII, is weaker and red-shifted relative to other bright epochs, closer to the HeI 4471 Å line. This effect, while very small, may indicate a slight shift in the continuum temperature at this slightly brighter epoch. As in other bright epochs, the HeI line shows an inverse P Cygni profile, i.e., redshifted absorption, suggesting absorption from infalling gas.

The strong increase in circumstellar emission, the red-shifted velocities of the Balmer lines, and the subtle change in the weak metal lines lead us to speculate that we are witnessing an accretion event at this unique epoch. Future modeling of this spectral emission may be able to constrain the temperature, density, and volume of the emitting gas.

4.6 Constraining Variability Models

4.6.1 Variable Extinction

The results presented here are consistent with a stable, multi-component (i.e., star, disk, circumstellar shell, wind) system in which the photometric and much of the spectral variability is caused by a featureless absorber along our line-of-sight. This obscuring screen acts as "nature's coronagraph", blocking the continuum source and some portion of the circumstellar environment. In this context, our spectra provide information on how each of the components in RR Tau is affected by the obscuration. Lines arising in the photosphere, (Balmer wings and weak metals) change with the continuum, resulting in constant EW, as is observed. The constant flux observed in [OI] indicates that the majority of the low density wind exists outside of the obscured region.

Our analysis of the strong metal lines indicates that the obscuration blocks the circumstellar gas producing the absorptions lines, revealing a tenuous emission line region around the star. The emitting volume must subtend a much larger solid angle than the obscuring

screen, which in turn is larger than the absorption region. Future modeling of the circumstellar line emission (Fig. 4.11) should yield the gas temperature, density, and radial extent.

Similar decreased absorption and increased emission in FeII lines in the UV is also documented for UX Ori and BF Ori (Eaton & Herbst 1995). This is referred to as "lifting the iron curtain" of UV absorption lines at minima. They deduce a large FeII emission region ($10^{14} - 10^{15}$ cm) around these stars.

Circumstellar Balmer emission lines become single-peaked for $V > 12$, as also reported during the minima of HR 5999 (Tjin a Djie *et al.* 1989). This indicates that the part of the circumstellar envelope responsible for the self-absorption is blocked by the obscuration (1), similar to the result we have found for the strong metal lines. However, we do not see a significant decrease in the Hα line flux, suggesting that the absorption is only a small component of the total flux.

In principle, the spectral behavior observed during minimal light can provide information on the nature of the obscuring screen itself. The multi-color photopolarimetric behavior of the system indicates a dusty absorber. Depending on the physics of the obscuring particles, one might expect to see additional gas absorption features in faint epoch spectra, which we do not detect. We have illustrated in §4.5.4 through very simple arguments that these data can constrain the physical extent of the obscuration. With detailed modeling, we expect that these data can place additional constraints on the location, density and composition of the obscuring matter.

4.6.2 Variable Luminosity

The other possible explanation for the photometric variability requires the continuum source itself to be variable, i.e., the bright state continuum source is physically distinct from the faint continuum source. One possibility is a binary system with a variable primary star such that the secondary star is visible during the primary star minima. This scenario would clearly predict a change in spectral type with system brightness, which we do not observe. We also find no evidence that RR Tau is a binary in either our photometric or spectroscopic

data.

In the variable accretion model suggested by Herbst & Shevchencko (1999), minima occur when the accretion is in a low state and a change in opacity causes the optically thick accretion region (which dominates the continuum at bright epochs) to become optically thin. One would expect a change in the observed spectral type of the system between photometric minima and maxima, although the interplay between changes in temperature and changes in surface area have not been modeled. In our analysis of the Balmer wings, we found that a simultaneous change to higher T_{eff} and lower surface area (higher log g), can go undetected. Lacking quantitative predictions, we suggest that an optically thick accretion region would exhibit higher T_{eff} and *larger* surface area (smaller log g) than the underlying star. The stable absorption lines in the blue forest argue against a change in T_{eff}. In addition, we do not see a correlation between Hα flux and system brightness which argues against the variable accretion model if Hα is an accretion diagnostic.

There is evidence for infalling matter in the inverse P-Cygni profiles of the CaII IR triplet and HeI 5876 lines, and we suspect accretion in the increased red-shifted emission seen on 19OCT97. However, if this is an accretion event, the increase in the V band is only $\sim$10%, nowhere near the factor of 10 change in brightness required between photometric maxima and minima. If the same circumstellar gas producing the variable metal lines (§4.5.4) goes from absorption to emission due to a decreasing continuum, we would expect significantly more emission at faint epochs. The kinematics of the absorbing and emitting gas is key to addressing this point– our data on the FeII(42) triplet lines suggest that the emission is blue-shifted with respect to the absorption. Higher resolution data is needed to quantitatively address this question.

4.7 Conclusions

We analyze twelve spectra of the UXOR star RR Tau spanning a period of 1.5 years and a factor of 10 variation in optical brightness. The data include 5 bright ($V \approx 11$) epochs, 3 intermediate ($12.0 \leq V \leq 12.6$), and 3 faint epochs ($13.2 \leq V \leq 13.7$). One unique epoch with $V = 10.9$ is considered separately.

Based solely on empirical analysis, free of model assumptions or parameters, we reach these conclusions.

1. The spectral type of the system is invariant under a factor of 10 change in brightness (§4.5.1).

2. Emission from the extended low density wind ([OI], [FeII]) exhibits constant flux with no dependence on V magnitude (§4.5.2).

3. Circumstellar hydrogen emission flux is variable, but independent of Vmagnitude. However the line profiles of Hα and Hβ become singly-peaked at faint epochs, indicating an absence of central absorption during photometric minima (§4.5.3).

4. Circumstellar gas responsible for permitted lines of CaII, FeII, NaI and OI is affected by photometric minima such that strong absorption in these lines disappears in concert with the stellar continuum. These metal lines are filled in by emission when the system reaches $\sim$ 10% of maximum light (§4.5.4).

These results are consistent with a variable extinction model in which an occulting screen obscures the star and some fraction of the circumstellar gas (initially responsible for the metal absorption lines). The screen does not occult the low density wind ([OI]), the bulk of the circumstellar hydrogen, or the region producing the weak metal emission. Our analysis show that the occulting screen is larger than the star but that the circumstellar envelope is significantly larger than the screen (§4.5.4). In the context of this model, the large temporal coverage, spectral range, and photometric range of these data offer the possibility of further constraining the location of the obscuring screen with respect to these circumstellar environments. Our results are not easily explained in terms of a variable accretion model.

In five of the six bright spectra spanning 1.5 years, the spectral features are very similar. However, one bright spectrum when the star is $\sim$10% brighter than its average bright state shows a three-fold increase in circumstellar hydrogen and metal emission, specifically CaII K, FeII(42) triplet, and OI 8446. We tentatively associate this epoch (19OCT97)

with a variable accretion event, independent of the mechanism associated with the deep photometric minima.

These spectra point out the importance of considering multi-epoch observations when doing spectral analysis of these volatile young systems.

Chapter 5

SPECTRAL VARIABILITY II: AB Aur, UX Ori, AND CQ Tau

5.1 Introduction

This chapter describes the spectral observations of three other monitoring targets: AB Aur, UX Ori, and CQ Tau. The first two of these stars are prototypes of their classes: AB Aur is the prototype Herbig Ae star; and UX Ori is the prototype (and namesake) of the UXORs. Both stars have been studied extensively in the literature. AB Aur, UX Ori, and RR Tau (Ch. 4) are all early A stars and believed to be similar in age, 2 - 4 Myr (Natta *et al.* 1997). CQ Tau is an F2 star that is also a member of the UXOR class. It is estimated to be somewhat older, >10 Myr (Rostopchina 1999).

The photometric behavior of these three stars is discussed in Chapter 2. AB Aur is photometrically stable, with $\Delta V \leq 0.25$ for the past ~20 years. It is known to vary spectroscopically and we have included it in our monitoring program to compare its variability (as a non-UXOR star) with the variability seen in the three UXOR stars (including RR Tau in the previous chapter). UX Ori and CQ Tau are both lower amplitude variables than RR Tau, with $\Delta V \leq 2.2$. We have poor photometry coverage of UX Ori and so can not report on correlated changes with system brightness, but discuss the behavior of the lines relative to each other. The spectra of CQ Tau are well matched with photometry measurements and span $\Delta V \simeq 0.7$. None of these three stars shows the dramatic spectra variability observed in RR Tau in our spectra, but none of the spectra capture as wide a range in optical brightness as we observed in RR Tau.

One additional star, CO Ori, was also observed on multiple epochs. CO Ori is a G5 star and a visual binary. The primary star exhibits strong photometric variability and CO Ori is often considered a UXOR star. The spectra show an increase in EW of the Balmer and CaII lines during photometric minima. However, we can spatially resolve the two components

and find that the strong Balmer and CaII emission are coming from the secondary. Besides very strong line emission, the secondary star exhibits a very red continuum apparent only in the reddest passband of these spectra, $\lambda > 8000$Å. We do not detect any strong emission lines in the photometrically variable primary star. Therefore we submit that CO Ori is not a UXOR star, but rather a variable primary star and a low mass pre-main sequence secondary star. CO Ori is not discussed further in this chapter. It is nonetheless interesting in its own right and will be the subject of a separate contribution.

5.2 The Spectra

The observations and data reduction are as described in Chapter 3. A log of observations of the stars in this chapter is given in Table 5.1. As with RR Tau, most of these observations were obtained during short time blocks, typically only an hour. For this reason, flux standards were not observed on all dates and therefore the data are not flux calibrated. Instead, data on all epochs have been normalized using a low order Legendre fit to the continua.

The spectra at all epochs for each of the three stars (AB Aur, UX Ori and CQ Tau) are shown in Figure 5.1. Each epoch is labeled, as are prominent spectral features. The spectra of CQ Tau are also labeled with the estimated V magnitudes at each epoch, discussed below.

5.2.1 AB AUR

AB Aur shows a number of lines in emission at all epochs. These include the cores of Hα and Hβ, the CaII IR triplet, HeI 5876, NaI D, and a weak [OI] line. The upper level Paschen lines are also filled in with emission. Prominent absorption is evident in the Balmer and Paschen lines, and the MgII 4481Å line. A number of weak absorption lines are also seen. Because the photometric behavior of AB Aur is very stable, with variations in flux of $\leq$ 10% ($\Delta V \leq 0.1$ mag), any significant changes in EW seen in these normalized spectra are due to changes in line flux, not in the continuum.

The spectroscopic behavior of this star has been studied extensively. A detailed line list identifying photospheric and non-photospheric lines is provided by Böhm & Catala (1993). AB Aur shows a number of circumstellar lines in emission, including HeI 5876, NaI D,

Table 5.1. Apache Point DIS Observations of Variability Targets

Object	Spec.Type	N_{OBS}	Epochs [UT]
AB Aur	A0	9	19Oct97,20Nov97,17Jan98,
			26Jan98,07Feb98,21Mar98,
			01Feb99,04Feb99,31Mar99
UX Ori	A2/3	10	19Oct97,20Nov97,24Jan98,07Feb98,
			10Mar98,25Mar98,04Jan99,
			04Feb99,06Mar99,29Mar99
CQ Tau	F2	13	19Oct97,20Nov97,15Jan98,24Jan98,
			07Feb98,24Feb98,05Mar98
			12Mar98,21Mar98,04Jan99
			01Feb99,06Mar99,29Mar99
CO Ori	G5	13	19Oct97,20Nov97,24Jan98,14Feb98,
			24Feb98,05Mar98,10Mar98,
			12Mar98,21Mar98,04Jan99,
			28Feb99,25Mar99,31Mar99

Figure 5.1 Multi-epoch DIS Spectra of AB Aur, UX Ori and CQ Tau. All spectra are normalized, and labeled with the UT date of observation. CQ Tau spectra are also labeled with the approximate visual magnitude. Prominent spectral features are indicated along the bottom of each plot.

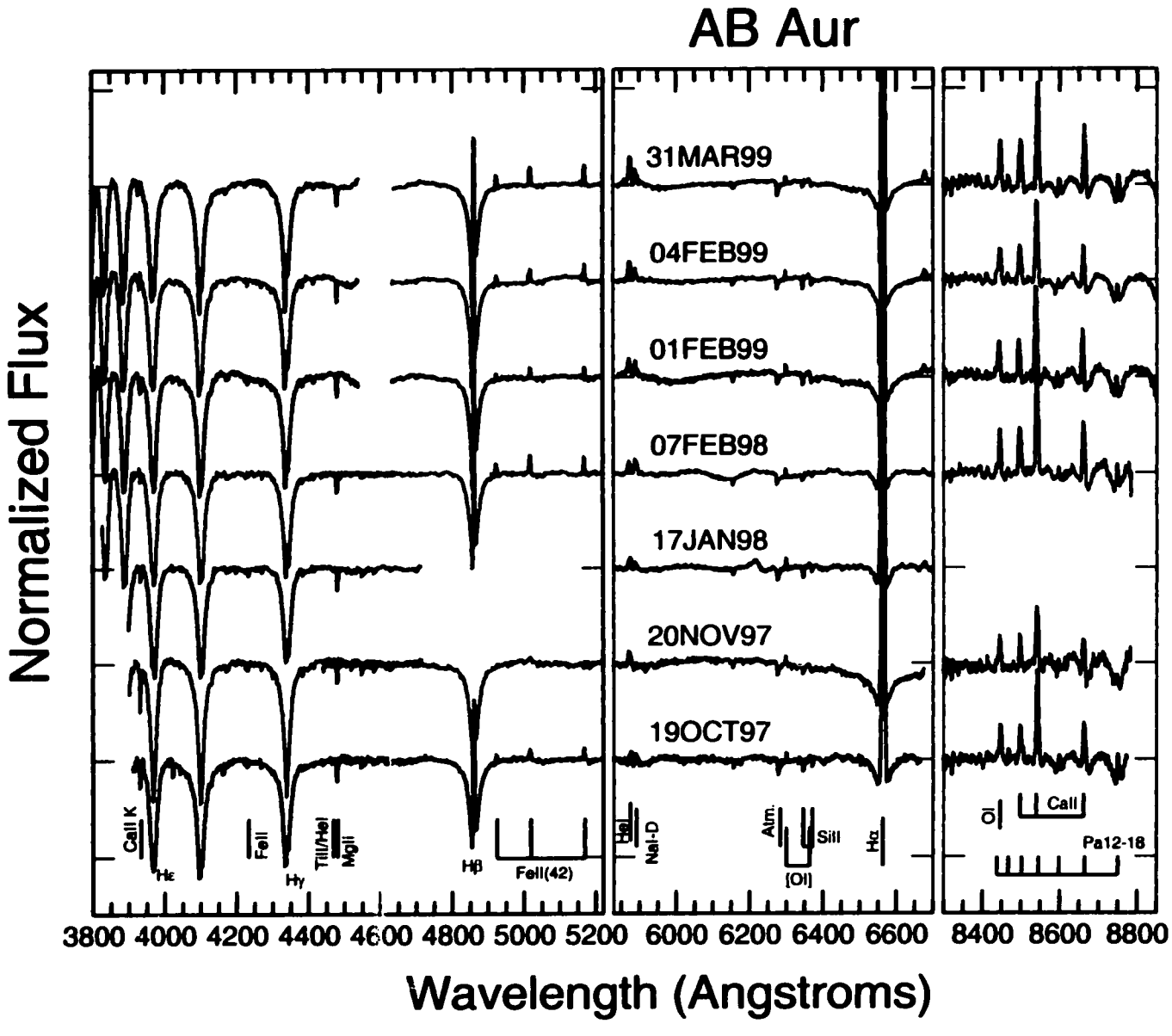
AB Aur
Normalized Flux
31MAR99
04FEB99
01FEB99
07FEB98
17JAN98
20NOV97
19OCT97
CaII K
Hε
FeII
Hγ
TiII/HeI
MgII
Hβ
FeII(42)
HeI
NaI-D
AlIII
SiII
[OI]
Hα
OI
CaII
Pa12-18
3800 4000 4200 4400 4600 4800 5000 5200 6000 6200 6400 6600 8400 8600 8800
Wavelength (Angstroms)

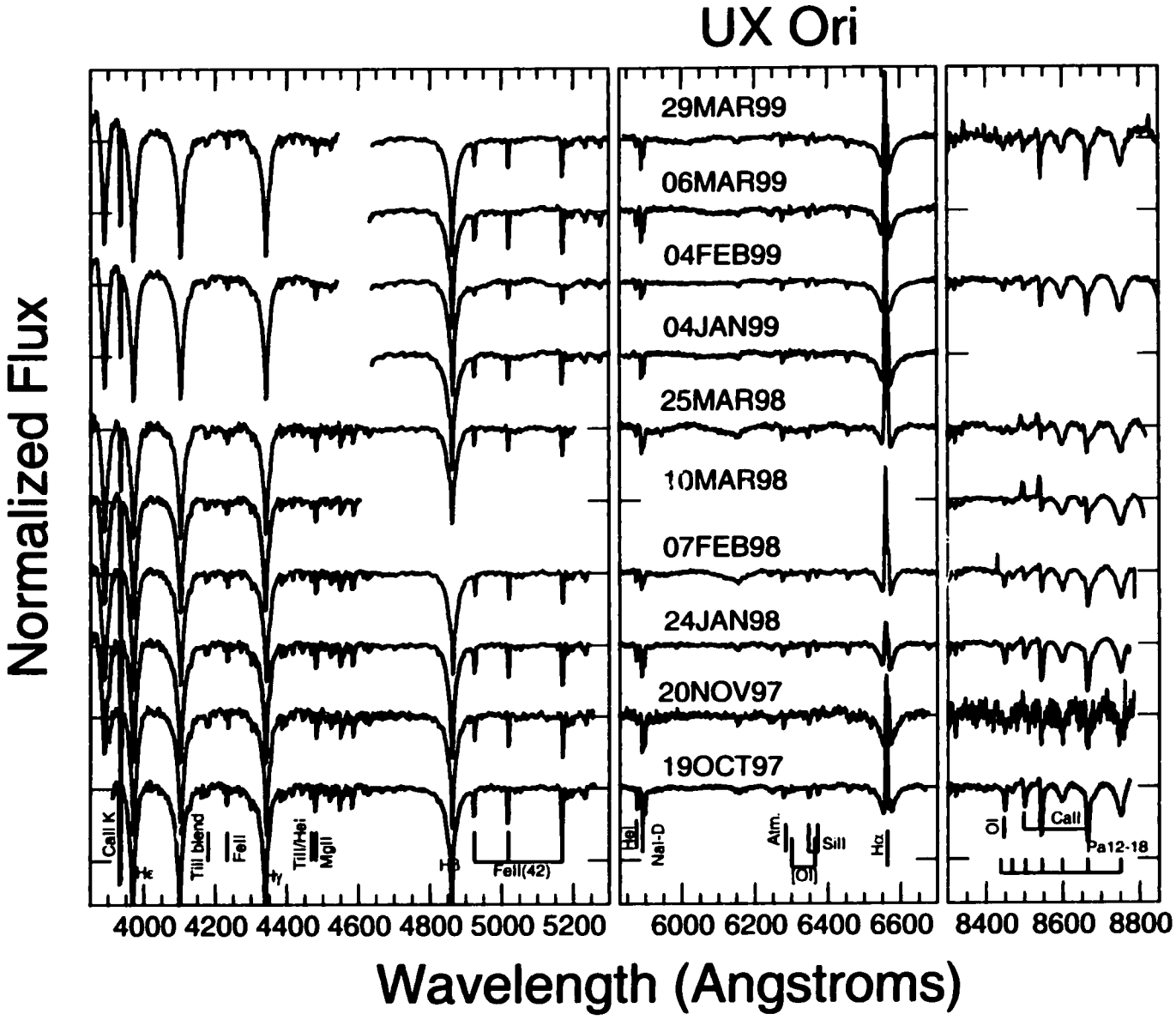
UX Ori
29MAR99
06MAR99
04FEB99
04JAN99
25MAR98
10MAR98
07FEB98
24JAN98
20NOV97
19OCT97
Normalized Flux
Wavelength (Angstroms)
4000 4200 4400 4600 4800 5000 5200
6000 6200 6400 6600
8400 8600 8800
CaII K
Hε
TiII blend
FeII
TiII/HeI
MgII
Hγ
FeII(42)
HeI
NaI-D
AlIII
[OI]
SiII
Hα
OI
CaII
Pa12-18

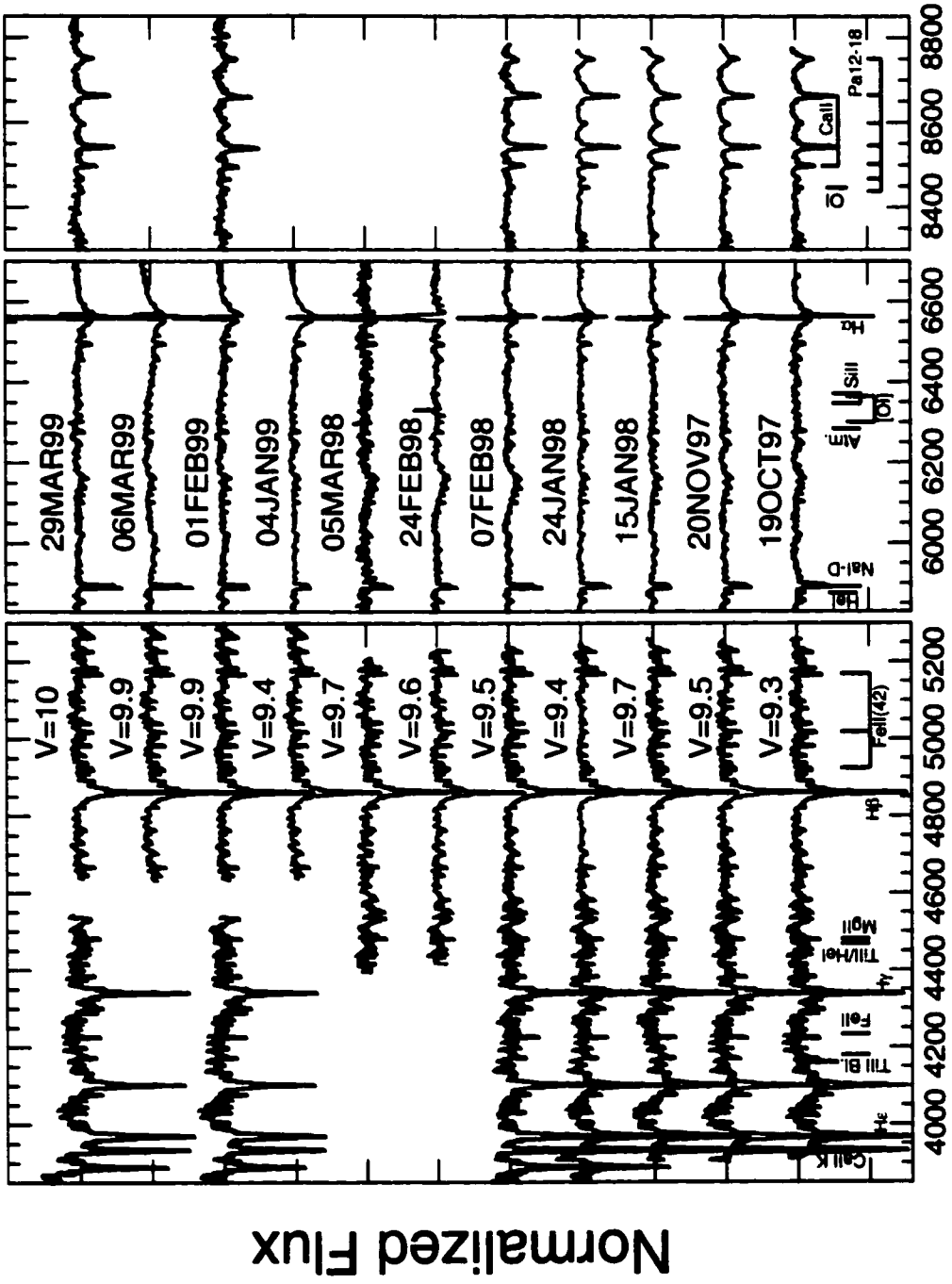
CQ Tau
Normalized Flux
Wavelength (Angstroms)
V=10
V=9.9
V=9.9
V=9.4
V=9.7
V=9.6
V=9.5
V=9.4
V=9.7
V=9.5
V=9.3
29MAR99
06MAR99
01FEB99
04JAN99
05MAR98
24FEB98
07FEB98
24JAN98
15JAN98
20NOV97
19OCT97
CaII K
He
TiII BL
FeII
TiII/HeI
MgII
Hγ
Hβ
FeII(42)
HeI
NaI-D
SiII
OI
CaII
Pa12-18
4000 4200 4400 4600 4800 5000 5200
6000 6200 6400 6600
8400 8600 8800

CaII K, CaII IR triplet and FeII(42) triplet. High spectral and time resolution studies have shown that both circumstellar and photospheric features are variable on timescales as short as hours (Catala *et al.* 1999; Catala *et al.* 1997; Böhm *et al.* 1996). These authors find periodic behavior in both the HeI 5876 line, with a period of 45 hours, and in the photospheric lines, with a period of 34 hours. They latter is matched by the rotational period of the star, and suggests azimuthal asymmetry in the star's atmosphere. They attribute the HeI 5876 line with a wind, and conclude that the longer period is either due to an equatorial wind with the star rotating faster at the equator, or a disk wind originating at 1.6 stellar radii (Catala *et al.* 1999). They find the variability in the Hα line to be psuedo-periodic, but complex.

Our spectra show emission in the cores of Balmer lines, at least through Hγ. Variability is apparent in Hα and Hβ (discussed below). The metal lines of the FeII(42) triplet, HeI 5876, NaI D, OI 8446 and CaII IR triplet are seen in emission on all epochs, and weakly variable. A weak [OI] line is detected with constant strength on all epochs. We have observed this star in order to contrast its behavior, as a photometrically stable star, with that of the UXOR stars. AB Aur does not show the dramatic variations seen in RR Tau and described in the last chapter. Never the less, spectroscopic variability is apparent. On 20NOV97, the FeII(42) triplet and NaI D lines essentially disappear in emission, at the same time that the circumstellar Balmer emission is much weaker. However, the HeI 5876, OI 8446 and CaII IR triplet lines are not significantly different on this epoch. The correlated variations clearly seen in RR Tau are not apparent in our AB Aur spectra.

5.2.2 UX ORI

The spectra of UX Orionis at all epochs are shown in Figure 5.1b. Although there are small variations in the strength of metal lines, and stronger variability in the cores of Hα, the spectra are generally very similar. The available photometry data for this star over the period of the spectral observations is poor (Fig. 5.2). UX Ori appears to be in or near bright state when most of the spectra were obtained, except possibly 24JAN98 (JD# 837 in Fig. 5.2), however the photometry points around that date are more than 2 days prior to

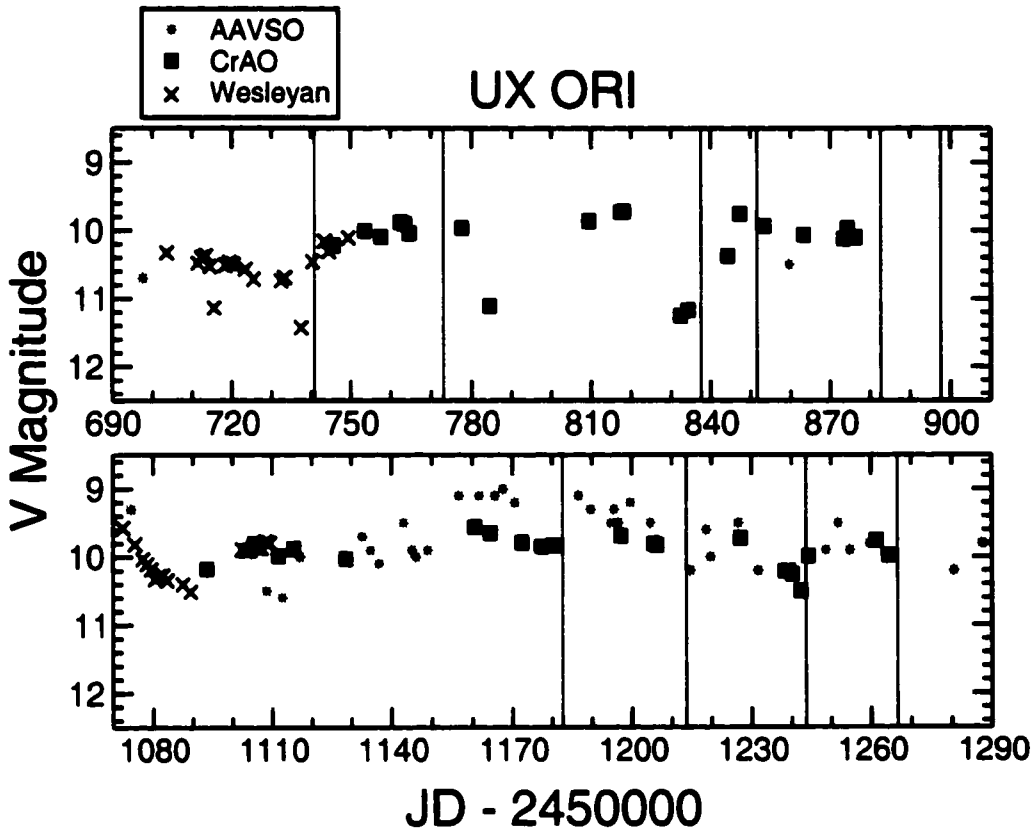

Figure 5.2 Light curve of UX Ori 1997 - 1999, combining three databases: Wesleyan (crosses), CrAO (squares) and AAVSO (stars). Epochs of spectral observations are shown as vertical lines.

the spectral observation. We can confidently determine its V magnitude on just two epochs: 10.5 on 19OCT97 (JD# 740) and 10.0 on 06MAR99 (JD# 1243). We find no features in the spectra on any of these three dates that appears linked to a change in the continuum. In particular, the [OI] line seen weakly in emission on all epochs, which was shown to be a reliable brightness indicator in RR Tau, shows essentially constant EW.

Without knowing the brightness state of the star, we can not conduct the type of analysis that was done for RR Tau in the previous chapter. If the star is in its bright state, or very near it, on all epochs, as suggested by the constant EW of [OI], it is not surprising that the spectra are very similar. The strongest variations are seen in the EW of the Hα core, while the upper level Balmer and Paschen lines do not change significantly. There is also

noticeable variations in the HeI 5876 and CaII IR triplet lines. Unfortunately, the epochs when these lines appear to be in emission (04JAN99 and 10MAR98, respectively) the data is missing in the other spectral regions prohibiting comparison. The FeII(42) triplet, NaI D, and OI 8446 lines are always in absorption with only small EW variations. However, it appears that these same lines that behaved together in RR Tau, also behave together in UX Ori. The variability is small, but similar across these lines. In addition, there are a number of weaker metal lines primarily between 4000 - 4600 Å that are associated with the spectral type of the star and appear to be more constant. The behavior of the hydrogen and CaII lines is discussed further in the next section.

5.2.3 CQ Tau

CQ Taurus is an F2 star and a known UXOR, with variable polarization of 6.4% (Yudin 2001). In Chapter 3 we assigned CQ Tau to Category III, meaning that it shows very few circumstellar features in its spectrum other than Hα in emission. It is also one of the oldest UXOR stars, with age estimates ranging from 10 Myr (Rostopchina *et al.* 1997) to >30 Myr (Natta *et al.* 2000b). The spectrum is rich in metal lines, as expected for its later spectral type. With the exception of Hα and Hβ, the spectra at each epoch look very similar. However, the wealth of lines makes detection of small variations in EW in these moderate resolution data difficult. No [OI] is detected in the star, and the FeII(42) triplet lines are essentially photospheric. A weak HeI 5876 line is detected which is not photospheric, and small EW variations are seen in the NaI D and CaII IR triplet lines.

For CQ Tau we have good photometric coverage during our spectral observations (Fig. 5.3). We have estimated the V magnitude at each spectral epoch in the same way as was done for RR Tau in the last chapter. Details of the light curve are shown in Figure 5.4 and the resulting magnitudes are listed in Table 5.2. Unfortunately, the intrinsic variability detected is ~1 magnitude, and errors are 0.2 - 0.3 magnitudes at V. Therefore fine distinctions between brightness levels and subtle line changes are probably not warranted. Variations in the cores of Hα are fairly dramatic and are discussed further in the next section.

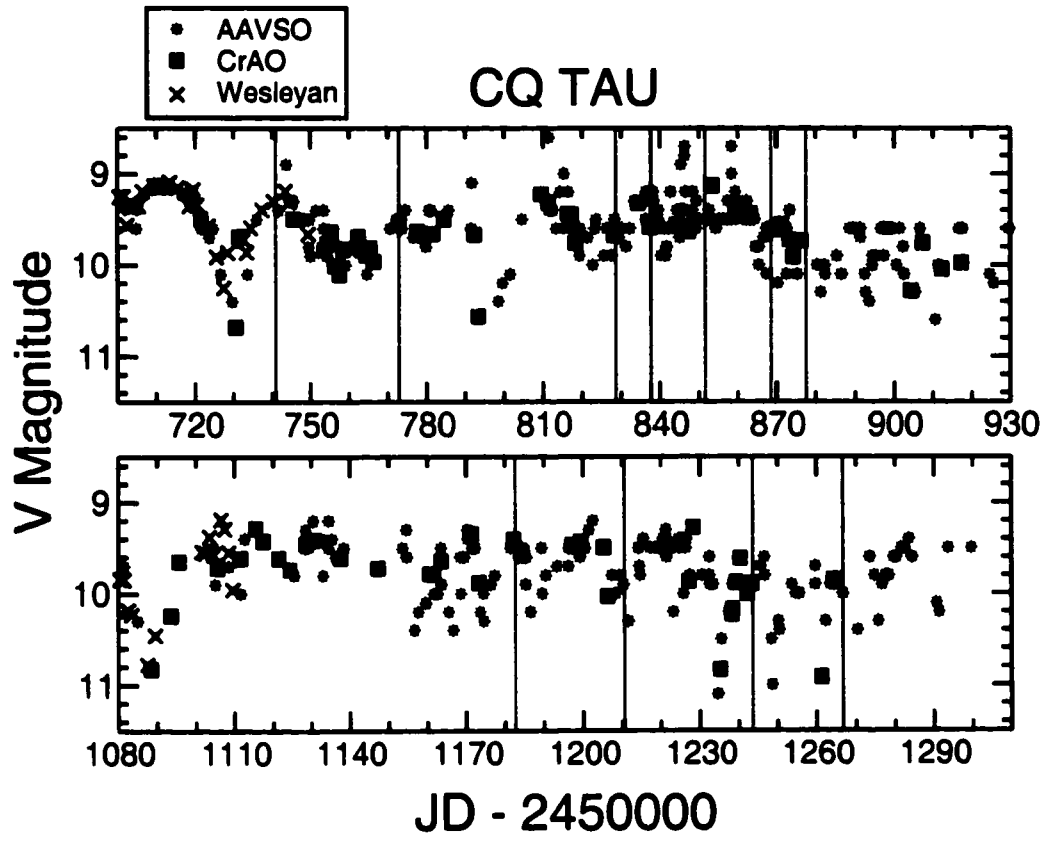

Figure 5.3 Light curve of CQ Tau 1997 - 1999, combining three databases: Wesleyan (crosses), CrAO (squares) and AAVSO (stars). Epochs of spectral observations are shown as vertical lines.

5.3 Discussion

5.3.1 Circumstellar Hydrogen

To isolate the circumstellar contribution to the Balmer lines, we have subtracted an appropriate Kurucz profile from each star, as described for RR Tau in the last Chapter. The stellar parameters used for each star are shown in Table 5.3. Values are rounded to the closest Kurucz Model grid point from those given in Grinin *et al.* (2001) for the UXOR stars, and Böhm & Catala (1993) for AB Aur. The wings of the Balmer Hβ, Hγ, and Hδ lines are shown for all epochs in Figure 5.5. The Kurucz spectrum for each line is overlaid on the data. The synthetic Kurucz profiles provide an excellent fit to the lines of AB Aur

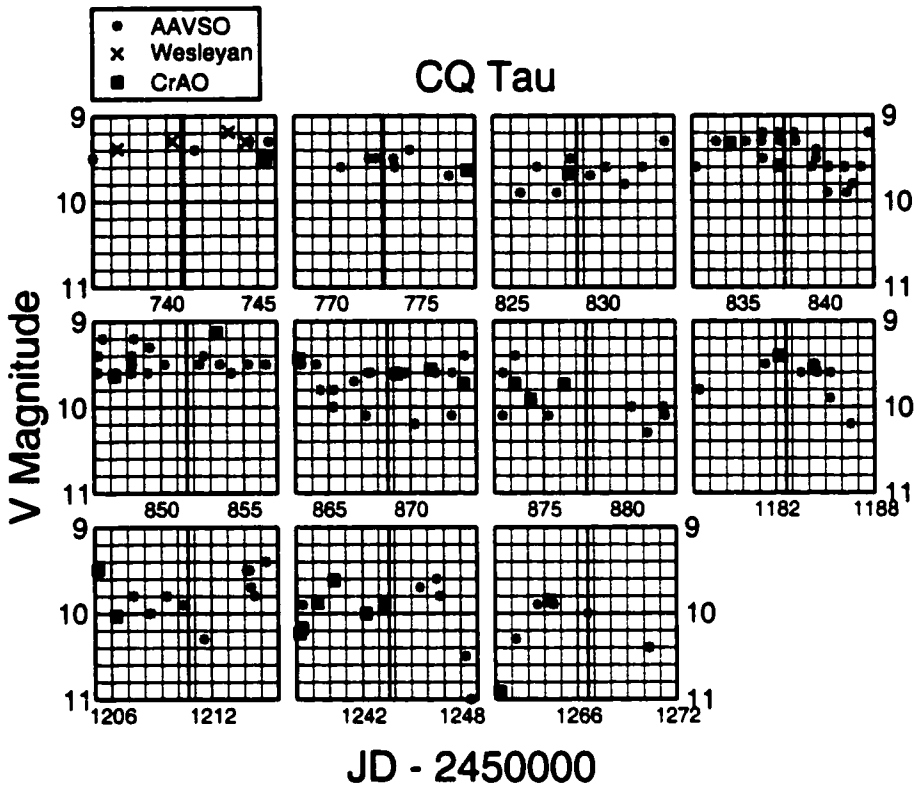

Figure 5.4 Detail of CQ Tau photometry showing datapoints within 5 days of each spectral observation, indicated by vertical blue lines.

and UX Ori. The fit to CQ Tau is less good, primarily due to the large number of strong metal lines in this later type star, which are not included in the Kurucz Balmer profiles. As with RR Tau, we find no measurable change at any epoch for the wings of the Balmer lines in each star. Thus we find no evidence for a change in the spectral types of these stars in our spectra.

After subtracting the Kurucz spectra, the residual flux represents the circumstellar contribution to the hydrogen lines. The circumstellar Hα and Hβ emission is shown at all epochs for each of the three stars in Figure 5.6.

In AB Aur, the circumstellar Hα and Hβ fluxes vary by a factor of two, but the emission profiles appear unchanged. The profiles are singly peaked and symmetric around the system velocity at all epochs. The central peaks and the full width at zero intensity are the same in Hα and Hβ, with velocity $\sim$600km s^{-1}. There is no evidence of central absorption, seen

Table 5.2. Visual Magnitudes for CQ Tau

Epoch	V	Uncertainty	Epoch	V	Uncertainty
19 October 1997	9.3	.1	05 March 1998	9.7	.3
20 November 1997	9.5	.1	04 January 1999	9.4	.1
15 January 1998	9.7	.1	01 February 1999	9.9	.3
24 January 1998	9.6	.2	06 March 1999	9.9	.1
07 February 1998	9.5	.2	29 March 1999	10.	.3
24 February 1998	9.6	.1			

Table 5.3. Stellar Parameters used for Kurucz Spectra

Object	T_{eff}	$\log g$	$v \sin i$	Reference
AB Aur	10000	4.0	80	Böhm & Catala (1993)
CQ Tau	7000	3.5	90	Grinin *et al.* (2001)
RR Tau	9500	3.5	140	Grinin *et al.* (2001)
UX Ori	9500	4.0	140	Grinin *et al.* (2001)

Note. — Values from references are rounded to the closest Kurucz model.

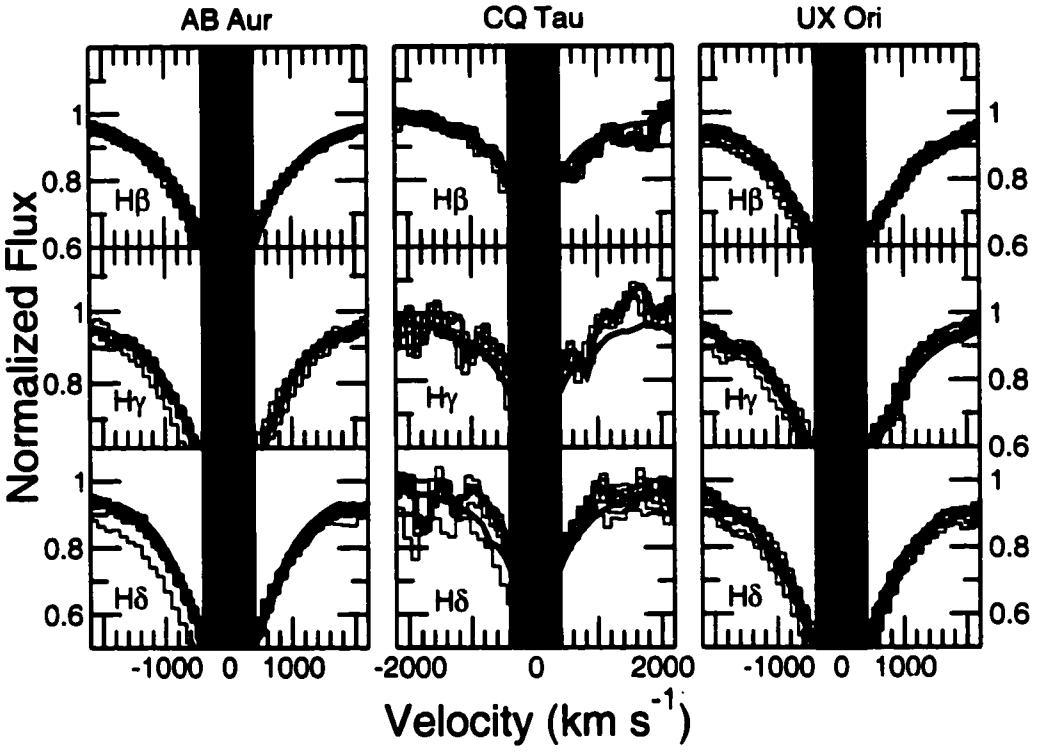

Figure 5.5 Hβ, Hγ, and Hδ wings for AB Aur, CQ Tau, and UX Ori. Data for each epoch are shown in blue. Overlaid in black are the Kurucz line profiles. The Kurucz model runs do not include all metals, resulting in a poorer fit to CQ Tau, an early F star.

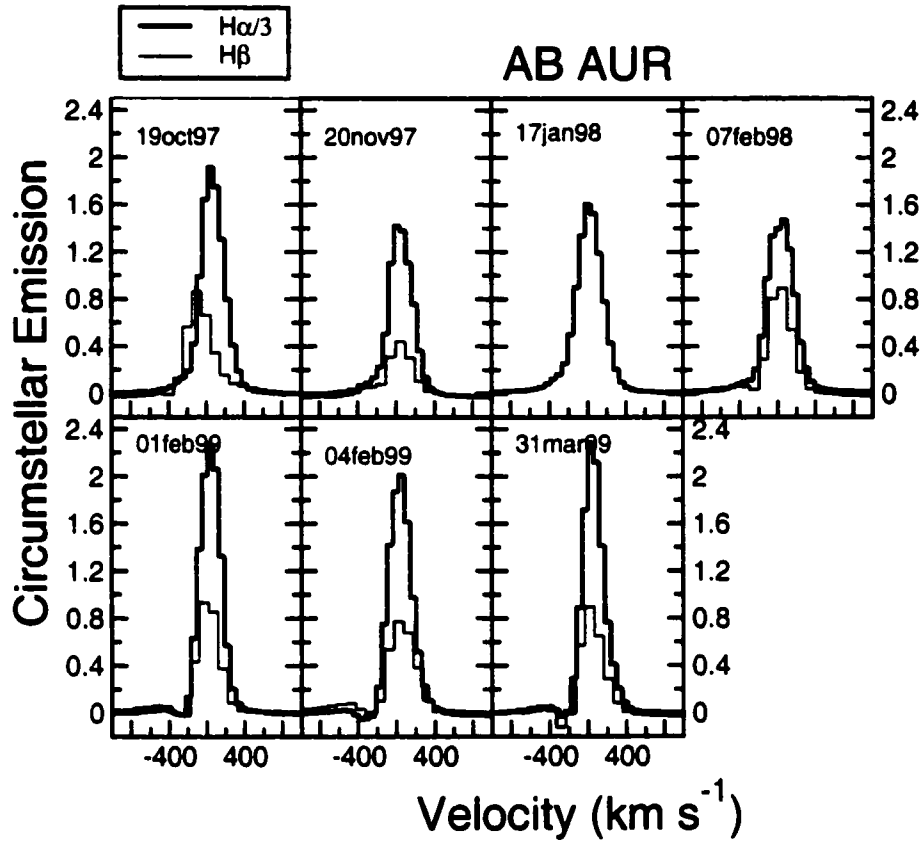

Figure 5.6a AB Aur circumstellar Hα and Hβ at each epoch.

to some extent in all three UXORs. There is a small but distinct dip on the blue side of the line, observed on three epochs in 1999. This P Cygni feature, indicative of outflow, is present in both Hα and Hβ at the same velocity, $\sim$ 300 km s^{-1}. It is not seen in the four epochs in 1998. The ratio of Hα to Hβ in AB Aur is roughly 6:1 on all epochs, a Balmer decrement a factor of 2 steeper than expected for hydrogen recombination. This suggests that the Hα line is pumped by collisional excitation, indicating high density origin. These profiles and the other emission lines seen in this star, including [OI], indicate that the Balmer emission in AB Aur is dominated by wind emission.

The circumstellar hydrogen emission lines in UX Ori and CQ Tau are similar. Both stars exhibit redshifted absorption in Hβ at all epochs, and double-peaked or asymmetric Hα. The blue peaks are always stronger than the red, indicating a slightly red-shifted central

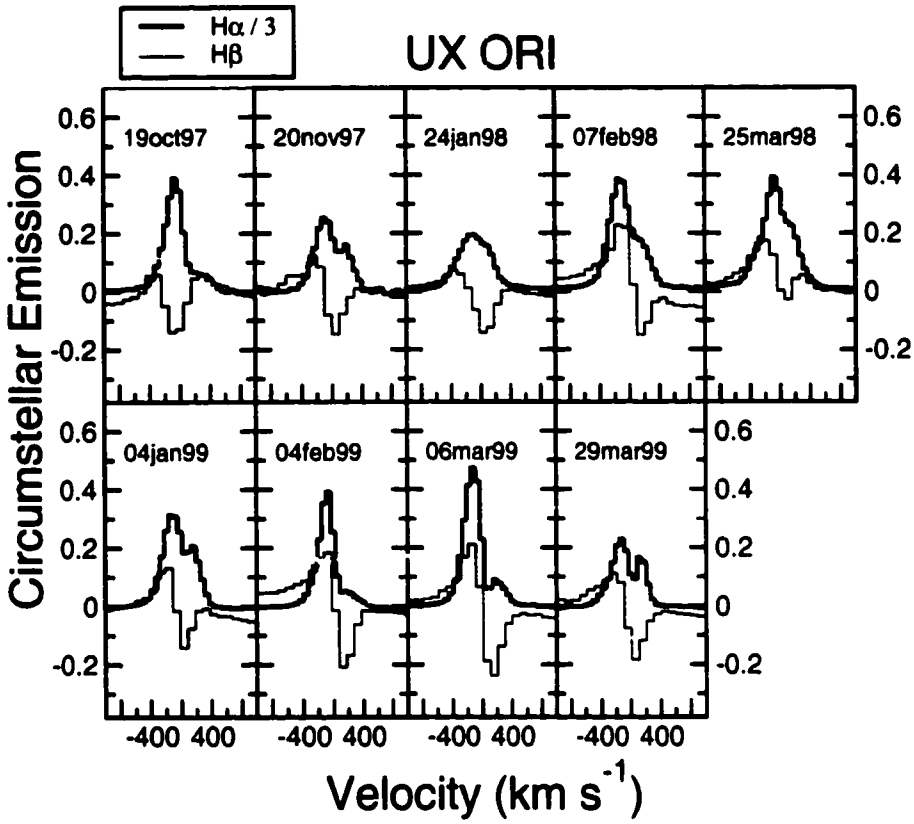

Figure 5.6b UX Ori circumstellar Hα and Hβ at each epoch.

absorption with velocity ~100km s^{-1}. Both lines, in both stars, are strongly varying. In CQ Tau, as in RR Tau, the variability observed in Hα and Hβ does not appear to be correlated with system brightness. The profiles in all three of the UXOR stars appear qualitatively different than the profiles observed in AB Aur. This may be a geometric effect, wherein the UXOR stars are seen more edge-on than AB Aur which has an inclination <45 degrees (Grady *et al.* 1999). Synthetic Hα profiles from magnetospheric accretion models in T Tauri stars indicate that system orientation is a major factor in determining the shape of hydrogen line profiles (Muzerolle *et al.* 1998b).

5.3.2 CaII IR Triplet

We now examine the CaII IR triplet lines in UX Ori. These lines exhibit similar profiles in UX Ori, RR Tau, and BF Ori (see Fig. 3.2). Hamann & Persson (1992) find that the CaII

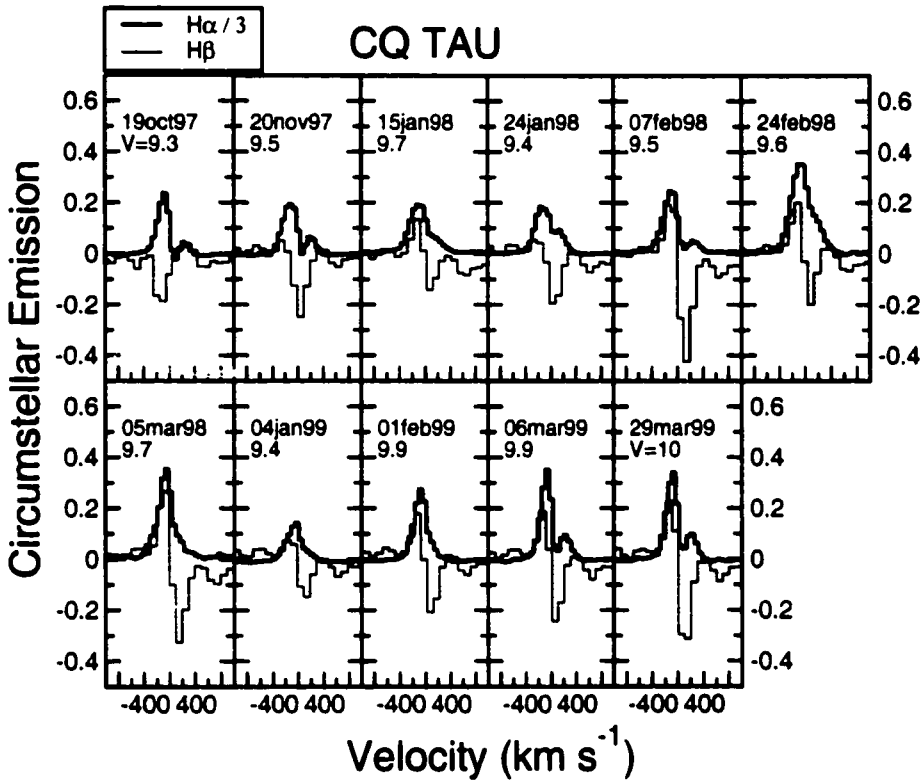

Figure 5.6c CQ Tau circumstellar Hα and Hβ at each epoch.

IR triplet lines of many Herbig stars originate in dense, optically thick emitting regions that can be several times the size of the stars. Their calculations are based primarily on stars showing strong CaII IR triplet emission, which does not include any of the UXOR stars discussed here. However, it is difficult to measure these lines in our moderate resolution spectra due to the severe blending of all three Ca II lines with the hydrogen Paschen lines of Pa13, Pa15 and Pa16.

Since the upper level Paschen lines in UX Ori are not varying significantly, we can more accurately subtract these lines from the spectra to uncover the shapes and fluxes of the CaII IR triplet. (Attempting this procedure with RR Tau was complicated by the variable Paschen emission.) We combine 7 epochs, excluding the low S/N spectrum of 20NOV97, to get a high S/N spectrum of the region. Gaussian line profiles are fit to the unblended Pa12, Pa14 and Pa17 lines, which bracket the lines blended with CaII. Using these Gaussians, we

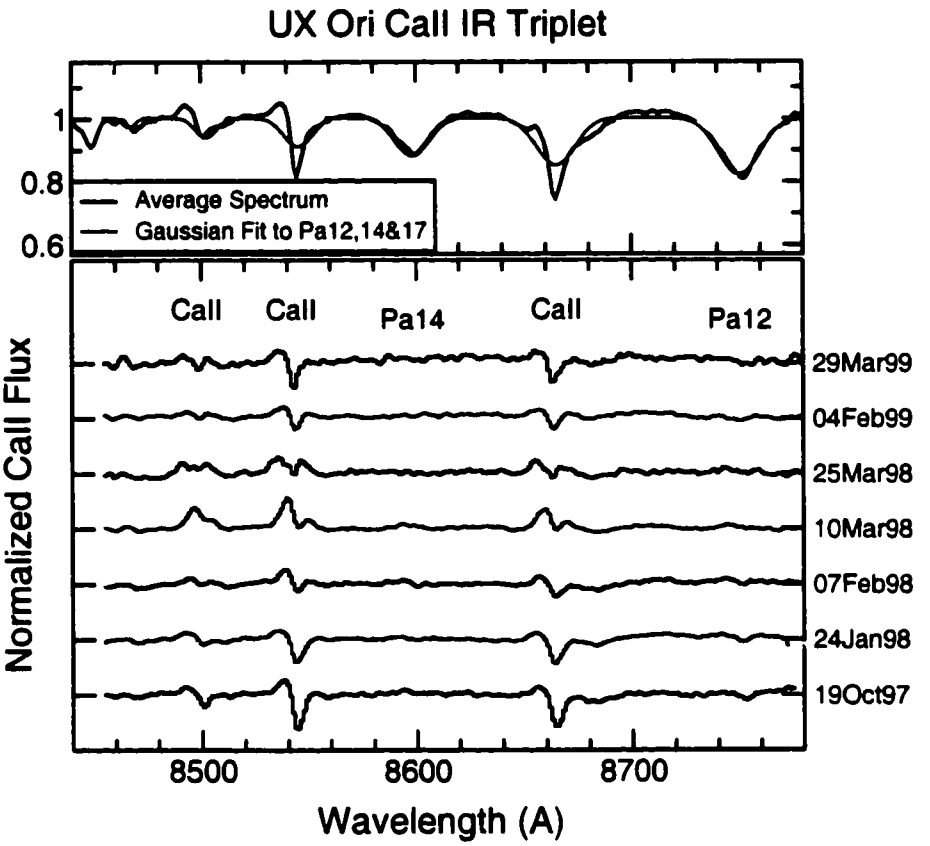

Figure 5.7 CaII IR Triplet: Paschen lines have been approximately removed by interpolating gaussian fits to Pa12, Pa14 and Pa17 (top panel). The difference spectra uncover the CaII emission on all epochs (lower panel). CaII lines are clearly inverse P Cygni, and variable.

interpolate between them to create a Paschen decrement from Pa12 to Pa17. The fit to the Paschen lines is shown in the top panel of Figure 5.7. The synthetic Paschen decrement is then subtracted from each epoch to expose the CaII lines. The Gaussian fits to the Paschen lines are approximate; however, as the same spectrum was subtracted from all epochs, the procedure is useful for uncovering variations in the CaII.

The difference spectra are shown in Figure 5.7. The accuracy of the Paschen line subtraction can be evaluated by the residual features around Pa12 and Pa14, which are essentially flat in all the residual spectra. The CaII lines are generally inverse P Cygni, or double-peaked with red-shifted central absorption. There is significant variability between the epochs, primarily in the emission component of the lines. The profiles appear very similar

to the Hβ line profiles (Fig. 5.3.1) on all epochs, suggesting a similar physical origin. The red-shifted absorption suggests infalling gas. Detailed analysis of these lines in UXOR stars, similar to that done by Hamann & Persson (1992) for other Herbig stars, requires higher resolution data but would be worthwhile to understand the behavior of the low ionization circumstellar gas.

5.3.3 Conclusions

We have presented repeated spectra of three additional stars: AB Aur, a non-UXOR, UX Ori, a young, early A type UXOR star, and CQ Tau, a slightly older early F type UXOR star. Our spectral coverage of these stars does not include the large range in system brightness that we captured with RR Tau (Ch. 4). It is not surprising then that these spectra do not show the dramatic spectral variations reported for RR Tau. In all three stars, the spectra are very similar between epochs. The wings of the Balmer lines are essentially constant in each star. There are small equivalent width variations in the same strong permitted lines reported for RR Tau and the variations also appear correlated across these lines. We find variability in the Hα and Hβ lines to be ubiquitious, but the shapes of the circumstellar hydrogen emission in AB Aur is qualitatively different than that found in the UXOR stars. The spectra of AB Aur are also different from the UXOR stars in that the metal lines are generally stronger in emission, particularly the CaII IR triplet and [OI] lines.

Chapter 6

NEAR-INFRARED *H* AND *K*: BRACKETT EMISSION

(Rodgers, Wooden and Woodward, to be submitted)

6.1 Introduction

We have collected low and moderate resolution *H* and *K* spectra of over 30 young stars, primarily Herbig Ae/Be stars and a few Vega-type main sequence stars. The scientific goal is to measure the hot, dense circumstellar gas through its Brackett emission and search for evidence of an evolutionary sequence in intermediate mass stars from very young embedded objects to main sequence Vega-like systems. This study was inspired by the ground-breaking work of Harvey (1984), who reported significant Brackett emission from a number of Herbig Ae/Be stars, and found the Brackett decrements were shallower than Case B, indicating high density for the emitting gas. Nisini *et al.* (1995), and others have assumed the Brackett emission originates from the base of a wind, and have used the line strengths to determine the mass loss rate. Whether the emitting gas is part of the wind or part of an accretion stream is a matter of debate that we take up in Chapter 7. In either case, the emitting gas must be quite hot and dense, suggesting a circumstellar origin close to the star.

The spectra show that the observed Brackett line strengths vary significantly from one object to another. The strongest Brackett emission is seen primarily in Herbig Be stars, while most of the Herbig Ae stars show essentially featureless ("flat") spectra in *H* and *K*, and the Vega-like stars exhibit photospheric absorption only. We have corrected the line strengths for photospheric absorption and veiling due to near-infrared continuum emission in order to isolate the circumstellar line emission. The circumstellar Brγ equivalent widths of the HAe stars are not correlated with effective temperature, but show positive correlation with excess near-infrared emission and negative correlation with system age. By the time

Table 6.1. Near-Infrared Spectrographs

Instrument	Telescope	Epoch UT	Å/ pix H	Å/ pix K	Δv [km s^{-1}] Brγ	Δv [km s^{-1}] Br11
GRIM II/f10	4-m APO	Nov 1997 - Mar 1998	18.2	13.8	505	493
CRSP	4-m KPNO	16 May 1998	25	12	694	429
IRS	Blanco 4-m, CTIO	17 June 1998	6.6	4.4	183	157

the young stars have reached the main sequence, they have lost the circumstellar emission in the near-infrared, both from hot dust in the continuum and from hot hydrogen gas.

6.2 Observations and Data Reduction

Three near-infrared long-slit spectrographs were employed over the course of this observing program. The majority of the spectra were obtained using the Grism Infrared Imager (GRIM II) on the Apache Point Observatory (APO) 3.5-meter telescope between February 1997 and December 1998. Some observations were made in June 1998 with the IR Spectrograph (IRS) on the 4-m Blanco telescope at Cerro-Tololo Inter-American Observatory (CTIO), in La Serena, Chile, and a few spectra were obtained in May 1998 by Chick Woodward on the 4-m telescope at Kitt Peak National Observatory (KPNO) using the Cryogenic Spectrograph (CRSP). The resolution of each instrument is provided in Table 6.1.

6.2.1 Observing Technique

Spectral observations in the near-infrared are complicated by strong and variable telluric absorption features, primarily OH and H_2O bands, between 1.2 and 2.5 μm. Ideally, one would like to observe a featureless source close in space and time to the target observations, and divide this spectrum into the target spectra to remove the atmospheric contamination. Occasionally this is accomplished with a nearby O star, however, these objects are not common and so are difficult to find close in space to the target objects. In practice, observers commonly use B and early A stars for this purpose and simply remove intrinsic

hydrogen absorption lines by interpolation. This is sufficient if one is interested in metal lines separated in wavelength from the Brackett lines. However if, as is the case here, one is interested in the hydrogen lines themselves, this procedure can produce unacceptable contamination in the final spectra from the hydrogen lines in the "atmospheric template". A second approach is to use early G stars, solar analogs, as the templates (Maiolino *et al.* 1996). These stars are divided by a solar spectrum to remove intrinsic features, leaving only the telluric absorption which can then be divided through the target spectra. Since very few exact solar analogs exist, this technique often leaves significant residuals of the intrinsic features in the atmospheric template.

Our observing technique is a hybrid of these methods. The procedure is described in the appendix of Hanson, Conti and Rieke (1996). Both A and G "standard" stars are employed in a three step process. A stars are observed immediately before or after the target observation, close in time and airmass. In addition, spectra of an early G star are obtained less frequently throughout the night. The G star spectra, with intrinsic features removed, are used to remove the telluric features from the A stars. This then allows more accurate fitting and removal of the hydrogen lines in the original A star spectra. Finally, the A star spectra (minus the hydrogen lines but with the telluric features) are divided into the target spectra obtained close in space and time.

6.2.2 GRIM II

Observations were made with the GRIM II instrument on several occasions between November 1997 and December 1998. The observations are listed in Table 6.2. Many of the targets were observed on multiple epochs in an effort to monitor for variability. On each date a number of early A stars were observed as standards and main sequence templates, as well as an early G star. Exposures of Argon arc lamps were made at the beginning and end of the night for the dispersion solution. A single object observation consisted of first imaging the field to center the object on the slit, then switching to grism mode to obtain a series of spectra at two locations along the slit in an ABBA pattern. This was repeated for each of the H and K' filters. The resulting spectra span 1.4 – 1.8 μm and 2.0 – 2.4 μm, respec-

Table 6.2. Apache Point GRIM II Observations

Object	Sp.Type	GRIM UT Epochs
Targets		
AB Aur	A0	15Feb97,17Feb97,15Jan98,19Jan98
BD+40 4124	B2	24May97,07May98,08May98
BD+61 0154	B8	18Jan97
CO Ori	G2	17Nov97,15Jan98,19Jan98,03Feb98,14Mar98
CQ Tau	F8	15Feb97,17Feb97,15Jan98,19Jan98,03Feb98
DG Tau	K/M	15Feb97,17Feb97,18Feb97,15Jan98,19Jan98
HD 34282	A0V	19Jan98,03Feb98
HD 35187	A2/3	19Jan98,03Feb98
HD45677	B3	15Feb97,18Feb97,19Jan98,03Feb98,14Mar98
HK Ori	A5	15Feb97,17Feb97,17Nov97,19Jan98,03Feb98
RR Tau	A2/3	15Jan98,19Jan98,03Feb98,14Mar98
T Ori	A3/5e	03Feb98
UX Ori	A2	18Jan97,19Jan98,03Feb98
V1686 Cyg	B2/3e	24May97,07May98
WW Vul	A0/3Ve	24May97,07May98
XY Per	B6/A5	16Feb97,15Jan98,19Jan98
Templates & Standards		
HD 27777	B8V	*various*
HD 33224	B8V	
HD 34317	A0V	
HD 35909	A4V	
HD 37439	A1Vn	
HD 37507	A4V	
HD 40335	A0V	

tively. The J band was not observed because two orders overlap within the J filter in this instrument. The resolution of GRIM II is determined by the focal length of the imager: $f5$, $f10$, and $f20$. $f20$ provides twice the resolution of $f10$, with half the wavelength coverage. Experimenting with $f20$ mode, we found that it produced significant fringing effect which could not be cleanly removed, resulting in much poorer quality data. We therefore used the $f10$ mode only.

Data reduction was performed with IRAF[1]. Raw images taken at alternate slit positions

[1]The Image Reduction and Analysis Facility, v2.10.2, operated by the National Optical

were subtracted from each other to remove dark current as well as sky emission lines. Dispersion calibration was performed independently for each slit position and then the images were combined. Modified A stars (having had their hydrogen lines removed as discussed above) were then used to remove telluric absorption features. The final image was multiplied by a blackbody to recover the continuum shape. This last step does not intend to provide true flux calibration, but only to correct for the division by the A star. An alternative would be to normalize the target and the A star before division, but then any information on the shape of the target star's continuum across the spectrum would be lost. However, after performing this procedure on the template A stars (one A star against another), we found that the shape of the continuum is not reliably reproduced. In the data presented here, the target spectra are normalized and we shall focus only on the Brackett lines.

6.2.3 IRS & CRSP Data

A single observing run was obtained on the Blanco 4-m telescope at CTIO on 16–18 June 1998. The weather was poor and useable observations were only obtained on 17 June 1998. For this observing run, we planned to observe a number of Herbig Ae/Be stars, zero-age main sequence stars with near-infrared excess and Vega-type stars. For the latter two, the targets were selected from Sylvester *et al.* (1996). We were able to obtain a small sample of targets from each group. In addition, a few spectra were obtained by Chick Woodward as part of an unrelated observing program with the CRSP at KPNO on 16 May 1998. Targets observed with the IRS and CRSP are listed in Table 6.3.

These data were obtained and reduced in a very similar fashion to the GRIM II data. The IRS has several modes, again trading off wavelength coverage for resolution. For these observations the resolution is roughly three times that of the GRIM II data, with correspondingly less coverage in each filter. Five filters were used to obtain Brγ, Br11 and Br12, Br13 through Br17, Paβ, and Paγ and HeI 10830Å. Each object was observed in all five filters before moving to the next object, resulting in spectra very close in time (within a

---

Astronomy Observatories.

Table 6.3. Cerro Tololo IRS & Kitt Peak CRSP Observations

Object	Sp. Type	Instrument & Epoch
HD 141569	B9V	CRSP, 16 May 1998
HD 142666	A8V	
VV Ser	A2IV	
R CrA	B8	IRS, 17 June 1998
HR 5999	A7III	
HD 141569	B9V	
HD 142666	A8V	
HD 143006	G6	
HD 144432	A5V	
HD 172555	A7V	
HD 176386	B9IV	

few minutes of each other), but also numerous filter changes over the course of the evening. Lamp exposures were obtained at the beginning and end of the evening. The dispersion solution was stable throughout the night, but the zero-point shifted between objects. To correct for this, sky lines in each filter were used with the IRAF "specshift" function to linearly shift the spectra to the correct position.

6.3 The Spectra

6.3.1 GRIM II Spectra

The spectra show a wide range of Brackett emission strengths, from very strong emission line objects to featureless spectra to objects with photospheric absorption profiles only. The objects that show strong emission in all Brackett lines are primarily Herbig Be stars or embedded objects such as R CrA and DG Tau (Fig. 6.1). The early spectral type means that these objects have weaker photospheric hydrogen absorption lines, which likely contributes to the strength of the observed Brackett emission.

In contrast, all of the Herbig Ae stars in this sample exhibit either moderate to weak Brackett emission or essentially featureless spectra at this resolution. The Vega-type stars

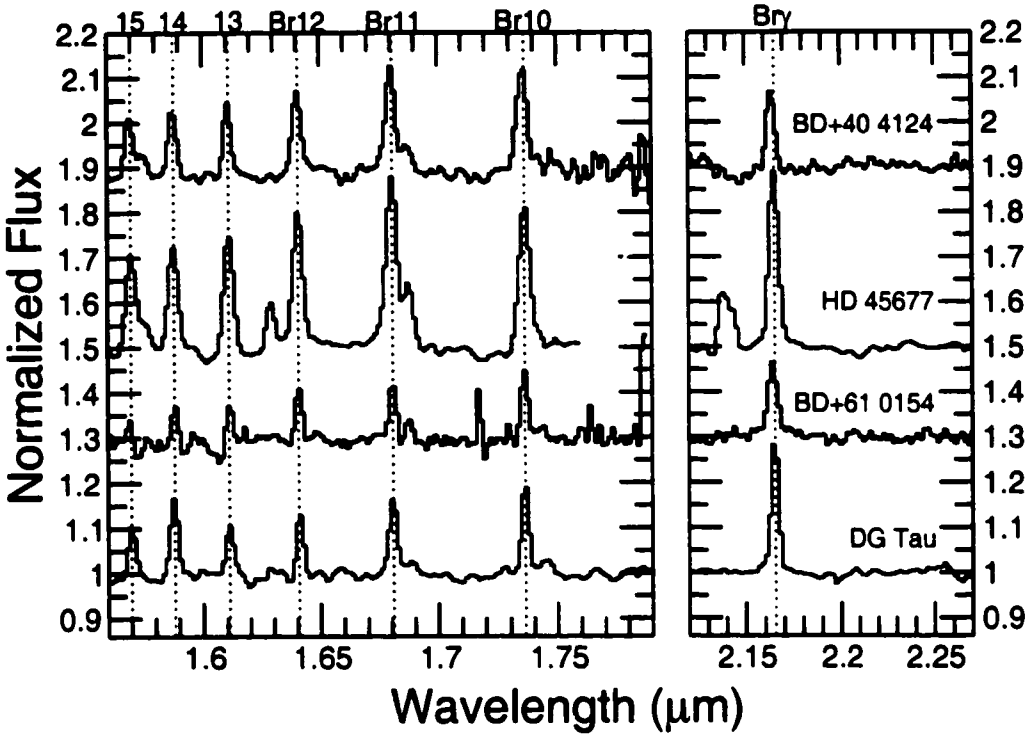

Figure 6.1 H and K spectra of the strongest Brackett line emitters in our sample. The Brackett decrements are clearly seen through Br15. The first two objects are early HBe stars, BD+61 0154 is a late Be star and DG Tau is a T Tauri star.

show photospheric absorption with no evidence of emission. A sample of these spectra are shown in Figure 6.2. In Figure 6.3 we plot the observed Brγ EW against spectral type. The HAe stars are clumped in a region of small Brγ EW, labeled as "flat" spectra. This trend is supported by the data presented in Harvey (1984). Of the 9 targets reported there, the 8 which show Brackett emission have spectral types A0 or earlier. The one exception is HK Ori, an ~A5 star. For the four targets in common (HK Ori, AB Aur, BD+40 4124, and BD+61 0154), our spectra are similar to Harvey's. The other five Harvey targets would fall in the upper left area of Figure 6.3.

It is the "Flat" spectrum targets that we are most interested in here. Clearly these objects have a significant non-photospheric component that is filling in the photospheric absorption. In the next section we explore the nature of the circumstellar component.

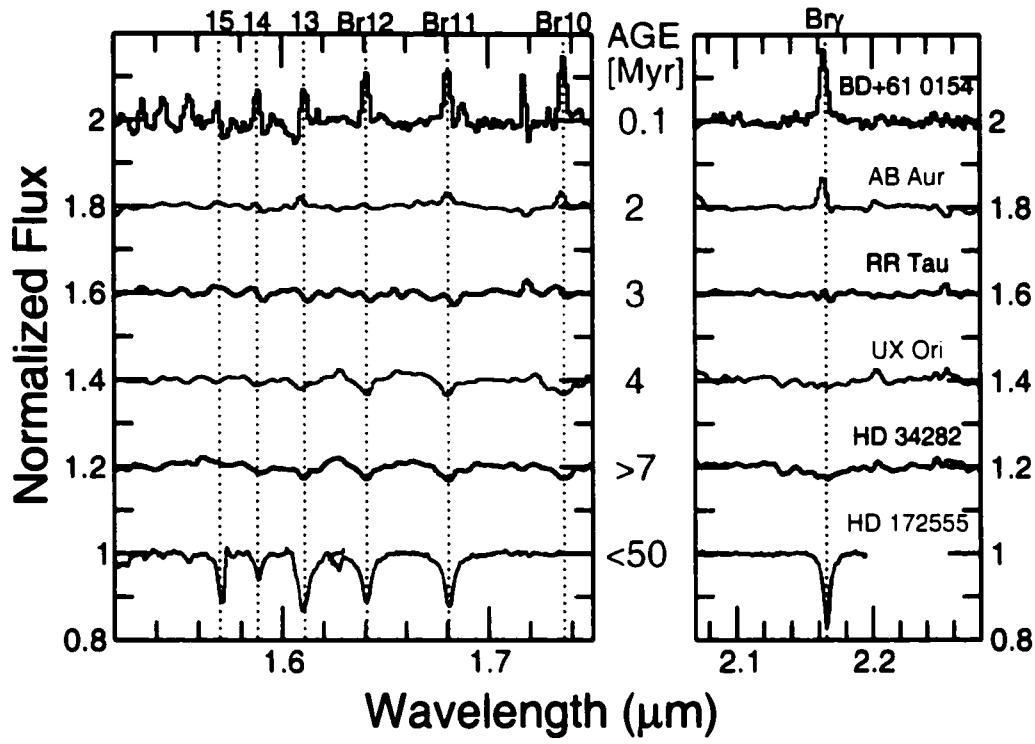

Figure 6.2 H and K spectra of a few targets, showing the range in Brackett features observed in our sample.

6.3.2 IRS Spectra

In addition to Brγ and Br11 - Br17, the IRS data cover the bluer lines of Paβ and Paγ, and the HeI 1.083μm line. The spectral resolution of these data, while still coarse ($\sim$ 150 - 200 km s^{-1}), does warrant some kinematic analysis. We have plotted the He I and Paγ lines in Figure 6.4. The targets are shown in order of increasing age, with the two youngest stars in the top row and the three main sequence objects in the bottom row. Despite the small sample size, the helium line shows a variety of complex profiles. It is not detected in any of the three main sequence stars in our sample, including two β Pic-like stars. The other five stars clearly show the line, with a broad, singly-peaked emission profile in the embedded object R CrA, to inverse P Cygni (infall) in HR5999 and HD142666, and P Cygni (wind) in HD144432 and HD143006. We caution that these are single epoch observations and it is quite likely that this line could vary dramatically at other epochs, as has been shown for

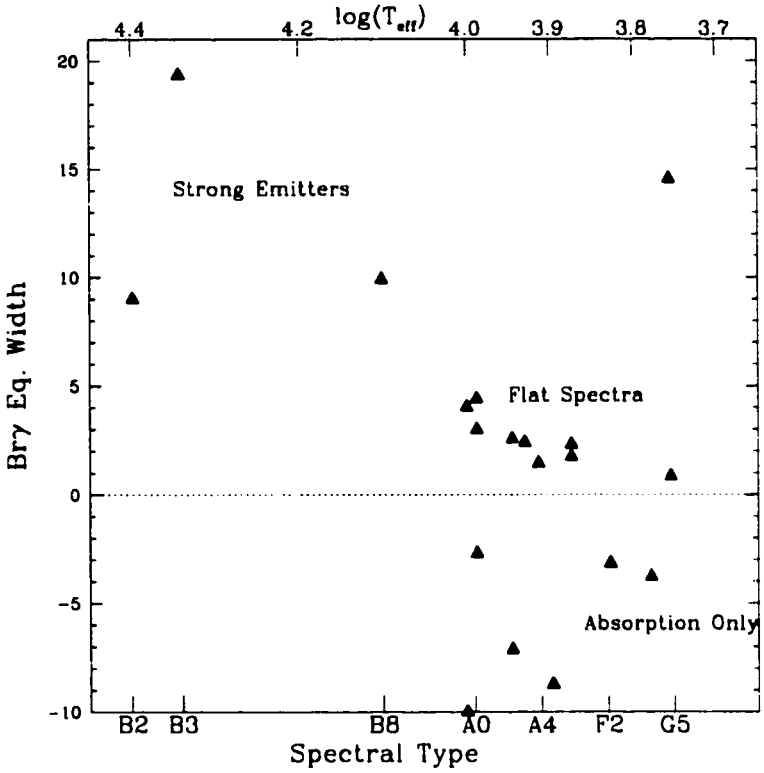

Figure 6.3 Brγ equivalent widths against Spectral type. The majority of the A stars exhibit featureless "flat" continua at the wavelength of Brγ. The strongest Brackett emission is observed in early B stars. The one exception is DG Tau, a low mass star with strong Brackett emission (the upper right point).

HeI 5876 in the optical (Ch. 4).

6.4 Discussion

6.4.1 K Veiling and Circumstellar Brackett Emission

There are two components that contribute to filling in the photospheric Brackett absorption in these objects. The first is veiling by excess near-infrared thermal emission from hot dust. The second is circumstellar Brackett emission from hot gas. In order to properly study the circumstellar line emission, it is necessary to remove both the photospheric absorption and the excess continuum emission. Ideally, one would subtract a template star with the

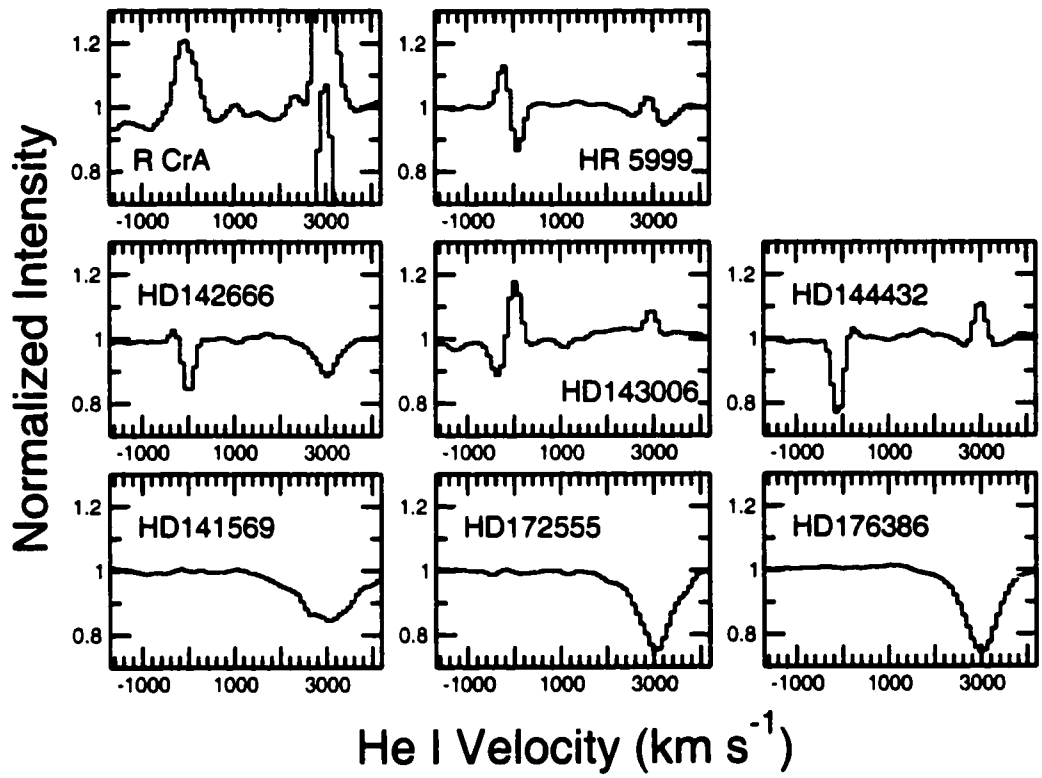

Figure 6.4 He I and Paγ emission from IRS data on 17 June 1998. Each plot is labeled with target name. Targets are plotted approximately in order of increasing age.

appropriate spectral type, scaled to the photospheric level of the target and veiled by an amount determined from the flux-calibrated spectra. An example of this procedure is given in the next chapter, using resolved data. Attempting such an exercise with our low resolution GRIM and CRSP data is of questionable utility. What is required is that the photospheric absorption wings be resolved from the emission cores in order to properly fit a main sequence template star, and that the spectra be flux-calibrated. Lacking this, we chose instead to look only at the equivalent width of the Brγ line. However, we do make corrections to the EWs for the veiled photosphere to recover the circumstellar line strength in an approximate way. We caution that we have used K' magnitudes from non-contemporaneous observations, both by us and from the literature. The photometric variability of these stars in the NIR is unknown. Based on the few, sporadic reports of NIR photometry of these stars we do not find evidence for dramatic changes in K' magnitude but variations at $\sim$.2 mag are seen.

AB Aur, which interestingly is optically stable ($\Delta V \leq 0.1$), varies by at least 0.4 magnitudes in K', from 4.4 in 1981 (Lorenzetti *et al.* 1983) to 3.97 ±0.01 on 10 December 1998 (Mount Lemmon Observing Facility).

We extract the circumstellar EW of Brγ in the following way. In the absence of excess emission, the observed K' magnitude is obtained from

$$(m_V - m_{K'}) = (M_V - M_{K'}) + A_V - A_{K'} \tag{6.1}$$

or

$$m_{K',ph} = m_V - (M_V - M_{K'}) - A_V(1 - A_{K'}/A_V) \tag{6.2}$$

where $m_{K',ph}$ is the observed photospheric flux at K', and we assume no veiling at V. The intrinsic $M_V - M_{K'}$ colors are a function of the spectral type (Johnson 1966) and we adopt the interstellar value for $A_{K'}/A_V = 0.112$. The excess continuum at K' is then simply the difference

$$K'_{exc} = m_{K',ph} - m_{K',obs} \tag{6.3}$$

and the veiling flux at K' is

$$F_{K',VEILING} = 10^{0.4K'_{exc}} - 1 \tag{6.4}$$

where the photospheric flux is normalized to 1.

Table 6.4 collects the necessary parameters, taken from the literature, along with the measured and corrected EWs of the Brγ lines in our sample. The uncertainty in the veiling is dominated by the variability in observed V, and possibly K'. For UXOR stars with large ΔV we have used the average bright state value. Sylvester *et al.* (1996) have calculated the excess magnitudes for some of our sample in a similar way (using Kurucz spectral energy distributions rather than $V-K'$ colors), and we have adopted their values. Also note that new K' photometry from Mt. Lemmon Observing Facility (MLOF) is reported in the table for AB Aur, CQ Tau, RR Tau, and UX Ori.

Having estimated the veiling, we add this flux to a normalized template of the appropriate spectral type, renormalize and measure the EW of Brγ in the veiled template. This

Table 6.4. Circumstellar Brγ Calculation Parameters

Object	m_V	m_K	Excess K'	Brγ_{OBS}	Brγ_*	Brγ_{CS}
AB Aur	7.05 (We)	4.16 (ML)	2.4	-4.40 ±0.15	1.06	-5.5
BD+40 4124	10.54 (Hi)	5.78 (Hi)	>1.9	-9.0 ±0.0	0	-9.0
BD+61 0154	10.38 (Hi)	5.70 (Hi)	2.8	-9.9 ±0.0	0.76	-10.66
CQ Tau	9.42 (Ro)	6.18 (ML)	1.5	3.17 ±0.18	2.75	0.42
HD 34282			1.9 (Sy)	2.71 ±0.17	1.76	0.95
HD 35187			1.0 (Sy)	7.13 ±0.27	6.16	0.97
HD 45677	8.05 (Sim)	4.62 (Sim)	>2.7	-19.36 ±0.13	0	-19.36
HD 141569	7.13 (Sy)	6.80 (Sy)	0.0	-2.99 ±0.13	10.6	-13.59
HD 142666			1.2 (Sy)	-0.55 ±0.13	2.92	-3.47
HD 144432			1.2 (Sy)	-2.30 ±0.14	2.92	-5.22
HD 172555			~0	8.74 ±1.21	8.59	0.15
HD 176386	7.28 (Bi)	6.66 (Bi)	0.0	9.98 ±0.05	10.6	-0.62
HK Ori	11.66 (Hi)	7.29 (Hi)	3.0	-1.44 ±0.08	0.72	-2.17
HR 5999	7.04 (Ma)	4.34 (Ma)	1.9	-1.74 ±0.01	4.75	-6.49
R CrA	11.52 (Bi)	3.54 (Bi)	5.5	-4.04 ±0.05	0	-4.04
RR Tau	11.0 (We)	7.29 (ML)	3.0	-2.56 ±0.05	0.95	-3.51
UX Ori	10.0 (We)	7.13 (ML)	2.5	-2.4 ±0.0	1.53	-3.93
VV Ser	11.63 (Ro)	5.61 (Hi)	2.8	-6.70 ±0.68	0.77	-7.47
WW Vul	10.5 (We)	7.26 (Sim)	2.6	-0.74 ±0.10	1.38	-2.12

Note. — Columns 2 - 5 are magnitudes; 6 - 8 are Equivalent Width (Å). See text for discussion. References in parentheses: Bi = Bibo & Thé (1991); Hi = Hillenbrand *et al.* (1992); Ma = Malfait *et al.* (1998); ML = Mount Lemmon Observing Facility (reported here); Ro = Rostopchina (1999); Sim = Simbad; Sy = Sylvester *et al.* (1990); vA = van den Ancker *et al.* (1996); vAb = van den Ancker *et al.* (1996b); We = Wesleyan database (Herbst & Shevchenko 1999).

is the EW "Correction" which is subtracted from the observed Brγ EW to obtain Brγ_{CS} , the circumstellar line strength. EW<0 indicates emission.

We have only a coarse sampling of template stars: B8, A1 and A4 for GRIM and CRSP data; A0 and A5 for IRS spectra. However, the variation in line depth is small ($\sim$ 10%) in these spectra, and the added veiling makes this effect negligible in most cases. The exception is CQ Tau, an F2 star for which we have used an A4 template that overestimates the photospheric absorption. The uncertainty in the K' magnitudes depends on the degree of photometric variability at K', which is unknown. We have estimated this uncertainty to be as much as 20%. The total uncertainty in the circumstellar Brγ EWs is conservatively estimated to be 35% (5% measurement error).

6.4.2 Disk Evolution

The results of this process is shown in Figure 6.5. From top to bottom, the panels plot the observed Brγ EWs, the calculated K' veiling flux, the Brγ correction, and the computed circumstellar BrγEWs, each as a function of effective temperature. Each source is numbered, with number increasing with age. Age estimates are not available for all objects (see Table 6.5); the position in the sequence for these stars is estimated based on their similarity to the stars with age estimates. The top panel shows a general trend of increasing emission with T_{eff}, with a large scatter. The second panel shows a significant correlation between age and veiling, with younger Herbig Ae/Be stars having it, and the older stars do not. The stars with significant veiling have a smaller EW correction (third panel), while the main sequence stars without veiling have a large correction due to photospheric absorption. This has the effect of reducing the scatter in the bottom panel. The circumstellar EWs show no significant trend with T_{eff}, but do separate by age. As with the veiling, the main sequence stars show essentially zero circumstellar Brγ emission, while the pre-main sequence Herbig Ae stars all exhibit some emission at Brγ. The exception is HD 141569 (#17) that has strong emission in the bottom panel. The emission in the core of Brγ is apparent in the IRS spectra. Another spectrum of this star with CRSP does not show this, although the lower resolution may be masking it. We don't know whether this star is unique among the

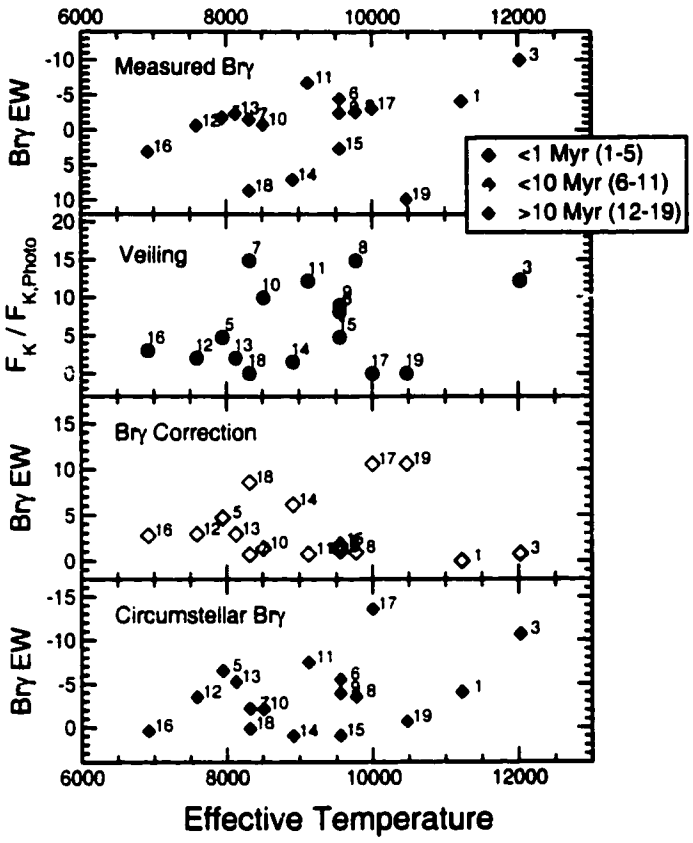

Figure 6.5 Derivation of Circumstellar Brγ EWs vs. Effective Temperature. Top panel plots observed Brγ EWs. Computed K veiling fluxes (second panel) are applied to templates to compute EW "corrections" (third panel). Difference of top and third panels is circumstellar EWs (bottom panel). See text for derivation.

ZAMS stars, or whether we have captured a unique epoch. The strong absorption seen in the IRS spectrum suggests that the calculation of essentially no veiling flux is correct.

Other properties of these systems, again collected from the literature, are given in Table 6.5, including system age. In Figure 6.6 we have plotted the estimated circumstellar Brγ EWs and the K veiling flux against age and variability (ΔV). We find the K veiling is not correlated with age for ages <10 million years. It appears that the excess continuum flux drops significantly around 10 Myrs. Similarly, we do not see a correlation between veiling flux and ΔV, suggesting that the variability phenomena is not directly linked to the amount of hot circumstellar dust in the system.

The data do suggest a correlation between circumstellar Brγ EW and age, with the strength of the Brγ line decreasing as the stars get older. Although the uncertainty is large in this dataset, the result is particularly intriguing because it shows a decreasing trend between 2 and 8 Myrs, in the range of ages where most Ae stars lie, and before the K continuum emission drops. In addition, there also appears to be a trend with variability, in

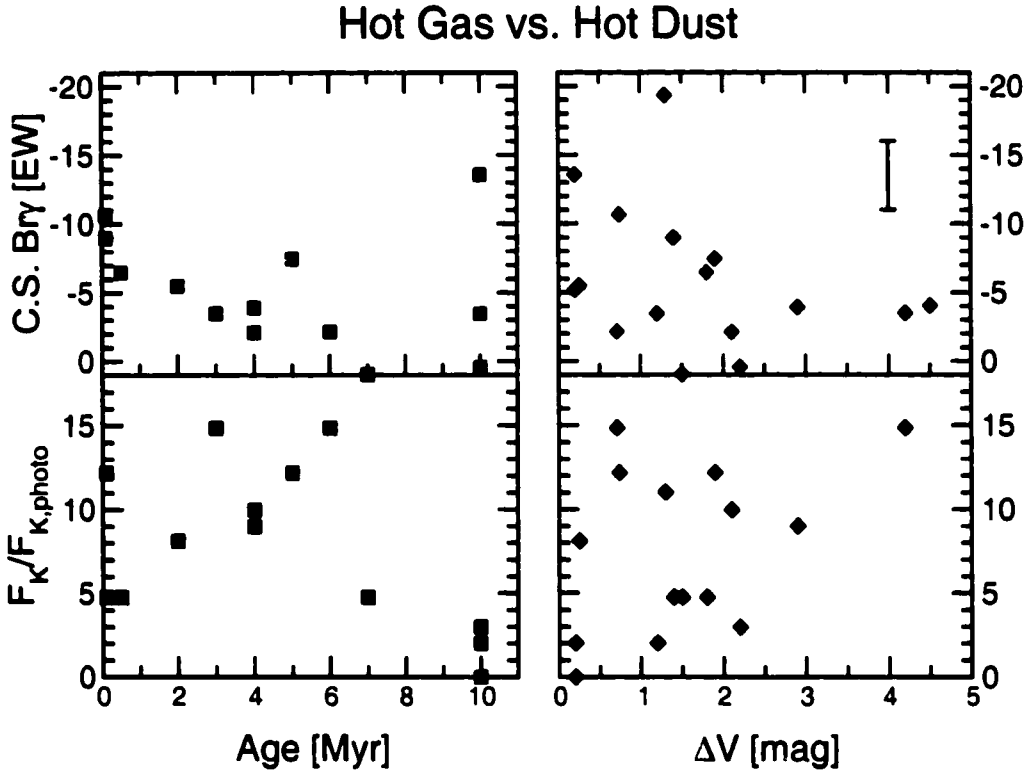

Figure 6.6 Circumstellar Brγ and K excess vs. Age and Variability. Uncertainty in circumstellar Brγ EW is shown as a vertical bar in the top right panel. Ages are not available for all objects.

6.5 Future Work

6.5.1 Brackett Decrements

The circumstellar Brackett decrement is a more sensitive diagnostic of temperature and density than the Balmer decrement in the high density regimes expected close the HAe

Table 6.5. Target Star Properties

Object	Sp.Type	log T_{eff}	log $L_*/L_\odot$	$M_*/M_\odot$	Age [10^6 yr][a]
AB Aur	A0Ve+sh (vA)	3.98	1.68	2.4	2.0 (6)
BD+40 4124	B2 (Na)	4.34	3.95	9	<0.1 (2)
BD+61 0154	B8 (Na)	4.08	2.59	4	0.1 (3)
CQ Tau	F2IV (Ro)	3.84 (Gr)	0.82 (Ro)	1.5	10 (16)
HD 34282	A0 (Na)	3.98	1.42	2.2	>7 (14)
HD 35187	A2-3IV/Ve (vA)	3.95			(13)
HD 45677	B2III-V[e](vA)	4.33	>2.60		(4)
HD 141569	B9.5Ve (vA)	4.00	1.35	2.3	>10 (17)
HD 142666	A8V (Na)				10 (15)
HD 144432	A5Ve (vA)	3.91	>1.48		(12)
HD 172555	A7V (So)				<50 (18)
HD 176386	B9IV (vAb)				>2 (19)
HK Ori	A5 (Na)	3.92	1.09	2.0	6 (7)
HR 5999	A5-7III/IVe(vA)	3.90	1.93	3.2	.50 (5)
R CrA	B8 (Bi)				(1)
RR Tau	A0III-IV (Ro)	3.99 (Gr)	1.57 (Ro)	2.5	3 (8)
UX Ori	A3III (Ro)	3.98 (Gr)	1.59 (Ro)	2.3	4 (9)
VV Ser	A2III-V (Ro)	1.51		2.1	5 (11)
WW Vul	A3III (Ro)	3.93 (Gr)	1.47 (Ro)	2.2	4 (10)

Note. — Reference in parentheses applies to the right of the reference, until replaced by another reference. References: Bi= Bibo & Thé (1991); Gr= Grinin *et al.* (2001); Hi= Hillenbrand *et al.* (1992); Ro= Rostopchina *et al.* (1999); Na= Natta *et al.* (2000b); vA= van den Ancker (1998)

[a]Number in parentheses is identifier in Figure 6.5.

stars. As an example, a number of line ratios from the theoretical work of Storey & Hummer (1995; Case B) are plotted for changing temperature and density in Figure 6.7. The Brγ/Br10 ratio is clearly a more sensitive discriminant of changing density conditions (bottom left panel) than Hβ/Hα. However, one needs fairly precise data to compare with such calculations. What is required is sufficient resolution to isolate the circumstellar line components while at the same time sufficient wavelength coverage to observe several Brackett lines, and preferrably flux calibrated spectra or contemporaneous photometry. This project, while challenging, offers a direct probe into density and temperature conditions present in the inner disk regions of these stars where the Brackett emitting gas is thought to originate. The curves shown in Figure 6.7 assume a Case B condition, wherein the Lyman lines are optically thick. Under very high density conditions, this condition may not be valid, and in fact this is indicated by work of Harvey (1984), at least for some Herbig Be stars. Beyond Case B, one approaches the Case C condition of optically thick Balmer lines, which results in line trapping and increased emission from higher level Paschen, Brackett and Humphrey lines. Comparison of these theoretical predictions with the observed Brackett decrements of HAe stars may place significant constraints on the location and conditions of the circumstellar gas responsible for the Brackett emission.

6.5.2 Variability

This program was originally undertaken with the hope of monitoring variability in hot dust and gas emission. We found the low resolution and inherent instability of the GRIM II instrument severely limited our ability to detect variability. Based on tests of the template stars on various epochs, we estimate our instrumental variability to be ~30%. We can say that we do not detect strong variability in any of our targets above this level. We do detect lower level variability that is probably real in at least some cases, based on the coordinated behavior across multiple lines. However, the quality of the data prohibit quantitative analysis.

Nevertheless, this is still a worthwhile undertaking. What is required is moderate resolution, broadband flux-calibrated spectra to look for changes in both continuum emission

(hot dust) and line emission (hot gas). Is either variable? Are they correlated? Is either correlated with optical variability in UXORs? These are questions which can only be answered with careful monitoring, but have profound implications for understanding the interplay between optical variability and circumstellar dust and gas.

6.6 Conclusions

We find the strength of Brackett emission in Herbig Ae/Be stars is diverse and somewhat correlated with age and spectral type. The strongest observed Brackett emission is seen in the Herbig Be stars, and in embedded objects such as DG Tau and R CrA. When present, strong Brackett emission is observed across the series from Brγ through at least Br17.

The majority of Herbig Ae stars show "flat" spectra in the near-infrared, with little observed Brackett emission or absorption. This is the result of a combination of circumstellar emission, photospheric absorption and veiling by excess continuum emission from hot dust. Isolation of the circumstellar component, while crude, suggests that emission is not correlated with effective temperature but does appear to correlate with system age, and in particular may offer an age diagnostic between 2 and 10 Myrs, at a time when the veiling flux is not correlated with age. Main sequence β Pic-like stars show photospheric absorption only. Veiling and circumstellar emission is absent in these stars (age $\gtrsim 10^6$ yrs).

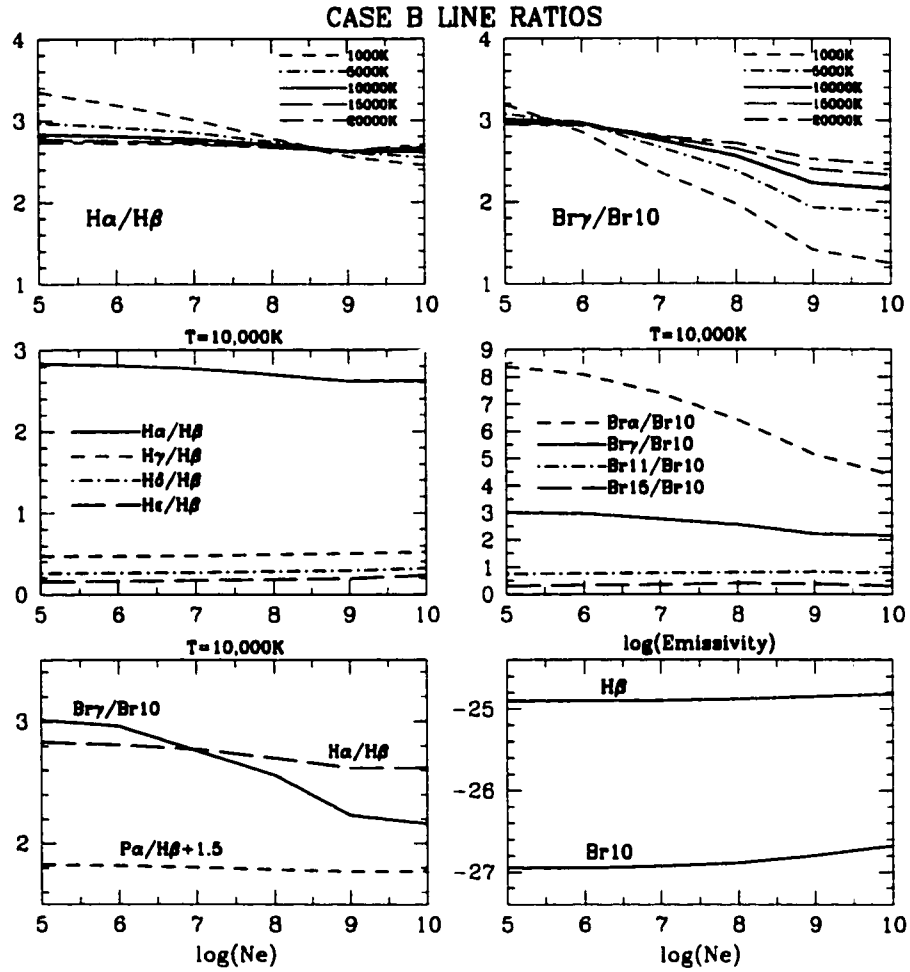

Figure 6.7 Theoretical Case B Balmer and Brackett Line Ratios based on data from Storey & Hummer (1995).

Chapter 7

BRACKETT GAMMA LINE PROFILES

(Rodgers, Woodward and Wooden, to be submitted)

The near-infrared spectra in the previous chapter showed that Brackett emission is associated with stellar youth and apparently correlated with near-infrared continuum excess. However, both accretion and winds are also associated with young stars, and the low resolution data do not provide the detailed line profiles needed to analyze line kinematics. To address the question of whether the Brackett-emitting gas is infalling or outflowing in young stars, we obtained high resolution Brγ profiles for a small number of targets. This chapter describes these high resolution near-IR spectra from CSHELL, and discusses their implications. We find that most of the target stars do not show significant Brγ emission or absorption, telling us that the flat spectra observed at low resolution are not just a result of unresolved data. Two stars that do show emission, AB Aur and UX Ori, show asymmetric profiles with red-shifted absorption and no evidence of blue-shifted absorption. These profiles suggest infall for the emitting gas.

7.1 Observations and Data Reduction

7.1.1 Observations

Data were obtained 2–6 February 1999 at the Infrared Telescope Facility (IRTF) on Mauna Kea, using the CSHELL instrument, with two-pixel resolution $\lambda/\Delta\lambda \approx$ 54,000. Four of the five nights were useable, under non-photometric skies. Brγ was observed on three nights, and one night was dedicated to Br11. Only the Brγ data are presented here. A summary of the observations are presented in Table 1. The spectral range of CSHELL is small, $\sim$50Å, much smaller than the width of Brγ in these A stars. To account for this, three

Table 7.1. IRTF CSHELL Brγ Observations

Object	Optical Spectral Type	UT Date	$\Delta\lambda$ [Å]	Comments
		Targets		
AB Aur	A0	02FEB99	132	1" slit
		06FEB99	132	2" slit
CO Ori	F9/G2	06FEB99	52	2" slit
CQ Tau	A8/F2	05FEB99	132	2" slit
DG Tau	K/M	05FEB99	52	2" slit
HD35187	A2/3	06FEB99	52	2" slit
HD45677	B2	05FEB99	94	2" slit
RR Tau	A3/4	06FEB99	52	2" slit
SU Aur	G2	02FEB99	132	1" slit
		06FEB99	52	2" slit
UX Ori	A2/3	05FEB99	94	2" slit
		Templates		
HD27819	A8	06FEB99	132	2" slit
HD27962	A2	05FEB99	132	2" slit
HD29526	A0	06FEB99	132	2" slit
HD34203	A0	02FEB99	132	2" slit
		Standard		
BS1656	G4	02FEB99	132	1" slit
		05FEB99	132	2" slit
		06FEB99	132	2" slit

grating settings were employed for most targets, one on either side of the center, providing a combined width of $\sim$1800km s^{-1} at Brγ. Along with the targets, main sequence stars of similar spectral type were observed as "templates". The G4V star BS1656 was observed each night at all grating settings and at multiple airmasses to monitor instrumental effects and changes in telluric absorption.

All observations were taken alternately at two positions along the slit (in an ABBA pattern) to facilitate sky subtraction. Four or five lamp lines were obtained at the beginning of each night to determine the dispersion solution and then flats and lamps were taken at or near (in space and time) each object during the night.

7.1.2 Data Reduction & Calibration

Initial data reduction was done with IRAF [1]. First, pairs of images at alternate slit positions were subtracted from each other to remove sky and bias/dark level. The sky-subtracted images were then flattened, trimmed and corrected for bad pixels using the IRAF routine *ccdproc*. The spectra were extracted from the 2-D images with *apall*, and then co-added. (The shift in the dispersion solution between the two slit positions was negligible– less than 1%.) The co-added spectra were wavelength-calibrated using the combined lamp dispersion solution, with the zeropoint determined by the lamp line taken at the object.

To correct for instrumental effects and telluric absorption, the G4V star BS1656 was employed. A solar spectrum, adjusted to the flux of BS1656, was divided into the observed spectra to produce a sensitivity function (including telluric effects) at each grating position on each night. Each object spectrum was then divided by the appropriate sensitivity function to obtain flux-calibrated spectra. The shape of the sensitivity function varied $\lesssim$ 5% from night to night; absolute flux levels varied by at most a factor of 2 from night to night and between grating settings due to the non-photospheric conditions. For each object (targets and templates), adjacent grating settings were combined by matching the average flux in the overlapping regions and scaling to the grating position with the largest flux (assuming only light loss). The flux adjustments were also of order a factor of 2, providing an estimate of the uncertainty in the flux calibration.

7.2 Results

The complete set of normalized Brγ profiles are plotted in Figure 7.1. In general, the spectra are very similar to the lower resolution spectra in Chapter 6. The strongest Brγ emission is seen in HD 45677, an early B star. The TT star DG Tau shows broad, blue-shifted line emission, which likely originates in the strong outflow associated with this source. Three A star templates of different spectral types are shown in the last three panels of the bottom row. With the exception of AB Aur, all of the HAe targets exhibit essentially flat spectra at

[1]The Image Reduction and Analysis Facility, v2.10.2, operated by the National Optical Astronomy Observatories.

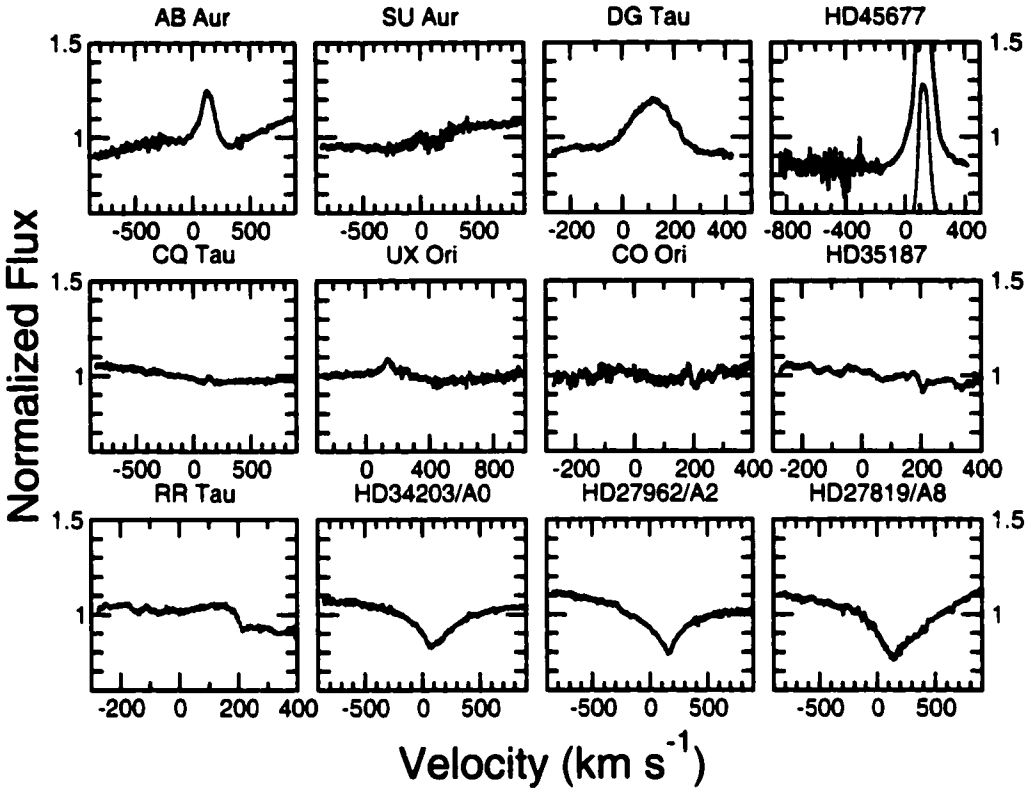

Figure 7.1 CSHELL Brγ profiles versus velocity for all targets. Note the x-axis is different in each plot, the y-axis is the same. No radial velocity corrections have been made. The second line shown in purple for HD 45677 is the original spectrum halved. Last three targets in the bottom row are main sequence A stars.

Brγ, showing neither strong emission or strong absorption. If the observed flux at Brγ were a combination of photospheric absorption and circumstellar emission, we would expect the two components to be resolved at this resolution. Instead, we see only the veiling continuum flux, confirming the results of the last chapter that the circumstellar Brγ emission varies across this selection of objects and disappears before the near-IR excess. Only AB Aur, which we identify as an emission star in Chapter 3, shows significant emission. Weak emission is seen in UX Ori and possibly CQ Tau.

7.2.1 Creating Photospheric Line Profile Templates

As discussed in Chapter 6, the excess continuum emission in the near infrared has the effect of "filling in" or veiling the photospheric absorption lines. In essence then, we can represent the line emission from the star with a 3-component model: photospheric absorption, approximated by a non-variable MS star of similar spectral type; IR continuum emission, approximated simply by an additive constant determined from the difference between the expected stellar continuum and the observed continuum flux near Brγ; and circumstellar line emission obtained by subtracting the first two components from the observed spectrum. With these high resolution spectra, we can recover the circumstellar line profiles, rather than simply the circumstellar EW as we did in the last chapter. We work in flux units, F_λ, where the wavelength dependence is implicit in the following equations.

Under the assumption that there is no excess emission at V (i.e., the V magnitude is purely photospheric) and after broadening the template star spectrum to the rotational $v \sin i$ of the target star, the two fluxes are related simply by the ratio of their radii and distances, which we will call D.

$$\frac{F_H(V)}{F_T(V)} = \frac{(R_H/d_H)^2}{(R_T/d_T)^2} = D$$

Then $\log(D) = -0.4(V_H - V_T)$, where V_H = the reddening-corrected V magnitude of the HAEBE star, and V_T = the V magnitude of the observed template. The expected photospheric flux of the HAEBE star at Brγ equals the observed template spectra multiplied by D.

The excess IR continuum (the second component) is determined empirically by taking the difference between the continua of the adjusted template flux and the observed flux of the target. Specifically, the observed target flux is approximated by a low order Legendre fit to the majority of the flux, while the template flux is approximated by a similar fit through the top of its flux in these flux-calibrated spectra. This is necessarily very approximate, due to the large uncertainty in the flux calibration, and the very small wavelength coverage of the spectra. The latter makes it difficult to determine where the continuum of each star lies. Alternatively, one could use the K veiling calculated in Chapter 6 from independent photometry measurements. Even given the uncertainty in the continuum flux in these

spectra, the simultaneous flux determination is preferrable. This excess value then is added to the (adjusted) template spectrum, and the result is subtracted from the target HAe star spectrum.

We illustrate this procedure with the UX Ori spectrum. In Figure 7.2 the CSHELL spectra of UX Ori and an A2 Template star, scaled to the V magnitude of UX Ori as described above, are plotted with the SED data of Hillenbrand et al (1992). The dashed line is the Hillenbrand *et al.* fit to the photometry and is the sum of the photosphere (short dashed line) and the Hillenbrand accretion disk (dotted line). The figure shows that the flux calibrated UX Ori spectrum and the adjusted A2 template are a good fit to the broadband data. It also highlights the near-IR excess, which is more than a magnitude at Brγ. To isolate the circumstellar Brγ line emission, a constant veiling flux of $3 \times 10^{21} W/cm^2/s/\text{Å}$ is added to the template, and the veiled template is subtracted from the UX Ori spectrum.

The three relevant spectra are plotted in the top panel of Figure 7.3: the original spectra of UX Ori and the A2 template, and the veiled template. The residual emission of UX Ori, that is the circumstellar Brγ component, is plotted in the bottom panel. The system velocity of UX Ori is not known; we have assumed the same value as for the template, $v = 35$ km s^{-1}, which is comparable to other stars in Orion. The velocity resolution is 6 km s^{-1}; given the uncertainty in the system velocity, we estimate the error in the zeropoint to be as much as 20 km s^{-1}. The shape of the Brγ emission is discussed in the next section.

7.3 Discussion

Four of the seven HAe stars in Figure 7.1 show no detectable line emission at Brγ. The above procedure was applied to the other three stars: UX Ori, CQ Tau and AB Aur. In UX Ori, the original template central line depth was 76% of the continuum; after adding the K excess flux, the line depth is $\sim$ 92% of the continuum. Thus, the effect of subtracting the veiled template is small, resulting in a slightly higher central peak and broader emission wings compared to the original UX Ori spectrum. In CQ Tau, a weak emission peak is barely detectable in Figure 7.1. CQ Tau has a smaller veiling flux than AB Aur or UX Ori, but also a weaker photospheric line. After correcting for these, the circumstellar Brγ emission

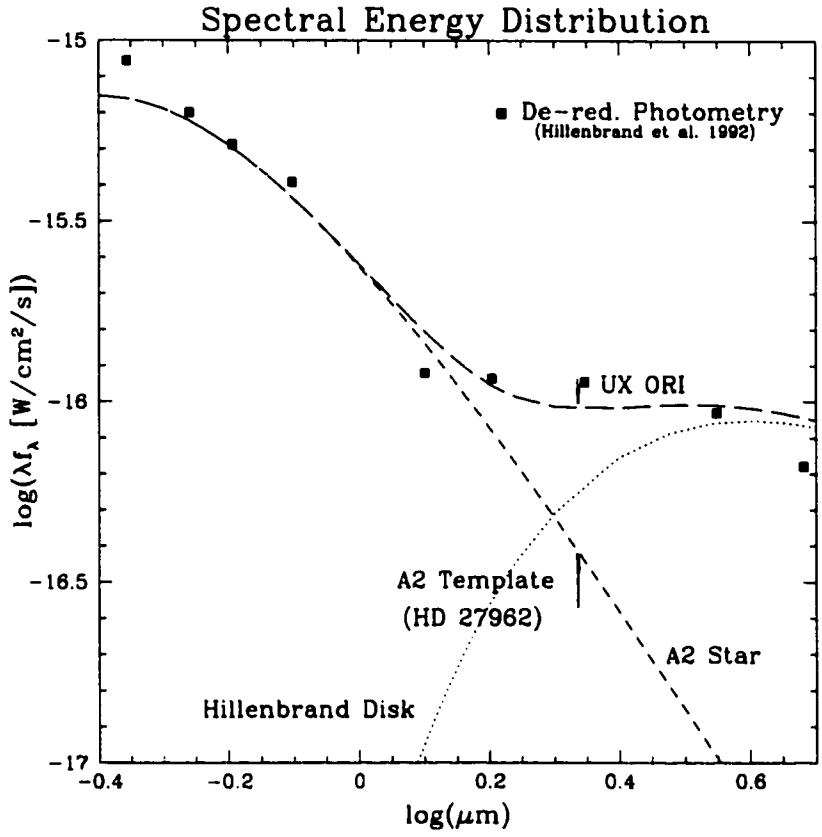

Figure 7.2 SED of UX Ori, overlaid with CSHELL spectra. Photometry points from Hillenbrand *et al.* (1992) are plotted along with their fit to the data (solid line) which is the sum of a blackbody photosphere (dashed) and a disk (dotted line). Two flux calibrated CSHELL spectra are shown: UX Ori (upper spectrum) and the A2 template star, scaled to the photospheric flux of UX Ori (lower spectrum). The flux levels of the spectra are well matched with the SED fluxes.

is still very weak, with a peak of order 1% above the continuum. In AB Aur, the depth of the photospheric absorpton in the original template was roughly 69% of the continuum level; however, because of the large IR excess, the veiled template line depth is 96% of the continuum. Therefore the circumstellar line emission in AB Aur is essentially equal to the original observed spectrum (to within the 5% error in sensitivity).

The circumstellar Brγ emission of AB Aur and UX Ori are plotted in Figure 7.4. Both lines are single peaked, but asymmetric in that the red side is significantly reduced in emission relative to the blue side. In AB Aur, an inverse P Cygni profile is clearly seen

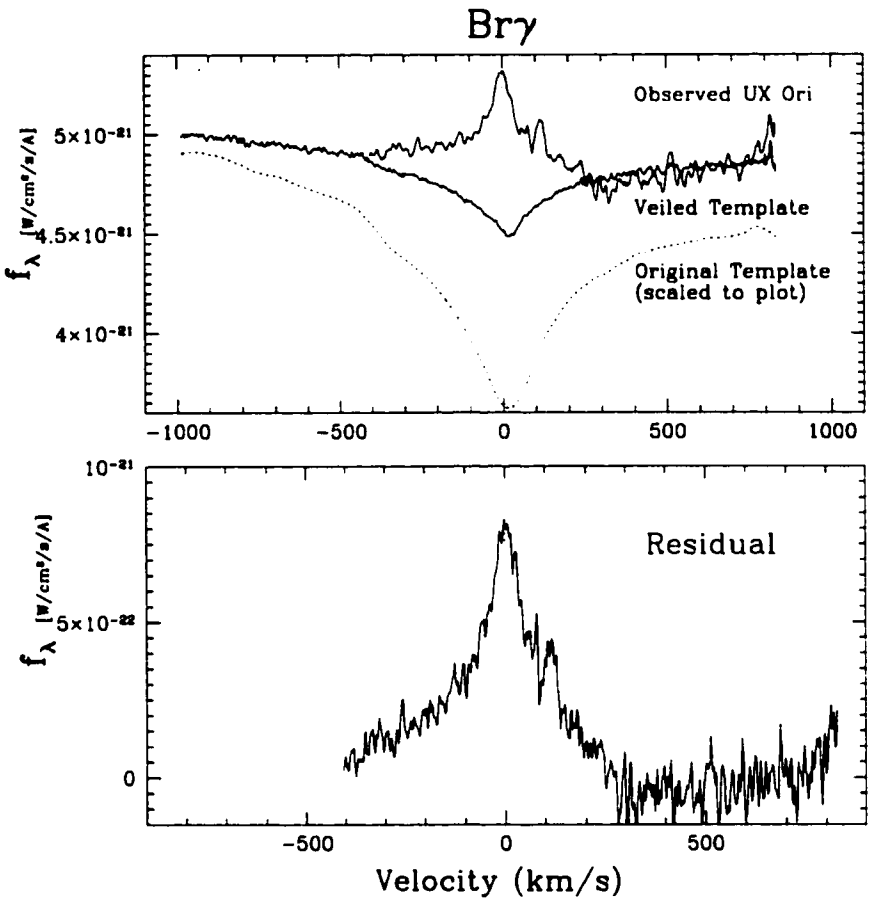

Figure 7.3 Circumstellar Brackett emission in UX Ori. Top panel shows observed emission in UX Ori (blue), observed template star (dotted) and veiled template (black). Bottom panel plots residual emission after subtracting the veiled template. This is the circumstellar Brγ emission.

with a peak velocity of $\sim$ 200km s^{-1}. The half width at the base on the blue side is $\sim$250 km s^{-1}. We see no evidence for blue-shifted absorption. In UX Ori, the core of the residual Brγ line is symmetric, exhibiting centrally peaked emission with a FWHM of 80 km s^{-1}. However, the wings of the line are clearly asymmetric. To the red, the central peak falls off more sharply than the blue side and there is a secondary peak at v = 110 km s^{-1}. To the blue, the decline is much flatter, such that the blue emission exceeds the red for Δv >200 km s^{-1}. Both stars exhibit an upward slope to the far-red side of the line, v > 400km s^{-1}, that is probably instrumental.

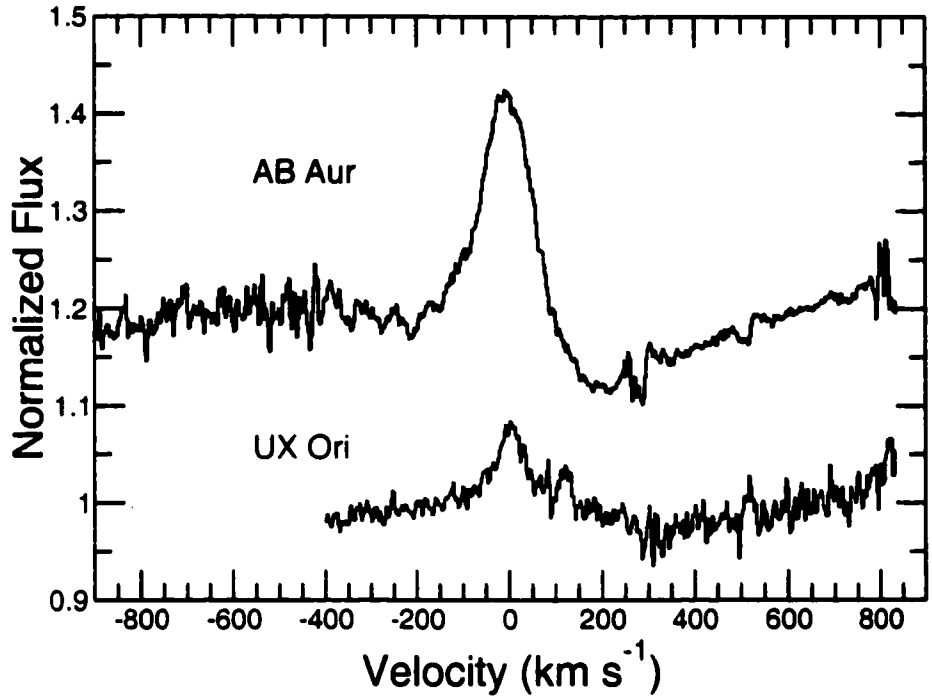

Figure 7.4 Normalized spectra of AB Aur and UX Ori. The AB Aur spectrum has been offset by 0.2. Inverse P Cygni absorption on the red side of the line is clearly seen in AB Aur. Although less apparent, the UX Ori line profile is also asymmetric with reduced emission in the red.

The circumstellar Brγ profiles of AB Aur and UX Ori are different than their Hα profiles shown in Chapter 5, suggesting that the two lines are dominated by emission from different physical regions. The Hα line of AB Aur does not exhibit red-shifted absorption, and in fact shows blue-shifted absorption on some epochs which is not seen in this Brγ profile (Fig. 5.6). Circumstellar Hα emission in UX Ori is double-peaked, with a slightly-redshifted absorption component. The UX Ori Brγ line is not double-peaked, although there is a small secondary peak on the blue side of the line. The Hα ($n = 3 \rightarrow 2$) line has contributions from many circumstellar regions, including possibly a wind, a disk atmosphere and an accretion stream. The Brγ ($n = 7 \rightarrow 4$) line must originate in a hot, high density region and is therefore likely to be less complicated and less saturated than the Hα line, providing a better look at activity in the very inner disk region.

Previous authors have assumed that Brackett emission in young stars originates at the

base of a wind. Nisini *et al.* (1995) use Brγ fluxes to estimate mass outflow rates in several HAEBE stars. This assumption may be incorrect. Muzerolle *et al.* (1998) find an empirical relation between Brγ line fluxes and accretion (as measured by UV veiling) in T Tauri stars. Najita *et al.* (1996) examine the Brγ profiles of a small set of T Tauri pre-main sequence objects, and suggest that the asymmetric line shapes suggest inflow, rather than accretion. Unfortunately, UV and optical veiling is not detected in HAe stars, and we know of no independent accretion diagnostic. However, the kinematics of the lines shown in this chapter are very similar to the Brγ profiles of the T Tauri stars described in Najita et al (1996), and we reach the same conclusion. The lack of blue-shifted absorption and the steeply decreasing red-side emission in the Brγ profiles of AB Aur and UX Ori favor an accretion origin, rather than a wind for the emitting gas.

7.4 Future Work

Synthetic line profiles based on the magnetospheric accretion model have been developed for T Tauri stars (Muzerolle *et al.* 1998b). These profiles are generally compared with Hα and Hβ line profiles in the literature. The results of this chapter indicate that the Brγ lines in AB Aur and UX Ori originate in accreting gas, and that these profiles are different from their respective Hα profiles, probably because the Hα lines include contributions from multiple circumstellar regions. We suggest that the Brγ line provides a more accurate diagnostic for testing accretion models. However, for Herbig Ae stars, model results appropriate to higher mass stars are needed for proper comparison with synthetic spectra.

Brγ profiles of additional stars are needed to clearly determine if the Brackett emission originates in infalling gas in HAe stars. If this is the case, coordinated monitoring of this line with optical brightness in UXORs will be important to access what role, if any, gas accretion plays in the photospheric variability of UXORs.

Chapter 8

DISK EVOLUTION AND STRUCTURE

Herbig Ae stars occupy a unique place in stellar evolution, in both the mass spectrum and the evolutionary sequence. Intermediate between the low mass T Tauri stars and the high mass O and B stars, research suggests Ae and Fe stars may be more similar to the former, but still significant theoretical and observational differences exist. In evolution, Herbig Ae stars are in a late pre-main sequence stage of star formation. Unlike low mass stars that occupy the vertical Hayashi tracks on the H-R diagram, intermediate mass stars evolve essentially *horizontally*, right to left, from the birthline to the main sequence. Therefore the effective temperature, and hence the spectral types of these stars change during the pre-main sequence lifetimes. Estimates indicate that the majority of Ae stars are located above but close to the zero-age main sequence on the H-R diagram (Natta *et al.* 1997; Rostopchina 1999). In addition, they are the evolutionary pre-cursors of β Pic-like systems, the young main sequence A stars that posess secondary debris disks, which suggest the presence of planetary bodies. That the HAe systems are in the beginning stages of planet formation is likely. There are many interesting questions we can pose about this group of stars. How does material accrete onto the star? How does the disk evolve and disperse? How is angular momentum dissipated? Are larger solid bodies forming, and if so, how? What is the structure of the inner disk, the outer disk?

Nearly all Herbig Ae stars exhibit photometric variability at some level, and roughly half show visible brightness variations of a factor of 4 or more ($\Delta V \geq 1.5$ mag; Ch. 2). These stars fall in the instability strip of the H-R diagram where temperature-sensitive opacity effects in the atmospheres of the stars cause small amplitude, periodic luminosity fluctuations. This behavior can account for variability up to a few tenths of a magnitude, and a few Herbig Ae stars have been identified as δ-Scuti type variables (Marconi & Palla 1998). The large amplitude variability however, has a circumstellar origin. If, as is commonly

believed, it is caused by obscuration of the central star by solid material in the circumstellar disk, then these stars offer a unique opportunity to study the structure of the circumstellar disks through their effects on the starlight.

In this thesis, we have used spectroscopy to probe the circumstellar line emission in HAe stars. These data provide direct access to the physics and activity of the circumstellar gas, that photometry alone can not. We have discovered new information about the evolution of hot gas and dust in the inner disk, and about the response of different circumstellar regimes to UXOR activity. To put these results in the larger circumstellar context, we now review briefly the nature of different types of young stellar disks, and their similarities and differences to Herbig Ae systems. We then discuss our main results in terms of disk evolution and structure. For the latter, we consider the empirical evidence associated with the UXOR phenomena against two variations of the obscuration model.

8.1 Young Stellar Disks

In the early 90s there was considerable controversy over whether Herbig Ae systems harbored circumstellar disks. After the ground-breaking paper by Hillenbrand *et al.* (1992), in which they fit the SEDs of some 30 HAEBES with disk reprocessing and accretion luminosity, other authors responded with alternative models (Hartmann & Kenyon 1996; Natta *et al.* 1993). Since that time the evidence for disks has grown, most notably due to resolved sub-mm observations of CO emission (Mannings & Sargent 1997; Mannings & Sargent 2000). These results confirm the presence of compact cool gas in a flattened structure around a number of HAe stars. At the same time, they do not rule out the presence of larger, unresolved envelopes as well. Estimates of disk masses are of order $0.5\mathcal{M}_{\odot}$, similar to T Tauri disk masses, and lead to the conclusion that only a disk configuration can harbor enough mass without obscuring the star (Natta *et al.* 1997). HST images of AB Aur (a non-UXOR star) show a circumstellar structure that appears disk-like with an inclination of less than 45 degrees (Grady *et al.* 1996). Nearly all HAe stars exhibit strong, optically thin silicate emission in the mid-infrared. This emission appears to vary on Keplerian timescales, months to years, and has been interpreted as originating in a disk atmosphere (Wooden *et al.* 2001).

Finally, a number of spectral similarities between HAe stars and T Tauri stars suggest a similar circumstellar environment, notably double-peaked Hα and Hβ profiles and inverse P Cygni profiles in lines such as CaII, NaI and HeI.

8.1.1 Be Disks

As already mentioned in Chapter 2, Herbig Be stars are very different from Herbig Ae stars and this applies to the evidence for circumstellar disks as well. In this thesis the spectra of HBe stars are clearly distinct from those of HAe stars. The optical spectra of Be stars exhibit strong hydrogen and metal emission lines, with either P Cygni profiles or forbidden emission indicating strong outflows (Ch. 3). In classical Be stars, strong winds are believed to create equatorial disks, unrelated to accretion activity. In the near-infrared, the Brackett emission in HBe stars is very strong. Both Brackett and Paschen emission is seen to very high upper levels ($n > 15$) in HD 45677, evidence of a large HII region. However, HBe stars do not exhibit significant excess continuum emission in the near-infrared. This is in contrast with HAe stars, which show more continuum veiling at K than Brackett line emission. The lack of hot dust and the strong hydrogen recombination emission are both a consequence of the much larger UV flux in Be stars compared to Ae or lower mass stars.

Theoretically Be stars are different as well. The pre-main sequence birthline intersects the main sequence for stellar masses $\gtrsim 10\mathcal{M}_{\odot}$, around early B spectral type. Stars with final mass greater than this do not have a classical pre-main sequence phase, and it may not be possible to build these stars via steady circumstellar accretion (Stahler *et al.* 2000). In addition, stars greater than $6\mathcal{M}_{\odot}$(~B5) are preferentially located in clusters, while young A stars are not (Testi *et al.* 1998). These results suggest that higher mass stars may form in a very different manner, through stellar aggregation. A thorough discussion of this intriguing idea is given by Stahler *et al.* (2000).

8.1.2 T Tauri Disks

The most well studied model for single star formation is the magnetospheric accretion model developed for T Tauri stars. In this model, a strong magnetic field created via a dynamo

inside these convective stars creates field lines that are coupled to the circumstellar disk at the Alfvén radius. This coupling creates an accretion stream from the disk to the star along the field lines and acts as a braking device, causing the star to spin down. Magnetic braking is needed to prevent the build-up of angular momentum on the star and account for the slow rotation rates of T Tauri stars. Hot spots associated with infalling material on the surface of the star emit UV continuum radiation which is manifested in a veiling of optical and UV spectral features. This model has been largely successful in explaining the wealth of data available on classical T Tauris, and is widely accepted (although see Alencar & Basri 2000). Measurements of the magnetic field strengths via Zeeman splitting are roughly consistent with mass accretion rates determined from the veiling continua.

Despite the observational similarities between Herbig Ae stars and T Tauri stars, there are theoretical and empirical difficulties in applying the magnetospheric accretion model to HAe stars. Stellar evolution models predict that HAe stars have radiative interiors, not convective, effectively eliminating the magnetic field generator. There are magnetic A stars, the Ap stars, but most main sequence A stars are not known to have strong magnetic fields. It is likely that pre-main sequence Ae stars harbor fossil fields, however efforts to measure the strength of the fields is hampered by the lack of significant metals in the photosphere and strong rotational broadening. Empirically, HAe stars do not exhibit the blue veiling continuum which is associated with accretion energy in T Tauris. This may be because the effective temperature of the stars is comparable to the accretion temperature, $\sim 10000K$. However, a careful analysis of AB Aur by Böhm & Catala (1993) places an upper limit on the mass accretion rate of $7.5 \times 10^{-8}\ \mathcal{M}_{\odot}\ \mathrm{yr}^{-1}$. This is more than 100 times less than the rate derived by Hillenbrand *et al.* (1992), using the excess near-IR luminosity at 3.5μm and a T Tauri like disk model. HAe stars are not generally slow rotators, with rotational periods of 1–2 days, thus removing the need for magnetic braking. In addition, HAe stars frequently show a dip in continuum emission in the near-IR that is not commonly seen in TTs, suggesting a difference in inner disk morphology. Recently, Natta *et al.* (2001) associate the near-IR continua emission with an inner disk "wall", unique to HAe stars.

8.2 Disk Evolution

Several authors have suggested an evolutionary scenario in HAEBEs based on their infrared spectral energy distributions (Hillenbrand *et al.* 1992; van den Ancker *et al.* 1997; Malfait *et al.* 1998). A similar scenario has been established in T Tauri stars for some time. (Adams *et al.* 1987). In the broad picture, the evolution from large infrared excess in very young stars to very little excess emission in main sequence stars is well-supported observationally and theoretically. However the evolution in near-infrared emission in HAEBEs is controversial. Malfait *et al.* (1998; Fig. 3) suggest that the decrease in emission in the near-infrared is associated with a clearing in the inner disk, possibly due to planet formation. But others have shown that thermal emission due to disk reprocessing may not account for all of the continuum emission; transient heating of small grains may also contribute (Natta *et al.* 1993). In addition, our calculations of the veiling fluxes at K' show that the excess emission is not well-correlated with age below 10 Myrs (see Fig. 6.6). Most HAe stars fall below this, with ages between 2 and 10 Myrs.

In Chapter 6, we find evidence of an evolutionary sequence in the strength of Brackett emission. The observed Brackett line emission evolves from the strongest line strengths, seen in the youngest stars, to esentially featureless flux spectra at intermediate ages (including UXOR stars), to photospheric Brackett absorption in Vega-like main sequence stars. More significantly, when the spectra are corrected for photospheric absorption and veiling, the circumstellar flux in Brγ is anti-correlated with age for ages from 0.5 to 10 Myrs. Although the sample size is small, the relation is apparent through intermediate ages (2 – 6 Myr), where no trend is seen in near-IR veiling flux (Fig. 6.6). This result suggests that hot gas may dissipate before hot dust in the inner disk. Interestingly, Natta *et al.* (2000) point out that disk mass estimates from measurements of CO (gas) in HAe stars are consistently lower than estimates based on millimeter measurements of hot dust.

Is the Brγ flux associated with accretion? The high resolution Brγ spectra in Chapter 7 show inverse P Cygni profiles in two stars (AB Aur and UX Ori), indicative of infall. Najita *et al.* (1996) reach the same conclusion based on similar spectra of seven low mass young stellar objects. Muzerolle *et al.* (1998) report an empirical correlation between Brγ

strength and accretion in T Tauri stars, using UV veiling to measure accretion. This accretion diagnostic is not available in Herbig Ae/Be stars, where no significant UV veiling is seen, presumably because the photospheric temperature is comparable to the blackbody temperature of the accretion luminosity. However, given that accretion is expected to be strongest in the youngest systems and decrease with age, the correlation between Brγ and age in our sample is consistent with their result and suggests that accretion may be similar in HAe stars and TT stars .

In the optical, the strength of circumstellar line emission may also indicate an evolutionary sequence, but the result is less clear. Of the three categories introduced in Chapter 3, we anticipated an age sequence from Category I to II to III, in analogy to the embedded, classical and weak-lined T Tauri stars, respectively. Instead, the Category I and III stars appear spread in ages between 0.1 and 10 Myr. The Category II stars, including all of the HAe stars and most of the UXORs in our sample, fall within a narrow age range, between 2 and 7 Myr. In these stars, Hα and Hβ emission is still prominent, but metal emission lines seen in the Category I objects are gone, or replaced with shell absorption lines.

Of the stars we studied in detail, we predict an age sequence of AB Aur— RR Tau— UX Ori— CQ Tau, based on the strengths of their circumstellar Brγ fluxes. This is consistent with age estimates from their H-R diagram positions: 2, 3, 4 and >10 Myr, respectively (van den Ancker *et al.* 1998; Rostopchina 1999), although the uncertainties in these ages is likely >1 Myr. Based on their optical spectra, these four stars were assigned to Categories I, II, II and III, respectively. The near-IR excesses we derived are similar between the first three stars (2.4, 3.0 and 2.5 magnitudes) and lower for CQ Tau (1.5 mag).

A fundamental question concerns whether the UXOR phenomenon is a particular evolutionary state of HAe stars, or a particular geometric configuration. Natta *et al.* (1997) investigate a number of variable and non-variable HAe stars and find no correlation between the two groups in disk mass or age. On the one hand, our spectra also show variable and non-variable Ae stars to exhibit similar features both in the optical and the near-infrared. At the same time, we find that all of the known UXOR systems present very similar spectra, with peculiar metal absorption and moderate Balmer and Brackett emission. No UXORs are found among the strong emission objects.

The age range of HAe stars with spectra similar to UXORs is very small, ~2 - 6 Myr, based on estimates from H-R diagram positions. This leads us to speculate that the UXOR phenomenon requires both a specific evolutionary state and a specific geometric configuration. The circumstellar disk must have evolved to a certain point for the cause of the obscuration to be present, and the system must have a favorable orientation for the effect to be observed.

8.3 Stellar Obscuration & Disk Structure

The suggestion that the photometric variability in HAe stars is due to stellar obscuration was first made by Wenzel (1969). Grinin *et al.* (1988, 1991) further developed the model and specifically showed how such obscurations can explain the "blueing" effect and the increased linear polarization during optical minima as a result of increased percentage of scattered starlight by dust. UXOR stars have been studied extensively by Grinin and collaborators and the "Grinin" obscuration model has been applied in detail to several UXOR stars including UX Ori, RR Tau, WW Vul, BF Ori and CQ Tau. (Grinin *et al.*1994; Rostopchina *et al.* 1997; Grinin *et al.* 1996; Kozlova *et al.* 2000). This work has been very important in describing the observed phenomena in terms of circumstellar obscuration and justifying the obscuration hypothesis, however, the nature of the obscuring material is not strongly constrained. Very little theoretical effort has been given to the feasibility of the model as a whole, and specifically the plausibility of large obscuring clouds existing in the disk as described by the model.

We briefly consider here two possibilities for the obscuring material. The first, occultation by circumstellar clouds in Keplerian orbits, is the mechanism assumed in the Grinin obscuration model, and is the most developed, but still faces difficulties. The second idea, occultation by dust rising out of the mid-plane of the disk due to some disk instability, does not yet exist as a formal model. However, the potential for such instabilities clearly exists and this model deserves consideration.

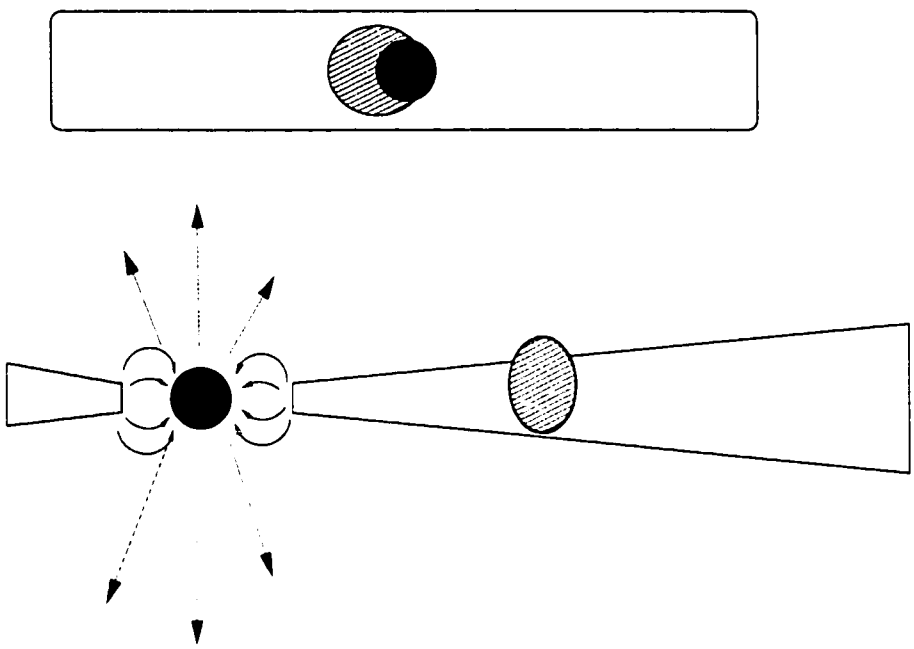

Figure 8.1 Schematic of Obscuration by orbiting cloud. In this edge-on configuration, the disk is assumed to be optically thin between the optically thick obscuring clouds. In another variation, the disk is not viewed edge-on but at a large angle (45 – 68 degrees), in which case the obscuring material must exist well above the disk plane.

8.3.1 Occultation by Orbiting Clouds

A schematic of this model is shown in Figure 8.1. Objections to this model concern the geometric configuration: assuming the clouds are orbiting in a Keplerian disk, this model requires these systems to be seen nearly edge-on, with very large ($\gtrsim R_*$), optically thick clouds embedded in an otherwise optically thin disk. Natta & Whitney (2000) have shown that the photometric and color behavior of UXORs at minima can be produced for a range of inclinations (45°- 65°) with a star surrounded by an optically thick flared disk, similar to disks associated with T Tauri stars. However, their model does not specify the location of the obscuration. The flared disk they describe has a maximum angular extent of ~10°above the equatorial plane, so the obscuring material must exist well above the disk to block the line of sight for inclinations of 45 - 65°. Bertout (2000) considered the possibility of the central star being observed through the optically thin disk atmosphere of a flared disk and found that the statistical probability is roughly consistent with the percentage of UXORs. In general, disk models predict settling of circumstellar dust into the disk mid-plane, so the mechanism by which large, optically thick clouds would be lifted into the tenuous disk atmosphere is unclear.

It is tempting to interpret these hypothesized circumstellar clouds in terms of protoplanetary blobs. The theorized sizes of protoplanetary envelopes are of the right order, with very large feeding zones of order R_*, (Pollack *et al.* 1996). However, these feeding zones grow within massive, optically thick disks. The orbiting obscuration model requires disks to be optically thin along line of sight between clumps, and optically thick within clumps. It has yet to be shown if large thick blobs can remain intact in such an environment.

In addition, timescales of photometric variability, particularly the shortest timescales (~days), seem incompatible with Keplerian motion in disks. There appear to be two frequencies of minima: large, long-duration dips of order weeks to months, and very short variations (usually within the longer dips) on timescales of days. The shorter timescales require either "holes" within the clouds, or clouds orbiting very close to the star. The lack of periodicity argues against close orbits, unless the bodies are accreting onto the star, as is suggested in the "evaporating infalling bodies" model.

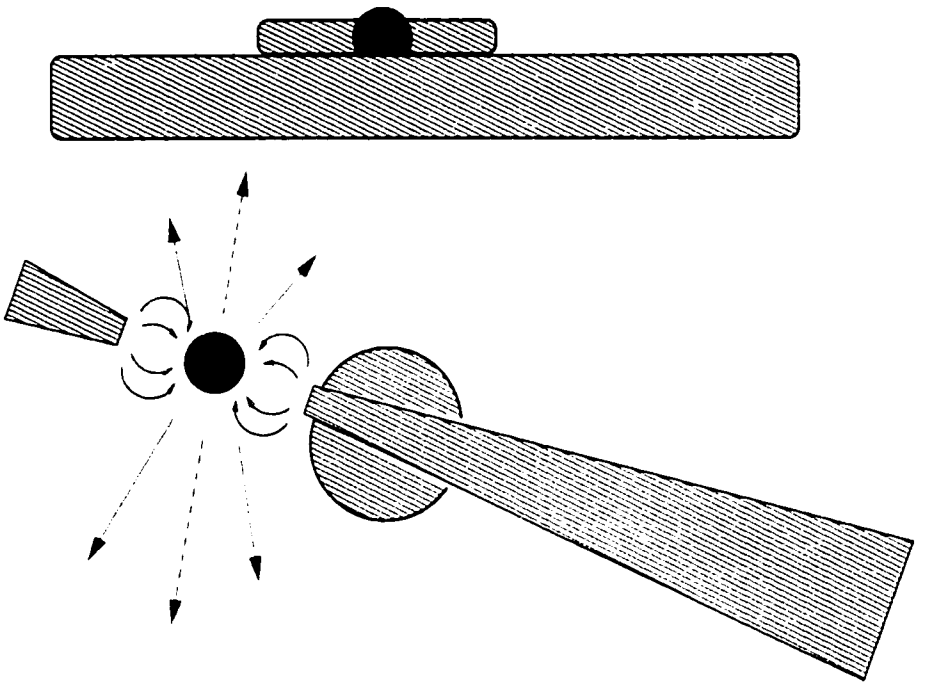

Figure 8.2 Schematic of Obscuration by intermittent disk instability. Disk inclination is large (45 - 68 degrees), but not edge-on. Central star is obscured by an instability in the disk, causing dust in the disk to rise well above the nominal disk height. Such an instability could be caused by a "warp" associated with azimuthal inhomogenities in the disk, or a "flare" related to variable disk accretion and/or magnetic activity.

This variation of the obscuration theory suggests that the occulting bodies are infalling "cometary" bodies (ie, "clumpy" accretion, Graham 1992), similar to the model developed for the young main-sequence star β Pictoris (De Winter *et al.* 1999; Grady *et al.* 1996). Such bodies could be infalling at any inclination, removing the need for an edge-on line of sight, but comets with very large ($\approx R_*$) dust comae or a very large number of them are required to obscure up to 90% of the starlight.

8.3.2 Occultation by "Puffed up" Disk Material

A second variation of the occultation model considers instabilities in the disk itself as the cause of the obscuration. A schematic of this model is shown in Figure 8.2. Although natural mechanisms exist to cause pre-main sequence disks to flare or "puff up", a model

does not exist specifically for HAe stars. The occulting material could be small grains rising up in the disk atmosphere, perhaps as a result of an accretion event or disk inhomogenity. An instructive analogy, developed for the large scale variability observed in FU Ori stars, can be found in Bell (1999; see Fig 2 for a much better schematic). In this model, the cause of the "volcano" region is an opacity effect associated with hydrogen ionization which causes the inner disk close to the star to flare up well above the mid-plane. In such a scenario, the flared region can block the line of sight to the star at inclinations significantly less than edge-on. In addition, the timescales for the obscuration to come and go are thermal, rather than Keperian, and can be quite short. However, in the Bell model, most of the luminosity during such a flare comes from the "volcano" region itself, therefore its not clear that such an event would be associated with a decrease in system brightness.

In search of diagnostics of this scenario, it is instructive to consider the data on R Cor Bor stars. These evolved stars also exhibit sudden drops in stellar brightness associated with obscuration of the star by circumstellar material. In this case the obscuring dust cloud is believed to be ejected from the stellar surface, and the recovery to normal brightness levels takes months to years. Although the scenario is very different, the exhibited behavior is very similar to UXOR stars. In particular, the spectral behavior of R Cor Bors during optical minima, which have been studied in some detail, bear striking similarity to the observed behavior of RR Tau shown in Ch. 4. At minima, broad absorption lines are replaced by narrow emission lines, slightly offset in velocity.

In the absence of a developed model, these comments are clearly speculative. However, there are aspects of the "puffy disk" scenario that appear to overcome the short-comings of the "orbiting cloud" model while still retaining the obscuration mechanism.

8.3.3 Variable accretion

It is possible that the photometric variability is not due to obscuration at all. An alternative model attributes the source of variability to a variable accretion flow onto the star (Herbst & Shevchenko 1999). These authors propose that the visible luminosity of the system is primarily accretion luminosity, rather than stellar. At maximum light we see the

optically thick surface of the accretion disk, while at optical minima a drop in the accretion rate causes this surface to become optically thin, allowing us to see the star. Note the fundamental difference: the obscuration models assume that the brightest state represents the true luminosity of the star, while the accretion model implies only at optical minimum do we see the luminosity of the underlying star. In this respect, this scenario is perhaps more similar to the FU Ori type outburst model (Hartmann & Kenyon 1996), than to the T Tauri accretion model that does not include a mechanism for such dramatic brightness variations.

We find little support for this model in our spectra of RR Tau. Specifically, if the source of the luminosity changed between maxima and minima, from accretion to stellar respectively, one would expect the spectral type of the system to change as well. We find no evidence for a change in spectral type, as discussed in Chapter 4. Additionally, one would expect spectral lines associated with accretion to be correlated with the system brightness. Neither Hα nor the wind lines ([OI], [FeII]) show any correlation. We find no simple explanation for the variability in the metal lines from absorption to emission, which is naturally explained with an obscuring screen. We do find evidence for accretion in HAe stars, and evidence for a variable accretion event in RR Tau. However, given the weak wind lines in most HAe stars and the lack of UV or optical veiling, it seems unlikely that the accretion stream would generate sufficient luminosity to dominate the light in these stars.

8.3.4 Empirical Evidence in this Dissertation

The main support for the obscuration model in our data comes from our observations of RR Tau, discussed in detail in Ch. 4). Briefly, the stability of the spectral type and of the extended wind emission, over a factor of ten in brightness argues against an intrinsic change in system luminosity. The correlated changes in brightness and spectra on short timescales: changing from faint to bright to faint again in $\sim$5 days, with spectral changes staying in sync with the photometry, are difficult to explain with large clumps in the disk as the source of the obscuration. This behavior may be better explained by a disk instability which can occur on very short timescales and have an immediate effect on the surrounding gas. Modeling of

the metal line flux may be key to sorting out this issue. The illustrative model developed in Chapter 4 finds that the obscuration is larger than the dense absorption region close to the star, but much smaller than the extended emission volume. Estimates of the density, temperature and volume of the metal emission regions should significantly constrain the affected volume, and provide specific information on the location of the obscuration region and its effects on the surrounding material.

Chapter 9

CONCLUSIONS

9.i Summary of Results

The main results of this dissertation, and their implications, are discussed in the previous chapter. Here we present a brief summary. Herbig Ae (HAe) stars are pre-main sequence stars of intermediate mass (2 - 5 $\mathcal{M}_{\odot}$). In evolution, they are intermediate between very young, embedded objects and young main sequence stars of spectral type B & A, specifically the Vega, or β Pic-like stars. As such they are the intermediate-mass counterparts to the low mass pre-main sequence T Tauri stars. HAe stars are similar to T Tauri stars in that they have significant infrared excesses and strong Hα emission lines, but they also emit many more UV photons and are massive (2-5 $\mathcal{M}_{\odot}$) enough to have fully radiative envelopes. Whether the magnetic accretion mechanism so popular with T Tauri stars applies to Herbig Ae stars is an open question. The majority of HAe stars reside above but very close to the zero-age main sequence on the H-R diagram. This, coupled with their optical visibility and predicted shorter pre-main sequence lifetimes suggest that these stars are in the late stages of star formation when planet formation activity is likely occuring.

A large fraction ($\sim$ 25 - 50%) of HAe stars exhibit large optical variability ($\Delta V > 1$, and sometimes as large as 4), commonly attributed to obscuration of the central star by circumstellar dust. In this dissertation, I report optical and near-infrared broadband spectra of a number of Herbig Ae (and a few Be) stars. My emphasis has been on the variable nature of these objects, and I have focused on the photometrically variable Ae stars, the UXORs. Low and high resolution near-infrared and optical spectroscopy provides a means to observe directly the hot gas and dust in the immediate circumstellar environment. These spectra provide diagnostics of the physics of the circumstellar environments of these stars that photometric data alone do not.

In both the optical and near-infrared, the Herbig Be stars separate from the Ae stars, showing much stronger hydrogen and metal emission. There are significant theoretical and empirical differences between Herbig Be and Ae stars and efforts to characterize and understand either are confused by datasets that combine the two.

Of the 22 Ae (and Fe) stars, the optical spectra of low amplitude variables span a range from strong emission objects to emission at Hα only, with some evidence of an evolutionary progression. In contrast, the high amplitude variables are concentrated in a group with moderate Balmer emission but peculiar metal absorption. Multi-epoch observations of the UXOR star RR Tau at different brightness levels from $V = 11$ to $V > 13.5$, reveal correlated changes in spectral behavior. The system shows photospheric line flux varies with system brightness while the wind lines ([OI], [FeII], and to a lesser extent Hα) emit constant flux, unaffected by the obscuration. Permitted metal lines (FeII, CaII, OI, NaI) change from absorption to emission when the star fades, and we suggest a model for this that attributes the absorption to a higher density region obscured with the star, while the metal emission comes from a more extended unobscured region.

Near-infrared spectra of a range of stars from embedded to Vega-like reveal an evolutionary sequence from strong Brackett emission in the youngest, embedded, sources (and Be stars), to photospheric absorption with little or no emission in Vega-like stars. The A stars fall between these two, exhibiting nearly featureless spectra in the near-infrared, with photospheric absorption veiled by strong excess emission and only weak Brackett emission. High resolution spectra of Brγ confirm this, showing essentially flat profiles for most sources. Two sources that do show circumstellar Brγ emission, AB Aur and UX Ori, exhibit inverse P Cygni profiles indicative of infall. The Brγ line in UX Ori looks very different from the Hα line, which is double-peaked with blue emission stronger than the red and a dip near the central wavelength, indicative of a disk profile. We contend that the Brackett line is more accurately probing the dense gas very near the star while the Balmer line contains a significant contribution from the disk atmosphere. Since most kinematic analysis of these stars has been based on Hα, these results point out the importance of using the near-infrared Brackett lines to effectively probe the inner disk accretion region.

Among the majority of the A stars that fall in the intermediate evolutionary state,

we find little evidence in optical or near-infrared spectra to distinguish between them. In particular, we find no evidence to suggest that the UXOR stars are in a different age group than similar less variable Herbig Ae stars. This favors a geometric origin for photometric variability, i.e., obscuration along the line of sight due to nearly edge-on view through the disk. However, the range of ages of Ae stars in this category is quite small, between 2 – 6 Myrs for most sources, based on their positions on the H-R diagram. It seems likely that the UXOR phenomenon then is a combination of both, such that the circumstellar disk must have evolved to a certain point for the cause of the obscuration to be present, and the system must have a favorable orientation for the effect to be observed.

9.2 Future Work

In this thesis I have concentrated on collecting and presenting a variety of spectroscopic data probing the circumstellar environments of Herbig Ae/Be stars. I have not attempted to model these data in any realistic way but rather have made a number of suggestions of things that might be learned with proper detailed modeling.

In the near-IR, the Brackett lines may provide a sensitive probe of hot, inner disk gas, just as the continuum is a diagnostic of the hot dust. The ideal dataset would be high spectral resolution, flux-calibrated spectra spanning H and K to explore the Brackett decrements of young stars of various ages. Such data are hard to come by with current instruments such as PHOENIX which offer high resolution but very limited spectral range. NIRSPEC, a NIR echelle instrument on the Keck telescopes provides both resolution and range, however simultaneous photometric observations would be needed to flux calibrate the spectra. In addition to NIR spectra, the question of NIR photometric variability remains largely unanswered. Whether such variability is expected is very model-dependent, however, empirical confirmation of its presence or absence will provide important constraints on existing models.

Much can still be learned from the optical spectra presented here, particularly in the case of RR Tau. These data have shown the importance of obtaining flux-calibrated data, in order to properly interpret variability in EW measurements. Through modeling, changes in

the flux of various metal lines with different excitation conditions, correlated with continuum variability, will provide information on the emitting volume of these gases and how they are affected by the obscuring material. Higher resolution flux-calibrated spectra will also be valuable for kinematic analysis of the circumstellar gas.

Of particular interest in the optical spectra is the FeII(42) triplet lines. These lines were observed in nearly every HAe star, either in emission or, in absorption with a significant circumstellar component. In MWC 1080 and HD 250550, the triplet lines show a P Cygni profile with velocities similar to Hα and Hβ, suggesting a common wind origin. However, in the UXOR star RR Tau, the [OI] wind line exhibits constant flux while the FeII(42) triplet lines vary dramatically from absorption at optical maximum to emission at optical minima. We suggest the absorption component originates near the star and this region is obscured during minima, revealing a more extended, weak emission region. Analysis of recently obtained echelle spectra will reveal what, if any, shift in velocity occurs between absorption and emission. Attempts to reproduce these FeII triplet lines with geometrically realistic models (i.e., disks) of Ae stars may provide important constraints on the different temperature and density regimes in their circumstellar environments.

BIBLIOGRAPHY

Adams, F. C., Lada, C. J., Shu, F. H. 1987, **ApJ**, 312, 788

Alencar, S. H. P. & Basri, G. 2000, **AJ**, 119, 1881

Backman, D. E. & Paresce, F. 1993, in *Protostars and Planets III*, eds. E. H. Levy & J. I. Lunine (Tucson: University of Arizona Press), p. 559

Bell, K. R. 1999, **ApJ**, 526, 411

Bertout, C. 2000, **A&A**, 363, 984

Bertout, C. 1994, in *Star Formation and Techniques in Infrared and mm-Wave Astronomy*, ed. T. P. Ray & S. V. W. Beckwith (Berlin: Springer-Verlag), 49

Bibo, E. A. & Thé, P. S. 1991, **A&AS**, 89, 319

Böhm, T., Catala, C., Donati, J. F. 1996, **A&AS**, 120, 431

Cabrit, S., Edwards, S., Strom, S. E. & Strom, K. M. 1990, **ApJ**, 354, 687

Catala, C., Donati, J. F., Böhm, T. 1999, **A&A**, 345, 884

Catala, C., Böhm, T., Donati, J. F., Simon, T., Jiang, S., Zhao, F. 1997, **A&A**, 319, 176

De Winter, D., Grady, C. A., van den Ancker, M. E., Perez, M. R., Eiroa, C. 1999, **A&A**, 343, 137

Eaton, N. L. & Herbst, W. 1995, **AJ**, 110, 2369

Finkenzeller, U. 1985, **A&A**, 151, 340

Finkenzeller, U. & Mundt, R. 1984, **A&AS**, 55, 109

Grady, C. A., Woodgate, B., Bruhweiler, F. C., Boggess, A., Plait, P., Lindler, D. J., Clampin, M., Kalas, P. 1999, **ApJ**, 523, 151

Grady, C., Perez, M., Talavera, A., *et al.* 1996, **A&AS**, 120 157

Graham, J. A. 1992, **PASP**, 104, 479

Grinin, V. P. 1988, **Sov. Astron. Lett.**, 14, 27

Grinin, V. P., Kiselev, N. N., Minikulov, N. Kh., Chernova, G. P., Voshchinnikov, N. V. 1991, **Ap&SS**, 186, 283

Grinin, V. P. 1994, in *The Nature and Evolutionary Status of Herbig Ae/Be Stars*, ASP Conference Series Vol. 62, eds. P. S. Th'e, M. R. Perez, & E. P. J. Van den Heuvel, (San Francisco: ASP), p.63

Grinin, V. P., Thé, P. S., de Winter, D., *et al.* 1994, **A&A**, 292, 165

Grinin, V. P. & Tambovtseva, L. 1995, **A&A**, 293, 396

Grinin, V. P. 1988, Kozlova, O. V., Thé, P. S., Rostopchina, A. N. 1996, **A&A**, 309, 474

Grinin, V.P., Kozlova, O.V., Natta, A., *et al.*, 2001, *in preparation*

Hamann, F. & Persson, S. E. 1992, **ApJS**, 82, 285

Hanson, M.M., Conti, P. & Rieke, 1996, **ApJ**, 107, 281

Hartmann, L. & Kenyon, S. J. 1996, **ARA&A**, 34, 207

Herbig, G. H. 1960, **ApJS**, 4, 337

Herbst, W., Herbst, D. K. & Grossman, E. J. 1984, **AJ**, 108, 1906

Herbst, W. & Shevchenko,V. S. 1999, **AJ**, 118, 1043

Hillenbrand, L. A, Strom, S. E., Vrba, F. J., & Keene, J. 1992, **ApJ**, 397, 613

Holtzman, J.A., Herbst, W., Booth, J. 1986 **AJ**, 92, 1387

Johnson, H. L. 1966, **ARA&A**, 4, 193

Kozlova, O. V. 2000, **Astron. Rep.**, 44, 36

Kurucz, R. L. 1979, **ApJS**, 40, 1

Lorenzetti, D., Saraceno, P., Strafella, F. 1983, **ApJ**, 264, 554

Malfait, K., Bogaert, E., Waelkens, C. 1998, **A&A**, 331, 211

Mannings, V. & Sargent, A. I. 2000, **ApJ**, 529, 391

Mannings, V. & Sargent, A. I. 1997, **ApJ**, 490, 792

Marconi, M. & Palla, F. 1998, **ApJ**, 507, 141

Muzerolle, J., Hartmann, L., Calvet, N. 1998, **AJ**, 116, 2965

Muzerolle, Calvet & Hartmann 1998, **ApJ**, 492, 743

Najita, J., Carr, J. & Tokunaga, A. 1996, **ApJ**, 456, 292

Natta, A., Prusti, T., Neri, R., Wooden, D., Grinin, V. P., Mannings, V. 2001, **A&A**, 371, 186

Natta, A., Grinin, V. P., Tambovtseva, L. 2000, **ApJ**, 542, 421

Natta, A., Grinin, V. P., Mannings, V. 2000, in *Protostars and Planets IV*, eds. V. Mannings, A. P. Boss & S. S. Russell (Tucson: University of Arizona Press), p. 559

Natta, A. & Whitney, B. A. 2000, **A&A**, 364, 633

Natta, A., Grinin, V. P., Mannings, V. & Ungerechts, H. 1997, **ApJ**, 491, 885

Natta, A., Prusti, T. & Kruegel, E. 1993, **A&A**, 275, 527

Nisini, B., Milillo, A., Saraceno, P. & Vitali, F. 1995, **A&A**, 302, 169

Rodgers, B., & Wooden, D.H., 1998, **BAAS**, #191.4709 (poster)

Rodgers, B., Woodward, C.E. & Wooden, D.H., 1999, *Protostars & Planets IV Conference* Santa Cruz, CA (poster)

Rodgers, B., Wooden, D.H., Grinin, V., Shakovsky, D., Natta, A., 2001, **ApJ**, submitted

Rostopchina, A. N. 1999, Astronom. Zhurnal, 76, 136

Rostopchina, A. N., Grinin, V. P., Okazaki, A., Thé, P. S., *et al.* 1997, **A&A**, 327, 145

Sorelli, C., Grinin, V., Natta, A. 1996, **A&A**, 309, 155

Stahler, S. W., Palla, F., Ho, P. T. P. 2000, in *Protostars and Planets IV*, eds. V. Mannings, A. P. Boss & S. S. Russell (Tucson: University of Arizona Press), p. 327

Storey, P. J. & Hummer, D. G. 1995, **MNRAS**, 272, 41

Strom, S. E., Strom, K. M., Yost, J., Carrasco, L., Grasdalen, G. 1972, **ApJ**, 173, 353

Sylvester, R. J., Skinner, C. J., Barlow, M. J., Mannings, V. 1996, **MNRAS**, 279, 915

Testi, L., Palla, F., Natta, A. 1998, **A&AS**, 133, 81

Thé, P. S., de Winter, D. & Pérez, M. R. 1994, **A&AS**, 104, 315

Tjin a Djie, H. R. E., Thé, P. S., Anderson, J., *et al.* 1989, **A&AS**, 78, 1

van den Ancker, M. E., Thé, P. S., *et al.* 1997, **A&A**, 324, 33

van den Ancker, M. E., de Winter, D., Tjin A Djie, H. R. E. 1998, **A&A**, 330, 145

Wenzel, W. 1969, in *Non-Periodic Phenomena in Variable Stars*, IAU Coll., ed. L. Detre (Budapest: Acad. Press), 61

Wooden, Woodward, Harker, 2001, in preparation

Wooden, D. H. 1994, in *The Nature and Evolutionary Status of Herbig Ae/Be Stars*, ASP Conference Series Vol. 62, eds. P. S. Th'e, M. R. Perez, & E. P. J. Van den Heuvel, (San Francisco: ASP), p.138

Yudin, R. V. 2000, **A&AS**, 144, 285

VITA

Bernadette Rodgers was born February 11th, 1963, in Kensington, Maryland, the 7th of 10 children in a catholic, Kennedy-era family. Family legend has it that she began to read the summer she was two, while helping her older sister prepare for kindergarden. This achievement won her the dubious honor of skipping kindergarden herself, effectively ending what might have been a promising art career. After a fairly rebellious but otherwise uneventful catholic school education, Bernadette moved a couple hours up the road to continue her education at the University of Delaware. Having been more interested in math and computers (and extracurricular activities) in college, she managed to avoid most science classes until her Senior year. It was in that year that she took an Introduction to Astronomy class with Dr. Harry Shipman, and got hooked on astronomy. But those were the days when Computer Scientists were just beginning to be in high demand, and Bernadette finished her B.S. in Computer and Information Science in 1984 and landed a good job with IBM Federal Systems Company in Gaithersburg, Maryland.

Bernadette worked for IBM from 1984 to 1993. While in Gaithersburg, she took up flying lessons from her father and got her pilot's license in 1986. That same year she moved with the company to Sunnyvale, California, near San Jose. She worked her way up the ranks on a large Air Force satellite control project, with the generic name of Data System Modernization (DSM), making her marks most notably in system testing and advanced application programming. At the same time, her interest in astronomy grew and she spent three of the nine years with IBM on an educational leave of absence. From 1987 to 1990, Bernadette attended New York University and obtained a Master's degree in Physics (taking most of the undergrad and graduate curriculum concurrently). It was at NYU that Bernadette met Al Glassgold, and began to really learn astronomy. Under Al's tutelage, she completed a master's thesis modeling the temperature in the circumstellar envelope of the red giant star α Orionis, or Betelgeuse.

Upon returning to California in 1990, she resumed her job with IBM but maintained ties with Al and the astronomy community. She began to infiltrate the Center for Star Formation group based at NASA Ames in Mountain View, California, and eventually accepted a job with Lockheed as a contractor at NASA Ames in order to spend more time there. After a brief stint testing software for monkeys to play video games in space, Bernadette decided to take the plunge and make astronomy her career. In the fall of 1994, she and her partner Peter Schneider loaded up the U-haul and moved to Seattle to attend graduate school at the University of Washington.

Their years in Seattle were the "busy years". While Bernadette worked full-time on her Ph.D., Peter, a master builder, spent his spare time rebuilding their 1914 bungalow from the foundation up. Their first child, Joshua Hanson Schneider, was born June 29, 1996, followed by their daughter, Amy DuBos Rodgers, on September 21, 2000. The couple was married on cinco de Mayo, dos mil uno. In August of 2001, the family will move to La Serena, Chile, where Bernadette will begin a Gemini Science Fellowship at the new Gemini-South Observatory.